Summer 2010

Experimental and computational investigations of hydrogen safety, dispersion and combustion for transportation applications

Shravan K. Vudumu

Department: Mechanical and Aerospace Engineering

EXPERIMENTAL AND COMPUTATIONAL INVESTIGATIONS OF HYDROGEN SAFETY, DISPERSION AND COMBUSTION FOR TRANSPORTATION APPLICATIONS

by

SHRAVAN KUMAR VUDUMU

A DISSERTATION

Presented to the Faculty of the Graduate School of the

MISSOURI UNIVERSITY OF SCIENCE AND TECHNOLOGY

In Partial Fulfillment of the Requirements for the Degree

DOCTOR OF PHILOSOPHY

in

MECHANICAL ENGINEERING

2010

Approved by

Umit O. Koylu, Advisor
Kelly O. Homan
Serhat Hosder
John W. Sheffield
Elvan Akin-Bohner

ABSTRACT

Hydrogen is an energy carrier that can be produced from a variety of sources, offering one of the viable solutions to the increasing demands for clean and sustainable energy. Compared to the conventional fuels, hydrogen has distinct properties that need to be properly accounted for during its safer storage and delivery as well as more efficient and cleaner utilization. The broader objective of this study is to contribute to the scientific knowledge necessary to overcome key technical barriers to the widespread implementation of hydrogen in transportation applications. Specifically, lower flammability limit of hydrogen is first measured with an enhanced experimental setup and then supported with a theoretical analysis in order to provide safety guidelines for hazardous conditions. Small and large hydrogen releases are computationally investigated under different conditions corresponding to potential accidental release scenarios. This involves quantifying the relative roles of buoyancy, diffusion and momentum during hydrogen transient mixing in air and the associated flammable zones in a simple geometry. The numerical predictions are extended to a practical geometry in which high-pressure unsteady hydrogen leaks occur due to a catastrophic failure of a storage tank in a typical mobile hydrogen unit. Additionally, the combustion, performance and emission characteristics of a hydrogen-powered internal combustion engine are simulated by incorporating fuel-specific sub-models into a quasi-dimensional model, which is subsequently validated against independent data and utilized to quantify the effect of exhaust gas recirculation on emissions of oxides of nitrogen. Such reasonably fast and accurate predictive tools are essential to effectively design and optimize hydrogen engines for higher efficiency and near-zero emissions in the automotive industry.

ACKNOWLEDGMENTS

I wish to express my sincere thanks to my advisor Dr. Umit O. Koylu for his invaluable guidance, advice and constant encouragement throughout the course of my research work. I am greatly indebted to him for his unwavering commitment, thought-provoking discussions, and constructive comments to improve my work.

I would like to thank my committee members Dr. Serhat Hosder, Dr. John W. Sheffield, Dr. Kelly O. Homan, and Dr. Elvan Akin-Bohner for their constructive suggestions, encouragement and for their invaluable time and efforts in examining my dissertation.

I also would like to thank the faculty and staff of the Department of Mechanical and Aerospace Engineering at Missouri University of Science and Technology for their support in executing and completing my research work.

I would like to acknowledge the National University Transportation Center and U.S. Defense Logistic Agency for financially supporting this research. I would also like to acknowledge the additional support in the form of Graduate Research Assistantship and Graduate Teaching Assistantship.

Finally, I would like to thank my family and friends for their support and interest during the course of my research.

TABLE OF CONTENTS

LIST OF ILLUSTRATIONS

Figure Page

LIST OF TABLES

NOMENCLATURE

Symbol	Description
A	cross-sectional area
A_s	heat transfer surface area
d	leak diameter
C_1, C_2,	constants in classical velocity decay scaling law (free jet)
C_3, C_4	constants in classical concentration decay scaling law (free jet)
D	diffusion coefficient
e	internal energy per unit mass
g	gravitational acceleration
h	enthalpy
I	unit tensor
$\vec{J}$	diffusion flux
k	thermal conductivity
L	length of the cylinder = 1 m
m	mass
$\dot{m}$	boundary mass flux
M_w	molecular weight
p	static pressure
P	pressure in the cylinder
Q	heat transfer rate

Ra	Rayleigh number $= \dfrac{g(\rho_{air} - \rho_{H_2})z^3}{\nu_{H_2}\alpha_{H_2}\rho_{H_2}}$
Re	Reynolds number $= \dfrac{V_e d}{\nu_{H_2}}$
Ri	Richardson number $= \dfrac{(\rho_{air} - \rho_{H_2})gd}{\rho_{H_2}V_e^2}$
S_L	laminar flame speed
S_T	turbulent flame speed
t	time
T	temperature
T_f	fluid temperature
T_{wall}	wall temperature
u	velocity
V	volume of the cylinder
$\vec{V}$	velocity vector
V_e	gas velocity at the jet exit
W_j	jet velocity at exit (free jet)
W_{cl}	jet centerline velocity at axial distance z from the jet exit (free jet)
X	mole fraction
X_{cl}	jet centerline mole fraction at axial distance z from the jet exit (free jet)
X_{dil}	diluent mole fraction
Y	mass fraction
z	position above the cylinder bottom or axial distance from the free jet inlet

Greek Symbols

α	thermal diffusivity
ϕ	equivalence ratio
μ	dynamic viscosity
ν	kinematic viscosity
ρ	density
$\overline{\overline{\tau}}$	stress tensor
∇	unit vector operator

Subscripts

u	unburned zone
b	burned zone

1. INTRODUCTION

It is well known that the combustion of fossil fuels is responsible for the majority of the green house gas emissions and a significant fraction of pollutant emissions in the world. The natural reserves of fossil fuels are also diminishing quickly. Hydrogen is considered to be one of the viable solutions to the increasing demands of clean and renewable energy due to the absence of carbon based pollutants, the abundance of hydrogen in nature, and the ability to generate hydrogen from various sustainable energy sources. It might also enable fossil fuel importing economies to become leading exporters of hydrogen. The transition from fossil fuels to such emerging energy technologies involves many challenges that must be overcome for widespread public use and acceptance. Hence development of a hydrogen economy demands research on hydrogen safety issues and its utilization in transportation applications.

1.1 BACKGROUND AND MOTIVATION

This research complements the ongoing research at Missouri University of Science and Technology to develop, demonstrate, evaluate and promote safe hydrogen-based technologies in real applications. This includes setting up a hydrogen fueling station and establishing a commuter bus service in rural Missouri and to understand feasibility and large-scale deployment of hydrogen technologies under diverse operating conditions. The University is also involved in the EcoCAR Challenge to re-engineer a conventional GM vehicle to a hydrogen fuel cell plug-in hybrid electric vehicle.

To promote the safe use of hydrogen-based technologies, it is important to thoroughly understand the unique properties of hydrogen, which is the smallest element.

As shown in Table 1.1, when compared to other traditional fuels like gasoline and natural gas, hydrogen has more energy per unit mass, wider flammability limits, lower density, higher flame speed and diffusion coefficient, and is easier to ignite. In addition, hydrogen does not give any odor, it is colorless, and hydrogen flame is almost invisible in day light.

Table 1.1. Important properties of hydrogen and comparison with traditional fuels

Characteristic	Hydrogen	Natural Gas	Gasoline	Significance
Heating value (MJ/kg)	120	50	44	higher heating value
Flammability limits in air (vol%)	4-74	5-15	1-7	wider limits
Density (kg/m^3)	0.082	0.67	4.4	lowest density
Diffusion coefficient in air (cm^2/s)	0.61	0.16	0.05	faster spread
Stoichiometric flame speed (m/s)	2.1	0.4	0.3	faster burning
Minimum ignition energy in air (mJ)	0.02	0.3	0.3	easier ignition

Many technical barriers to the implementation of a hydrogen economy exist due to the lack of established scientific and technical knowledge that is needed to support the development of codes and standards to mitigate potential fire and explosion hazards. Fire safety of existing hydrogen applications is generally provided by experience from other traditional fuels whose properties are drastically different (as shown Table 1.1) from those of hydrogen. It is therefore essential to recognize the properties of hydrogen and help establish the safety codes and standards for an effective transition to hydrogen-based technologies (Dahoe and Molkov, 2007; Houf and Schefer, 2008). In addition, one of the

disadvantages of hydrogen is related to its real and perceived safety issues (Rodgers et al. 2010).

To accelerate the utilization of hydrogen in transportation applications, the existing engine design methods and manufacturing plants can be fitted with minor modifications. This permits the mass production of hydrogen engines in the near term while other technologies, such as fuel cells, need a complete re-design of vehicles in the long term. Consequently, hydrogen fuel-specific predictive engine models that take the distinct properties of hydrogen into account are required to help develop hydrogen engines during this transition period (White et al., 2006; Verhelst et al., 2006).

1.2. THESIS OBJECTIVES

The present study is divided into four stages that are discussed below.

1.2.1. Establishing the Lower Flammability Limit. When hydrogen concentration decays in surrounding air during an unintended release, there exists a concentration range below and above which the mixture will not ignite. The leanest and richest concentrations that can support flame propagation are called lower and higher flammability limits. The knowledge of the lower flammability limit value is very important for safety purposes. Although previous studies are available on hydrogen flammability limits, the contradictory values reported in the literature make it difficult to know the correlation between the flammability limits measured with various methods and the exact physical conditions for extinguishing related flames in real accidents. Therefore, an experiment is designed in this study to determine the lower flammability of hydrogen in air that will be independent of the experimental setup (as practical as

possible) and to obtain a value that would be observed in free space. The measured result is also supported with a theoretical analysis.

1.2.2. Buoyancy-Dominated Small Leaks. Buoyancy-driven diffusion of hydrogen in enclosures is of interest in transportation applications because hydrogen gas can disperse very quickly with its lowest molecular weight and high diffusion coefficient (Swain et al., 2003; Cisse and Karim, 2007). These properties can be used to avoid the formation of flammable mixtures after accidental hydrogen releases and to prevent further development towards hazardous concentrations (Dahoe and Molkov, 2007). Based on properties alone, hydrogen poses an increased risk primarily due to the increased probability of ignition. But, the increased buoyancy effects might change this probability depending on the actual physical condition (Crowl and Jo, 2007). Although there are reports on hydrogen simulations for predicting radiative heat fluxes and flammability envelopes for unintended releases, there are few past investigations on the transient behavior of hydrogen mixing at short times. The present study therefore focuses on the fundamental features of hydrogen transient dispersion for different cases within a unit-length vertical cylinder that can be used as a benchmark problem for simulating more complicated and practical hydrogen release scenarios with complex geometries. The computational parameters are varied so that the flow conditions are controlled by either buoyancy or molecular diffusion or a small jet momentum. The details of the temporal and spatial distributions of hydrogen in air and the resulting flammability zones are explored with implications in the safe practices of hydrogen delivery to various hydrogen technologies.

1.2.3. Momentum-Dominated Large Leaks. Due to its low density, hydrogen is often compressed to high pressures for storage in fueling stations, hydrogen-powered vehicles, and other industrial applications. Extending the simple geometry in Stage 3 to a practical and complex geometry, this part of thesis focuses on a momentum-dominated major leak from one of the high-pressure (485 bars) hydrogen storage cylinders in a typical mobile hydrogen unit (MHU) used in fueling stations. Computational Fluid Dynamics (CFD) is used to simulate a potential accidental scenario in which there is a catastrophic failure of a pressure relief device or a small crack in a storage vessel. As the exit flow chokes at the sonic velocity, a careful approach to the computational model is necessary in this unsteady, three-dimensional, compressible and turbulent flow. Initially, the applicability of the various effective diameter approaches available in the literature to overcome the numerical difficulty of solving the complete underexpanded jet is assessed, and later the transient mixing behavior of momentum-dominated hydrogen leak is studied in the MHU.

1.2.4. Hydrogen-Fueled Internal Combustion Engines. The unique properties of hydrogen also make it a favorable fuel to be used in engines. Hydrogen internal combustion engines have the potential for high power because of more energy per unit mass and high flame speed, high efficiency because of high flame speed that causes high rate of pressure rise in the cylinder and hence near constant-volume combustion. They also have near-zero emissions, except NO_x at higher loads, because of the absence of carbon in the fuel molecular structure. In this study, the performance, combustion and emission characteristics of a hydrogen-fueled engine when used in a vehicle are investigated. The objectives of this part are to develop a hydrogen fuel-specific predictive

one-dimensional engine model based on two-zone combustion methodology, validate it against independent experimental data for widespread implementation, and demonstrate its utilization for finding operating conditions for higher performance and lower emissions.

1.3. BROADER IMPACTS

Development of a hydrogen economy is important to dramatically reduce dependence on foreign oil and help secure our energy. It would also help to reduce carbon emissions from energy production and consumption including green house emissions from cars and trucks. Since hydrogen can be produced from a number of domestic sources (electrolysis of water, reforming natural gas, nuclear and solar high-temperature processes, coal gasification), it assists in diversifying the energy source beyond petroleum to fuel the transportation needs. Hydrogen's use as a major energy carrier, in addition to the introduction of other fuels, would also provide the nation a more efficient and sustainable energy infrastructure, with a variety of options for central and distributed fuel production and electric power generation.

To overcome the technical barriers during the implementation of a hydrogen economy, this research is expected to help develop the much-needed safety codes and standards (based on sound scientific and technical knowledge), ventilation system designs, and optimal locations of hydrogen detectors for hydrogen-powered technologies in transportation applications. It will be important to develop and implement an outreach program, in collaboration with other programs at the local, state and national levels, which is necessary to gain public acceptance for the safe use of alternative fuels to power

the transport systems that are independent of the fossil fuels. This study should also assist the automobile industry to design hydrogen internal combustion engines during the initial stages of the hydrogen economy.

2. EXPERIMENTAL STUDY AND THEORETICAL ANALYSIS ON LOWER FLAMMABILITY LIMIT OF HYDROGEN IN AIR

2.1. INTRODUCTION

Safety is a critical issue for the design and operation of transportation vehicles using hydrogen. This is because hydrogen has drastically different properties when compared to other traditional fuels, as mentioned in Section 1. Key concerns are its low ignition energy, low luminosity, high flame speed, and wide flammability range. Flammability limits, the lowest and highest concentrations below and above which the fuel-air mixture can no longer be ignited, are very important when considering safety issues and associated risk analyses. They are useful for developing safety codes and standards, providing design criteria for refueling stations, and operating various hydrogen-powered technologies safely.

As extensively discussed below, the flammability limits of hydrogen have remained as an empirical observation in the literature. In this study, effort has been made to develop a simple ideal experiment to observe the lower flammability limit of hydrogen in air that would be less dependent on the apparatus itself and to support the present observations with a theoretical analysis.

2.2. BACKGROUND AND MOTIVATION

Although much research has been conducted in the field of flammability limits, there are still many questions that cannot be answered adequately (Wierzba and Wang, 2006), mainly due to the contradictory values of the flammability limits reported in the literature. Table 2.1 shows some of the experimental studies done on the lower

flammability limit of hydrogen with a brief summary of their experimental setup and the reported results.

Table 2.1. Experimental studies in the literature on hydrogen lower flammability limit

Source	**Lower flammability limit (% of H_2)**	**Experimental set-up**	**Notes**
Coward and Jones (1952)	4.15 (upward) 6.7 (horizontal) 9 (downward)	Bureau of Mines experimental set up. Tube: dia. 5 cm, length 150 cm	Considered to be the earliest and most extensive study
Kumar (1985)	4 (upward) 6.5 (horizontal) 8.5 (downward)	Test tube: dia. 5 cm, length 180 cm	H_2-air mixtures
Hustad and Sonju (1988)	5 (upward)	Test tube: dia. 10 cm, length 300 cm with thermocouples	H_2, CH_4, CO, air mixtures and dependence on temperature
Medvedev et al. (2001)	4 (upward)	Test tube: dia. 12 cm, length 60 cm	H_2-air mixtures in the presence of ultrafine droplets of water (fog)
Swain et al. (2005)	5-10 (upward)	Sliding cylinder piston mechanism. Test tube: dia. 10.16 cm, length 19.1 cm	Various ignition energies and electrode gaps
Ciccarelli et al. (2006)	4.5 (upward)	Cylinder test vessel with a mixing fan: dia. 25.7 cm, length 25 cm	H_2-air mixtures at various initial temperatures
Villegas et al. (2005)	5.8-13	Volume around a shaft: dia. 7.87 cm, length 10 cm	H_2-air mixtures with various gap sizes
Wierzba and Wang (2006)	3.9 (upward)	Stainless steel test tube with a vacuum pump: dia. 5.08 cm, length 100 cm	Dependence on temperature
Weissweiller (1936)	5	Sphere: 0.81 L	H_2-air mixtures
Yaew and Shnidman (1938)	4.6	Bomb: 0.35 L	H_2-air mixtures

Safety studies are concerned with experimentally-determined limiting concentration beyond which combustion can be assured not to occur. From Table 2.1, it can be seen that the experimental determination of lower flammability limit of hydrogen is inextricably interwined with the apparatus and varies between 3.9% and 13% by volume in air. These values are dependent on many factors such as shape and dimension of vessel, direction of flame propagation, temperature and pressure of the mixture, ignition energy and location of ignition source, addition of diluent gas, turbulence, and criteria of flammability (see Table 2.2).

For quick reference and comparison purposes, one of the most commonly referred method to observe lower flammability limit developed by Coward and Jones (1952) is presented here. Figure 2.1 shows the schematic diagram of the test apparatus. The experimental set-up is based on a vertical open ended transparent tube. The use of a transparent tube permits direct visualization of the flame and flammability is based on the propagation of the flame over a predetermined section of the tube (5 feet = 1.52 m).

In Figure 2.1, ***a*** is the glass tube in which the mixture is tested. Its lower end is closed by a lightly lubricated ground-glass plate ***b***, sealed with mercury ***c***. It is evacuated by a pump through the tube ***j***. The vapor or gas under the test is drawn from its liquid (if required) in the container ***p***, in the amount measured by the manometer ***k***. Air or other atmosphere is then admitted through the drying tube ***q*** until atmospheric pressure is reached. The air and gas to be tested are then thoroughly mixed by circulation, by suitably raising and lowering the mercury vessel ***g*** repeatedly for 10 to 30 minutes. The mercury seal is then removed, the glass plate ***b*** is slid off the tube, and the flammability is

tested by sparking at ***y*** or by passing a small flame across the open end of the tube. The tube used was 5 cm (~2 inches) in diameter and a height of 150 cm (~5 feet).

Table 2.2. Effects of various factors on the flammability limits

Factor	**Effect**
Temperature	By increasing the initial temperature, the lower limit decreases and the upper limit increases, thus widening the range of flammability (Coward, 1952).
Pressure	Normal variations of atmospheric pressure do not appreciably affect the limits of flammability. Reduction in pressure below 1 bar generally narrows the range of flammability and at a suitably low pressure the limits coincide, below which no mixture can propagate flame (Coward, 1952).
Ignition energy	The mixture should be provided with enough ignition energy (depends on spark gap). If adequate ignition energy is not provided, limits of ignitibility and not limits of flammability may be measured (Zabetakis, 1965).
Shape and dimension of the vessel	For a cylindrical vessel of small diameter with a large height, the flammability limits are primarily determined by the quenching effect of the wall. (Takahashi, 2003).
Direction of flame propagation	For upward propagation, the buoyant acceleration of a burned gas is in the direction of propagation, and hence the buoyant velocity adds to the rate of advance of flame front. For horizontal flame propagation, the buoyant flame acceleration is perpendicular to the direction of propagation. For downward propagation, the buoyant acceleration is opposed to the direction of propagation, and hence the buoyant velocity reduces the rate of advance of flame front. Hence, the limits for upward propagation are wider than those for horizontal and downward propagation of flame.
Turbulence	With suitable amount of turbulence produced either by a fan or stream movement of the mixture widens the range of flammability (Coward, 1952).
Diluent	The addition of increasing amounts of a chemically inert substance to the mixture narrows the range of flammability and ultimately becomes non-flammable (Coward, 1952).

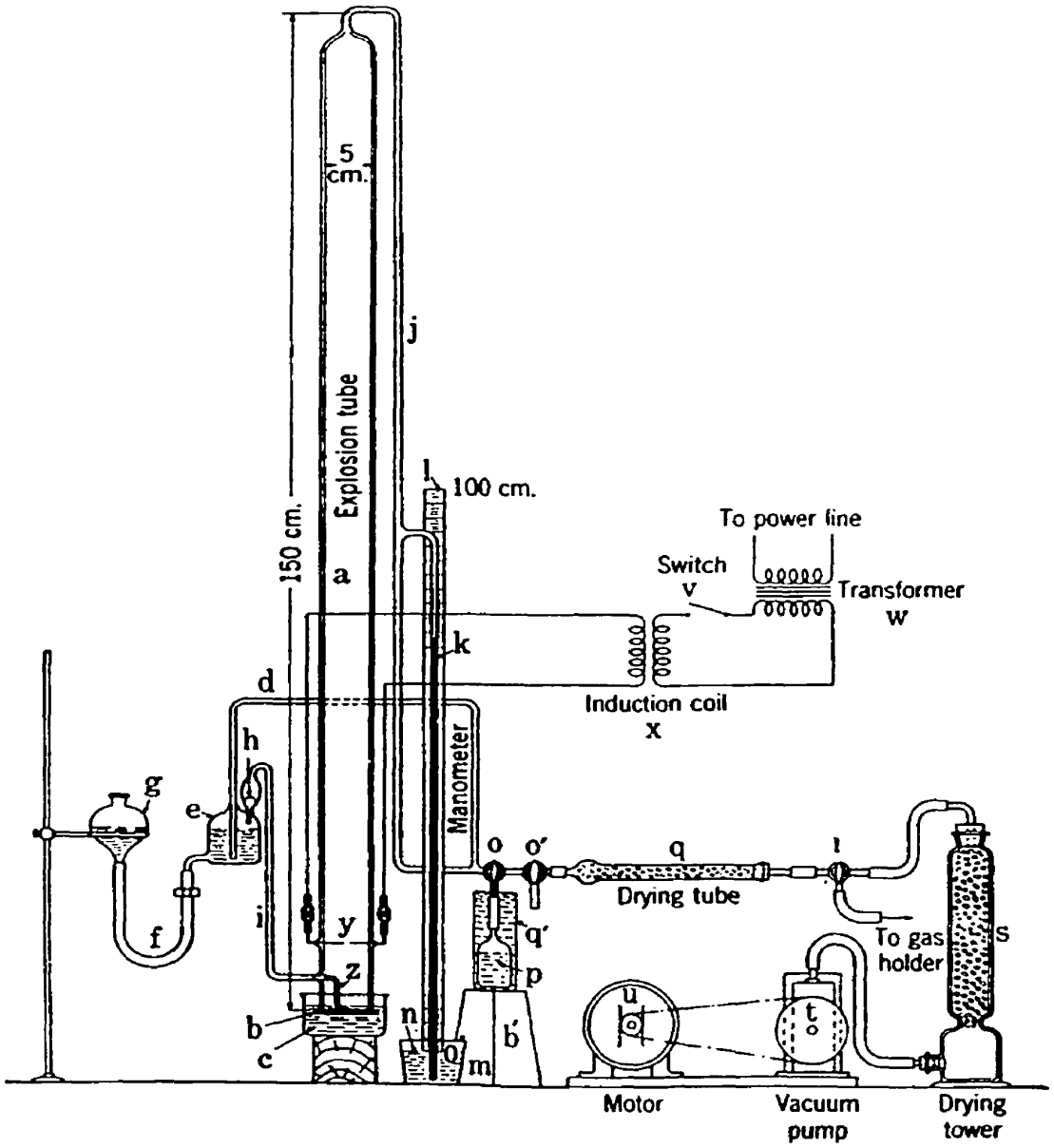

Figure 2.1. Schematic diagram of the test apparatus developed by Coward and Jones (1952) to observe flammability limits

The experimental set-up shown above together with the different lower flammability limit values reported in Table 2.1 and their dependence on experimental set-up (Table 2.2) indicates that it is difficult to conduct the experiment and to know the

correlation between the flammability limits measured with various methods and the exact physical conditions for extinguishing flames related in the real accidents.

2.3. OBJECTIVES

The objective of this study is to design a simple yet effective experiment to determine the lower flammability of hydrogen in air that will be independent of the experimental setup (as practical as possible) and to obtain a value that would be observed in free space. The result will also be supported with a theoretical analysis.

2.4. EXPERIMENTS TO OBSERVE LOWER FLAMMABILITY LIMIT

Figure 2.2 shows the initial experimental configuration designed and set up in this study. A compressed hydrogen gas cylinder (30 cc, 2000 psig, 70 ^{o}F, 99.999% purity, double-stage stainless steel regulator) was used with a compressed air gas cylinder (232 cc, 2000 psig, 70 ^{o}F, single stage brass regulator) to get various concentrations of hydrogen and air. Two mass flow controllers (Omega FMA 5500 series) were used to measure mass flow rates of hydrogen and air. Different percentages of hydrogen and air mixtures were formed in the vertical acrylic cylinder (diameter: 10.16 cm, length: 19.3 cm) that was closed on the bottom with a piston and on the top with a flexible latex membrane. The bottom of this cylinder had a spark plug to ignite the mixture with a push button piezoelectric igniter.

Figure 2.2. Initial experimental setup used in the present study

A custom made LabVIEW program (Figure 2.3) was employed with National Instrument's USB 6009 data acquisition card to precisely control the amount of hydrogen and air sent through the mass flow controllers while filling up the acrylic cylinder. When the program was run, the mass flow controllers sent the desired amount of hydrogen and air simultaneously. To ensure that there was no hydrogen leak from the cylinder, polypropylene connection tubes and Swagelok compression fittings, a hydrogen gas detector was used. Initially, bubble testing was done but since this was not a continuous monitoring system, needed to be applied directly on the source, and did not measure the concentrations, a hydrogen gas detector was essential. The detector (Matheson IQ350) was based on solid state or electrochemical bead sensor that could measure hydrogen concentrations from 50 ppm to 5000 ppm. Before starting the experiment, all the

connections were checked with the detector. It was also kept near the experimental setup during all the experiments for safety purposes.

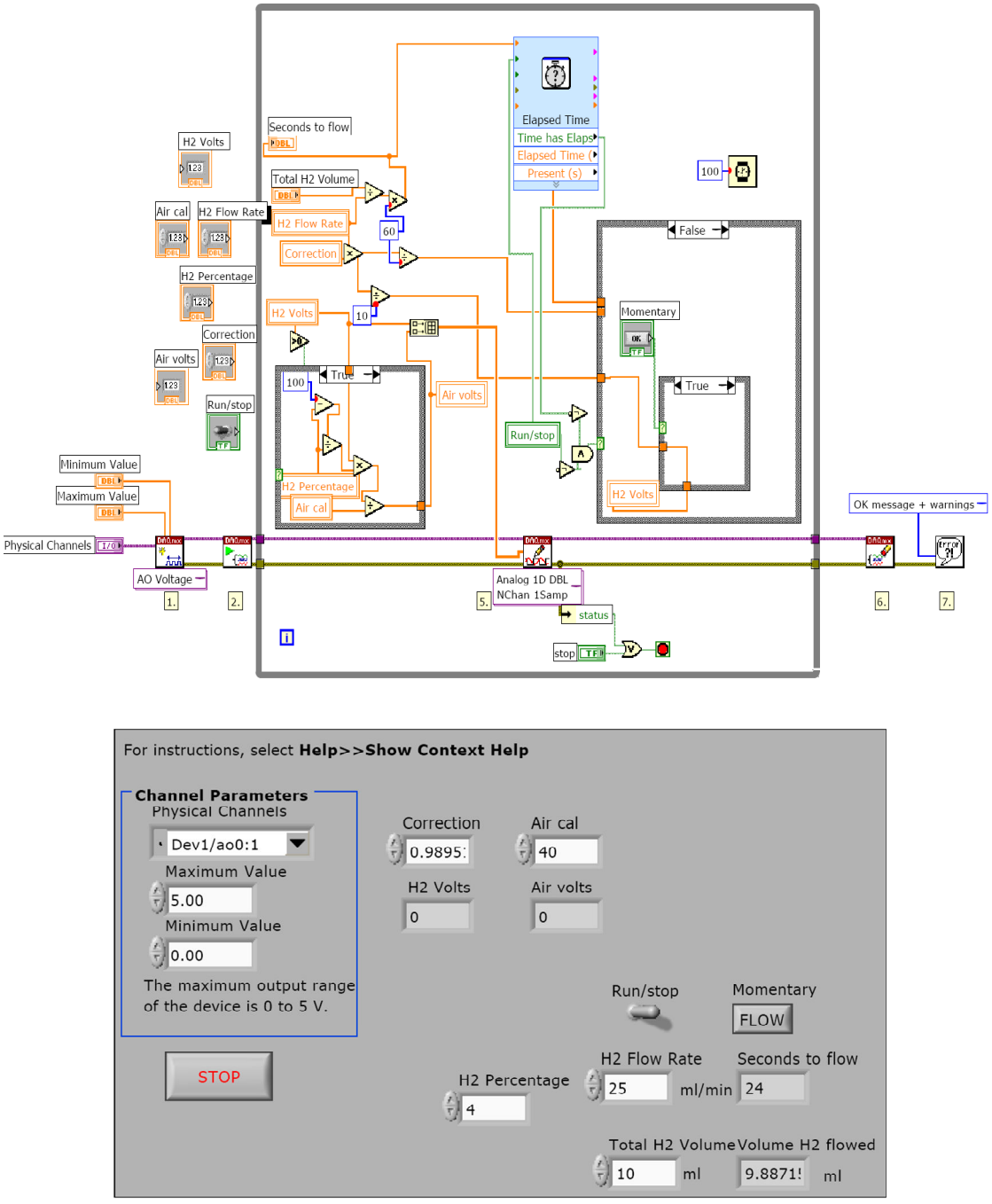

Figure 2.3. LabVIEW program (top: block diagram, bottom: front panel) used to control the mass flow rate of hydrogen and air

The experiment was conducted with hydrogen concentrations from 3% to 8% by volume in air. It was found that the mixture would not ignite below a hydrogen concentration of 5.5% (lower flammability limit), as shown in Table 2.3. When the mixture in the cylinder ignited, the hydrogen flame was almost invisible in the cylinder but as the flame propagated, the latex membrane got burst and the burning of the membrane gave color confirming the reaction. Since the cylinder was in the vertical position and hydrogen diffuses very fast in air, the local concentration of hydrogen at the bottom of the cylinder could be less than 5.5% and more than 5.5% near the top of the cylinder with a total average concentration of 5.5% in the cylinder when the ignition occurred. Due to this preferential diffusion of hydrogen, the local concentration of hydrogen near the spark plug was not known at the time of ignition and therefore the value of 5.5% observed as the lower flammability with this experiment might be questionable. To overcome this issue, the initial experiment was modified as shown in Figure 2.4.

Table 2.3. Hydrogen lower flammability limit based on the initial experimental setup

Source	**Lower flammability limit (% of Hydrogen)**	**Experimental set-up**	**Notes**
Missouri S&T: Experiments (2007)	5.5 (upward) average	Test tube: dia. 10.16 cm, length 19.3 cm (acrylic transparent tube)	Unknown effect of preferential diffusion

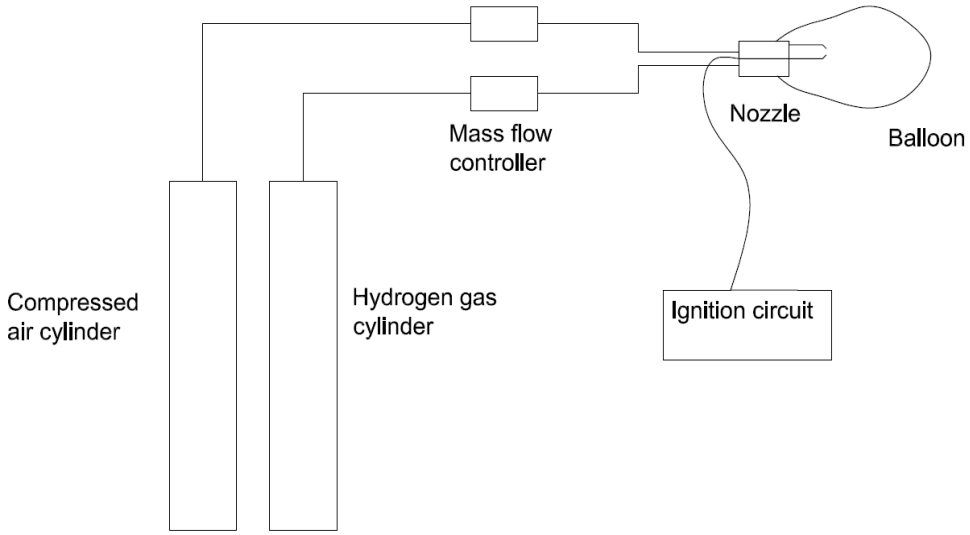

Figure 2.4. Schematic of the modified experimental setup used in the present study

In the modified experiment, instead of a vertical cylinder, a balloon was used to minimize the buoyancy effects and preferential diffusion/mixing of hydrogen within the container. The approximate diameter of the balloon just before ignition was 20 cm, containing a larger volume of hydrogen-air mixture than the initial experiment. Since the modified experiment had a larger mixture volume before ignition, heat transfer losses to the walls would be less. The minimum ignition energy of hydrogen in air at stoichiometric condition ($\Phi = 1$) is 0.02 mJ and at approximately $\Phi = 0.1$, the minimum ignition energy is 10 mJ, but in the initial experiment, the amount of energy supplied by the spark plug was not exactly known. Therefore, in the modified experiment, a custom made capacitor discharge ignition circuit (using $E = 0.5CV^2$, E = energy produced, C = net capacitance, V = voltage across the capacitor) was used to vary the ignition energy from 47 mJ to 686 mJ, providing more energy than required to make sure the limits measured were the flammability limits and not the ignitability limits. With the modified

experiment that was significantly improved and made nearly independent of experimental conditions, the lower flammability limit was found to be 4.5% concentration of hydrogen in air by volume as shown in Table 2.4.

Since the effect of preferential diffusion of hydrogen in air seemed to have a significant effect on the hydrogen concentrations in a vertical cylinder (from the initial experiment conducted), CFD tools were used later on (Section 3) to understand the transient mixing behavior of hydrogen in air and the formation of flammable envelopes in a vertical cylinder.

Table 2.4. Hydrogen lower flammability limit based on the modified experimental setup

Source	Lower flammability limit (% of Hydrogen)	Experimental set-up	Notes
Missouri S&T: Experiments (2007)	4.5	Balloon	~20 cm diameter before ignition

2.5. THEORETICAL ANALYSIS TO PREDICT LOWER FLAMMABILITY LIMIT

When a flame propagates, various processes cause energy to dissipate from the combustion wave and quench its propagation. Therefore, flammability limit occurs when the thermal energy produced by combustion of the limiting mixture is just equal to the energy dissipated. Considering a one-dimensional, constant area, laminar flame, the important processes that affect flame propagation in a tube and hence that are responsible for lower flammability limit are: (a) natural convection or buoyancy - this is especially important for hydrogen due its lowest molecular weight, (b) conduction and convection

heat transfer losses to the walls - important when observing lower flammability limit in small tubes as shown in Figure 2.5.

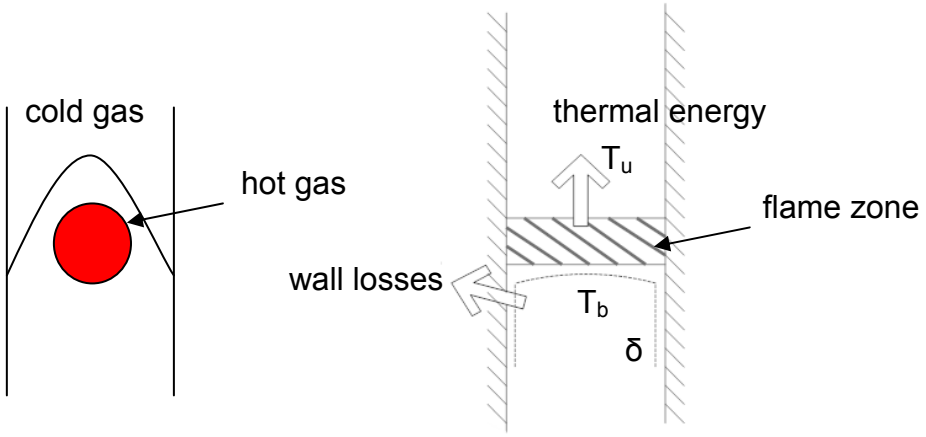

Figure 2.5. Schematic showing buoyancy effects (left) and heat transfer losses (right)

Considering only natural convection or buoyancy, the flame propagates into a velocity gradient that stretches it, so the limit in effect becomes the blow off limit due to buoyancy.

Kinetic energy change per unit volume across the propagating flame is given by

$$\Delta KE = \frac{1}{2}\rho_b S_b^{\,2} - \frac{1}{2}\rho_u S_u^{\,2} \tag{1}$$

Force produced due to combustion is given by $\dfrac{\Delta KE}{\Delta x} = \dfrac{\frac{1}{2}\rho_b S_b^{\,2} - \frac{1}{2}\rho_u S_u^{\,2}}{\frac{\alpha}{S_u}}$ (2)

where, S is the velocity and Δx is the flame thickness

Pressure gradient due to density difference is given by $(\rho_u - \rho_b)g$ (3)

Equating 2 and 3, and using the mass conservation, $\rho_b S_b = \rho_u S_u$, gives the limiting burning velocity as

$$(S_u)_l = \left(2\alpha g \frac{\rho_b}{\rho_u} \right)^{1/3} \tag{4}$$

By including the effect of flame stretch when a hot gas rises in a cold gas (Landau and Lifshitz, 1987) and assuming the flame temperature is 900 K (Kumar, 1985), the limiting velocity considering only buoyancy becomes:

$$(S_u)_l = \left(\frac{3}{8} \frac{\rho_u - \rho_b}{\rho_u + \rho_b} \alpha g \frac{\rho_b}{\rho_u} \right)^{1/3} = 4.38 \text{ cm/s} \tag{5}$$

Now, considering only the effect of conduction and convection heat transfer losses to the wall,

Energy produced per unit time per unit area is given by $S_u \rho_u C_p (T_b - T_u)$ (6)

Rate of heat loss due to cold walls per unit area is given by $\frac{k}{\delta}(T_b - T_u)$ (7)

From Equations 6 and 7, after multiplying with the appropriate area and including the effect of additional perimeter due to the boundary layer δ as shown in Figure 2.5 results in Equations 8 and 9.

$$S_u \rho C_p (T_b - T_u)\pi r^2 = \frac{k}{\delta}(T_b - T_u)2\pi r \Delta x(1+\beta) \tag{8}$$

$$=> \frac{(S_u)_l r}{\alpha} = \left[\frac{2}{\delta}(1+\beta)r\right]^{1/2} = 2.5 => (S_u)_l = \frac{0.0346}{r} \text{ cm/s} \tag{9}$$

Adding the effects of both buoyancy and heat transfer losses, the net limiting velocity becomes

$$(S_u)_l = \left(\frac{3}{8}\frac{\rho_u - \rho_b}{\rho_u + \rho_b}\alpha g \frac{\rho_b}{\rho_u}\right)^{1/3} + \left(\frac{2.5\alpha}{r}\right) \tag{10}$$

$$(S_u)_l = 4.38 + \frac{0.0346}{r} \text{ cm/s} \tag{11}$$

where r is the radius of the vessel (in m).

With the calculated limiting burning velocity from Equation 11 for a particular vessel, the equivalence ratio and hence the volumetric concentration of hydrogen can be calculated from the burning velocities vs. equivalence ratio graphs and equations provided by Liu and MacFarlane (1983). Figure 2.6 shows the variation of lower flammability limit value calculated from the above analysis and the experimentally reported values from literature. It shows that the lower flammability limit value approaches 4.5% as the diameter of the vessel increases - the value that would be obtained in free space. 4.5% was also the value obtained in this study with the modified experiment proving that the experimentally observed flammability limit was less dependent on the apparatus and thus representing the value that would be obtained in free space. This value of 4.5% has also been reported by Ciccarelli et al. (2006) who did

experiments in a larger vessel (diameter = 25.7 cm) compared to other studies and the mixture was thoroughly mixed with a fan before ignition to reduce the effect of preferential diffusion of hydrogen, again supporting the present conclusion that 4.5% is the true lower flammability limit value of hydrogen in air (by volume).

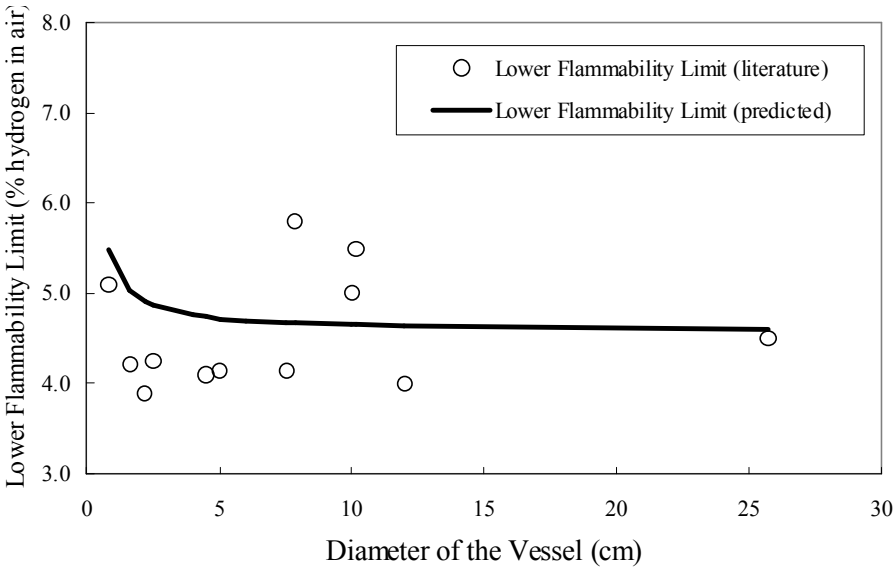

Figure 2.6. Variation of the lower flammability limit with diameter of the vessel

2.6. SUMMARY AND CONCLUSIONS

It was found from literature that the flammability limit values have remained as an empirical observation and dependent on the experimental setup used to observe these limits. Contradictory values of the flammability limits have been reported and the correlation between the flammability limits measured with various methods and the exact physical conditions that would occur in real accidents was not known. In this study, effort has been made to develop a simple ideal experiment to observe the lower flammability

limit of hydrogen in air that would be less dependent on the apparatus itself and support the result with a theoretical analysis.

Initially, a simple experiment was designed to observe the lower flammability limit of hydrogen in a vertical cylinder, but the effect of preferential diffusion of hydrogen and amount of ignition energy provided were not precisely known. The experiment was therefore modified with a custom-made ignition circuit and a larger mixture volume was collected in a spherical balloon. The lower flammability limit of hydrogen was found to be 4.5% after reducing its dependence on the apparatus itself as much as possible.

A theoretical analysis was done to predict the lower flammability limit of hydrogen considering the effect of the most important factors: natural convection or buoyancy and heat transfer losses to the walls. It was found that the lower flammability limit value was dependent on the radius of the vessel and approached a value of 4.5% as the diameter of the vessel increased. Thus, the concentration at which hydrogen would ignite in free space is 4.5%, a value consistent with the measurements conducted in this study.

This research will be important for understanding safety issues that need to be fully addressed by developing proper codes and standards that are critical for the design and operation of hydrogen-powered transportation vehicles.

3. DETAILED SIMULATIONS OF THE TRANSIENT MIXING, LEAKAGE AND FLAMMABILITY OF HYDROGEN IN AIR IN SIMPLE GEOMETRIES

3.1. INTRODUCTION

As discussed in detail in the previous section, there is an envelope (approximately 4% and 75% by volume) beyond which the hydrogen-air mixture can no longer be ignited as the hydrogen concentration decays in surrounding air during an unintended release. These lowest and highest concentrations below and above which flame propagation cannot be sustained are called lower and higher flammability limits. Hydrogen flammability limits and their implications on fire safety and prevention are important in many applications such as hydrogen-powered transportation vehicles, hydrogen fueling stations, storage facilities, pipelines and other supplementary infrastructure. Buoyancy-driven diffusion of hydrogen in enclosures is also of interest in such applications because hydrogen gas can disperse very quickly with its lowest molecular weight (Swain et al., 2003; Cisse and Karim, 2007). These properties can be used to avoid the formation of flammable mixtures after accidental hydrogen releases and to prevent further development towards hazardous concentrations (Dahoe and Molkov, 2007). Based on properties alone, hydrogen poses an increased risk primarily due to the increased probability of ignition. Note, however, that the increased buoyancy effects, which are relatively difficult to assess, might change this probability depending on the actual physical condition (Crowl and Jo, 2007).

There are reports on hydrogen simulations for predicting radiative heat fluxes and flammability envelopes for unintended release (Houf and Schefer, 2007) and accidental hydrogen release from pipelines (Wilkening and Baraldi, 2007). Studies on the dispersion behavior of hydrogen in urban and residential areas (Venetsanos et al., 2003; Schmidt et

al., 1999; Olvera and Choudhuri, 2006) and the design of passive ventilation systems for the safe use of hydrogen (Swain and Swain, 1996) have been conducted. Based on the previous research, dispersion in a confined area is recognized as one of the most dangerous scenarios (Matsuura et al. 2008). The dispersion behaviors of hydrogen and other traditional fuels like methane, ethane and propane in an open vessel were studied to highlight the differences among these fuels (Cisse and Karim, 2007). However, there are few past investigations on the transient behavior during the process of mixing of hydrogen at short times.

The present study focuses on the fundamental features of hydrogen transient dispersion for different cases in simple geometries that can be used as a benchmark problem for simulating more complicated and practical hydrogen release scenarios with complex geometries. Exploration of the details of the temporal and spatial distributions of hydrogen in air and the resulting flammability zones has implications in the safe practices for hydrogen delivery to fuel cells as well as the ventilation of hydrogen accidental leakage in closed and partially closed environments (e.g., parking garages, road tunnels, fuel cells, mobile hydrogen units). These simulations will also be useful for effective design of future experiments such as the deflagration experiments conducted by Groethe et al. (2007) on a 1/5-scaled road tunnel with hydrogen release from a fuel cell vehicle. Limited number of computational fluid dynamics (CFD) simulations is available on the consequence analysis and safety verification of hydrogen fueling stations (Shigeki, 2008). Results obtained in this investigation are expected to be utilized for developing the necessary fire safety codes and standards for hydrogen-powered transportation vehicles and for the prevention and safe handling of hydrogen fires and detonations.

3.2. GEOMETRY AND RELEASE SCENARIOS

3.2.1. Geometry. In the present work, different cases representing fundamental dispersion and leak phenomena are investigated within a vertical cylinder of 1 m height and 0.5 m diameter. Experiments conducted to find the transient dispersion behavior of hydrogen have the inherent problem of delayed or uncertain response times associated with the available hydrogen sensors (Matsuura et al. 2008; Shigeki, 2008; Jordan et al., 2007; Tanaka et al., 2007). Since the accurate predictions of formation and decay of flammable zones are difficult with experiments and theoretical hand calculations (Zhang et al., 2007), advanced CFD tools are used here after benchmarking with the already-available classical free jet decay scaling laws. These computations also provide deeper insight into the detailed hydrogen behavior with time. Two-dimensional simulations of the cylinder are performed here to capture important information instead of the complete 3-D simulations due to the prohibitive computer run time required by such simulations (Wilkening and Baraldi, 2007). This is deemed to be sufficient and accurate for the axisymmetric unit-length cylinder geometry.

In the following, three different release cases are studied to consider potential representative risk scenarios and relative effects of diffusion, buoyancy and jet momentum. The first case involves a small amount of hydrogen concentrated at the cylinder bottom in order to assess the effect of only buoyancy on mixing with the overlaying air. The second case induces a small hydrogen jet leak at the cylinder bottom in order to investigate the relative influences of buoyancy and momentum on mixing with the overlaying air. In the last case, the hydrogen is concentrated and leaked at the top of a closed cylinder which forces the lighter hydrogen to mix with heavier air underneath such

that concentration-driven diffusion and momentum-driven mixing work in the opposite direction to the gravitational force. In all the cases discussed below, the gravitational force acts in the downward direction.

3.2.2. Hydrogen Concentrated Near the Cylinder Bottom. Hydrogen is initially concentrated in the lower 10% volume of the cylinder with the remaining upper portion being air. At time t = 0 s, the hydrogen is released to allow mixing with the overlaying air in the absence of a momentum-forced jet. Figure 3.1 shows half portion of the axis-symmetric vertical cylinder enclosure considered in this study. Cases with different top conditions are studied: (a) the top of the cylinder is completely open to the outside atmosphere, (b) the top of the cylinder has a circular opening of 0.25 m diameter (half the diameter of the cylinder) at the center, and (c) the top of the cylinder is completely closed. These cases are considered to understand the similarities and differences regarding the mixing processes of hydrogen-air and the corresponding flammable zones in closed, partially open, and open geometries.

3.2.3. Small Hydrogen Leak at the Cylinder Bottom. Understanding the flammability envelope from a small-scale hydrogen leak and its transient dispersion properties is important for the safe use of hydrogen (Matsuura et al., 2008; Houf and Schefer, 2008). Consequently, small continuous hydrogen leaks from two different holes of diameters 2 mm and 10 mm at the bottom center of the vertical cylinder are also considered. Both these conditions yield laminar flows at the jet exits with Reynolds numbers of 1000 and 50, respectively. Relative to the previous pure concentration-driven dispersion case, the jet momentum will force the hydrogen flow upwards and consequently influence the unsteady fluid dynamics.

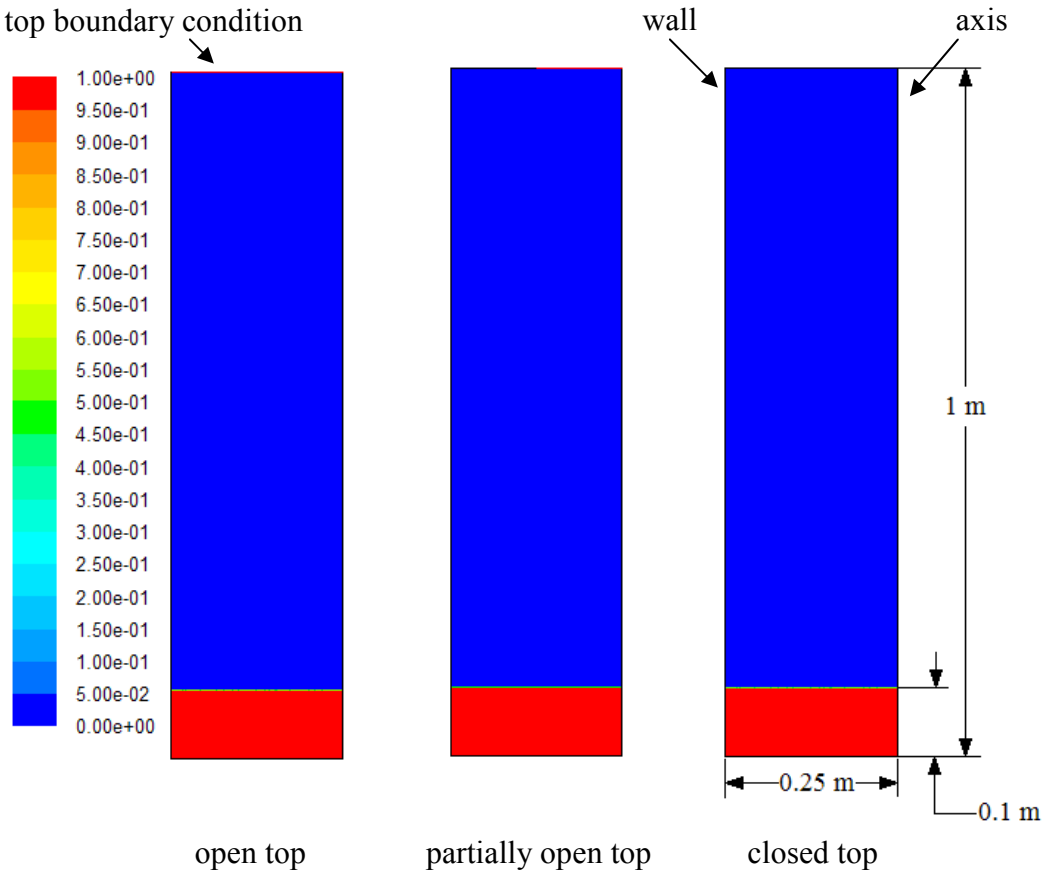

Figure 3.1. Geometry and initial mole fraction of hydrogen for three cylinder top conditions

3.2.4. Hydrogen Concentrated and Leaked at the Cylinder Top. Two additional cases, in which hydrogen accumulation/leak is at the top of the closed vertical cylinder, are explored. This is equivalent to reversing the direction of the gravitational force in the previous cases such that the effects of buoyancy relative to diffusion and momentum on the transient mass transfer process can be quantified. These cases may be relevant to possible accidental scenarios in practical applications where the hydrogen release is near the top of an enclosure.

3.3. COMPUTATIONAL MODEL

3.3.1. Governing Equations. For all the cases identified above, the complete set of transient equations for the conservation of mass, momentum and energy as well as the non-reacting transport equations (2 species – hydrogen and air) are considered as follows:

Mass conservation:

$$\frac{\partial \rho}{\partial t} + \nabla.(\rho \vec{V}) = 0 \tag{1}$$

Momentum equation:

$$\frac{\partial}{\partial t}(\rho \vec{V}) + \nabla.(\rho \vec{V}\vec{V}) = -\nabla p + \nabla.(\bar{\bar{\tau}}) + \rho \vec{g} \tag{2}$$

where $\bar{\bar{\tau}} = \mu\left[(\nabla \vec{V} + \nabla \vec{V}^T) - \frac{2}{3}\nabla.\vec{V}I\right]$ is the stress tensor.

Energy conservation:

$$\frac{\partial}{\partial t}(\rho E) + \nabla.(\vec{V}(\rho E + p)) = \nabla.\left(k\nabla T - \sum_j h_j \vec{J}_j + (\bar{\bar{\tau}}.\vec{V})\right) + \rho(\vec{V}.\vec{g}) \tag{3}$$

where $E = h - \frac{p}{\rho} + \frac{V^2}{2}$ and $h = \sum_j Y_j h_j$.

Species transport equation:

The conservation equation to predict mass fractions for the i^{th} species, Y_i, is given by:

$$\frac{\partial}{\partial t}(\rho Y_i) + \nabla.(\rho \vec{V} Y_i) = -\nabla.\vec{J}_i \tag{4}$$

Mass diffusion:

$$\vec{J}_i = -\rho D_i \nabla Y_i \tag{5}$$

Composition-dependent thermal conductivity and viscosity for multi-component mixtures are based on the kinetic theory, that is:

$$k = \sum_i \frac{X_i k_i}{\sum_j X_j \phi_{ij}} \text{ and } \mu = \sum_i \frac{X_i \mu_i}{\sum_j X_j \phi_{ij}} \tag{6}$$

where $\phi_{ij} = \dfrac{\left[1 + \left(\dfrac{\mu_i}{\mu_j}\right)^{1/2} \left(\dfrac{M_{w,j}}{M_{w,i}}\right)^{1/4}\right]^2}{\left[8\left(1 + \dfrac{M_{w,i}}{M_{w,j}}\right)\right]^{1/2}}$

A laminar flow analysis is used in this study for two main reasons. Earlier studies have clearly shown that turbulence models tend to overpredict mixing of gas released from slow leaks (Barley et al., 2007; Papanikolaou and Venetsanos, 2005) and that laminar analysis is more suitable for the purpose of safety engineering (Barley et al., 2007). Reynolds numbers at the leak exits were always low enough to be in the laminar regime while Rayleigh number, which is indicative of flow type in buoyant flows due to temperature difference, was also in the laminar or transition regime (~10^9).

3.3.2. Solution of the Governing Equations. The above equations are simultaneously solved using the advanced fluid dynamics software ANSYS FLUENT 6.3, which has been demonstrated to be suitable for analyzing buoyancy-driven flows (Shigeki, 2008; Jordan et al., 2007; Barley et al., 2007; ANSYS FLUENT, 2010; Prasad et al., 2008; Swain et al., 2007). A second order implicit scheme is used for the unsteady flow equations to obtain better accuracy (ANSYS FLUENT, 2010). The governing equations are solved sequentially (i.e., segregated from one another) using a segregated solver suitable for low speed incompressible flows. Because the governing equations are non-linear and coupled, the solution loop must be carried out iteratively in order to obtain a converged numerical solution. The standard SIMPLE algorithm (Versteeg and Malalasekera, 2007) is employed to effectively handle pressure-velocity coupling. To accommodate the highly diffusive nature of hydrogen in air, a fine mesh size (minimum size = 0.1 mm) and a small time-step (0.001 s) are used. About fifty iterations are performed at each time step for achieving convergence at every time step. Different grid sizes are tested to ensure that the simulations are independent of the grid size. During the computations, absolute convergence criterion for continuity, species and energy equation residuals are 10^{-5}, 10^{-5} and 10^{-6}, respectively, which are satisfactory for such flows. Stationary, no-slip and adiabatic wall boundary conditions are applied on the walls of the cylinder. When necessary, a pressure outlet (open to atmosphere) boundary condition is applied at the top boundary.

3.4. RESULTS AND DISCUSSION

3.4.1. Benchmarking the Computational Method. To obtain confidence in the modeling results, unignited free jets were simulated and compared with experimental data, correlations and simulation results obtained from the literature. For benchmarking, two cases of steady unignited incompressible turbulent free jets were considered: (1) air jet releasing into air from an orifice of 2 cm with *Re* = 13200 and (2) hydrogen jet releasing into air from an orifice of 2 cm with *Re* = 13200. The velocity and concentration decay along the axis (shown in Figure 3.2) are compared with classical decay scaling laws taken from experiments and simulations available in literature (Houf et al., 2009).

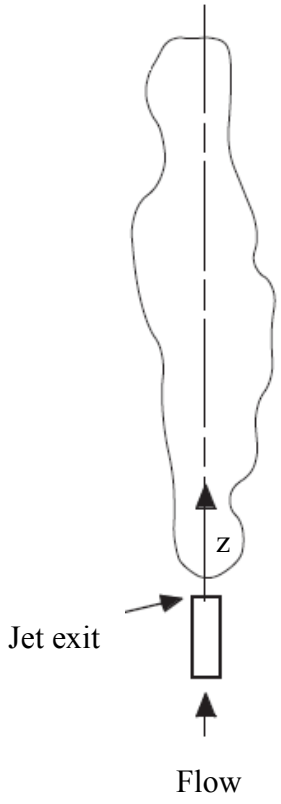

Figure 3.2. Schematic of free turbulent jet

3.4.1.1. Unignited incompressible turbulent air jet. The velocity decay scaling law for air jet releasing into air is given by Equation 7, where W_j is the jet velocity at exit, W_{cl} is the jet centerline velocity at axial distance z from the jet exit and d is jet or orifice diameter. C_1 and C_2 are constants that vary depending on the jet conditions, non-similar region of the jet, the turbulence model used, and discretization scheme used (Houf et al., 2009). Figure 3.3 shows the velocity decay profile of the air jet. It was found that the current study simulations shown by blue line are within the minimum and maximum ranges reported in the literature (Houf et al., 2009) and shown by red and green lines.

$$\frac{W_j}{W_{cl}} = \frac{1}{C_1}\left(\frac{z}{d}\right) + C_2 \tag{7}$$

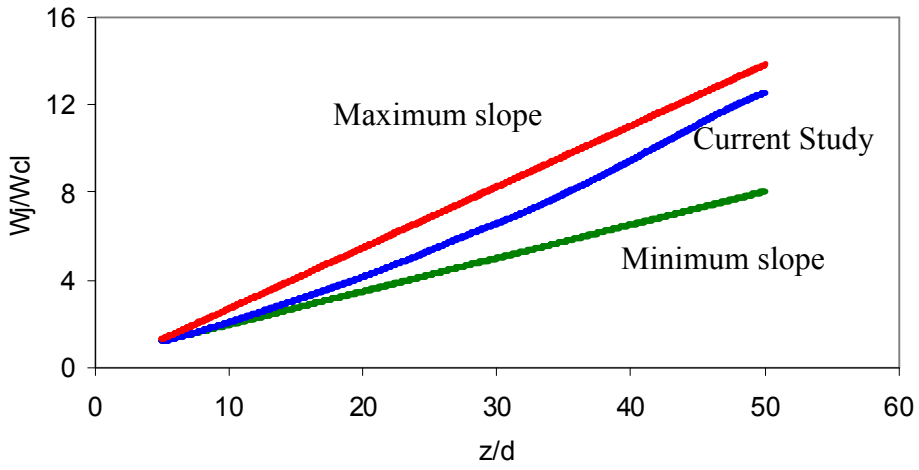

Figure 3.3. Air jet velocity decay profile in air

3.4.1.2 Unignited incompressible turbulent hydrogen jet. When the density of the jet (hydrogen) differs from that of the ambient fluid (air), the centerline velocity decay law is modified by replacing the jet diameter d with d^* as shown in Equation 8, where ρ_j is the density of the jet and ρ_{amb} is the density of ambient air. The classical velocity decay law is given by Equation 9. Similarly, the decay law for the centerline mole fraction is given by Equation 10 where d' is defined by Equation 11.

$$d^* = d\left(\frac{\rho_j}{\rho_{amb}}\right)^{1/2} \tag{8}$$

$$\frac{W_j}{W_{cl}} = \frac{1}{C_1}\left(\frac{z}{d^*}\right) + C_2 \tag{9}$$

$$\frac{1}{X_{cl}} = \frac{1}{C_4}\left(\frac{z}{d'}\right) + C_5 \tag{10}$$

$$d' = d\left(\frac{\rho_{amb}}{\rho_j}\right)^{1/2} \tag{11}$$

Figures 3.4 and 3.5 show the results of hydrogen jet velocity decay and concentration decay profiles, respectively. Again, the current simulations indicated by blue lines are mostly with-in the minimum and maximum ranges specified in the literature (Houf et al., 2009) and shown by red and green lines.

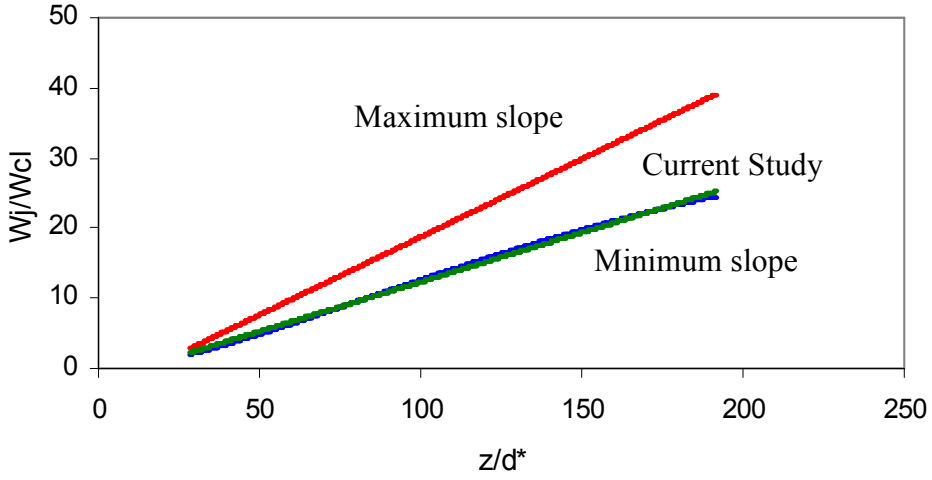

Figure 3.4. Hydrogen jet velocity decay profile in air

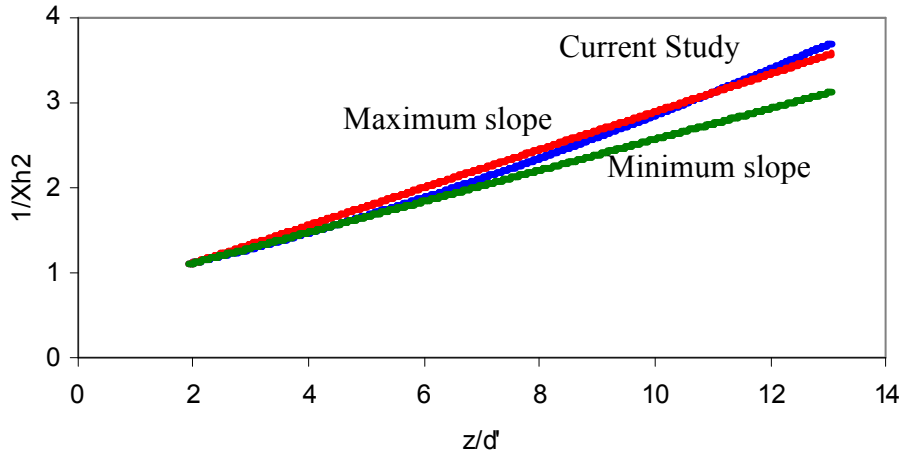

Figure 3.5. Hydrogen jet concentration decay profile in air

3.4.2. Hydrogen Release Near the Container Bottom. Initially, the lower 10 cm of the cylinder is filled with pure hydrogen, which is suddenly released at time $t = 0$ s and starts mixing with the overlaying air that occupies the top 90% (by volume) of the cylinder. Since hydrogen has high diffusion coefficient in air and very low density compared to air, it rapidly moves upward with the development of temporal and spatial

concentration distributions within the unit-length vertical cylinder. With the commencement of mass transfer, the flammable mixtures begin to form depending on axial and radial locations at a certain time.

3.4.2.1. Hydrogen concentration distributions. Hydrogen mole fraction contours for the open cylinder top are shown in Figure 3.6 at different time steps. The mixing process between these two gases with substantially different densities takes place by the combined effects of buoyancy and diffusion in the flow. The hydrogen concentration distribution depends on the convective mass transfer driven by buoyancy and molecular diffusion driven by local concentration gradients. At very short times (e.g. t = 0.1 s), hydrogen starts to disperse due to the local concentration difference where the distribution stays almost one dimensional in the axial direction. The buoyant force evidently assumes the predominant role after this initial time. As time progresses, hydrogen rapidly moves up, and its concentration decays from the initial high value forming a distribution that strongly depends on radial and axial positions across the cylinder. At these later times, the formation of small local pockets of higher hydrogen concentrations as well as the air entrainment to the lower cylinder portions along the centerline can be seen in Figure 3.6. Hydrogen covers nearly all the cylinder volume as it reaches the cylinder top at about t = 5 s. Such a short time for the hydrogen to begin escaping from the unit-length vessel is associated with the strong buoyancy effects driven by the large differential between the molecular weights of hydrogen (2 kg/kmol) and air (29 kg/kmol).

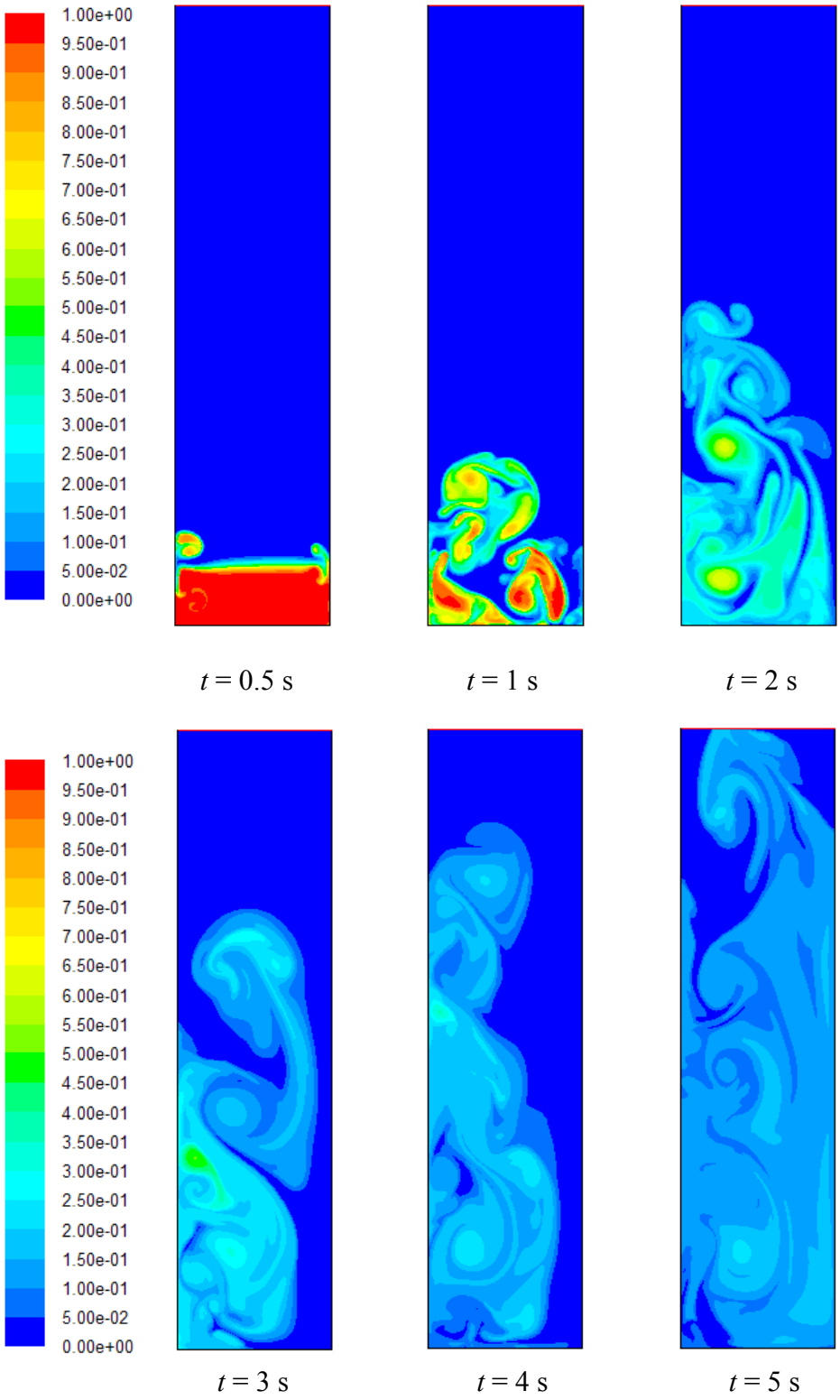

Figure 3.6. Hydrogen mole fraction contours for open cylinder top at different times

The present results are qualitatively similar to a recent study on hydrogen dispersion in an open-top configuration (Cisse and Karim, 2007). However, there are some quantitative differences noted during the computational simulations (Vudumu and Koylu, 2008) when the identical geometry and conditions given in (Cisse and Karim, 2007) are considered. For example, there is more than a factor of two difference between the computed times for the arrival of the hydrogen to the top of the cylinder. This is attributed to the formulation of the problem for this open-top vessel configuration as the complete set of governing equations is employed here while the Boussinesq approximation and associated equations were utilized in (Cisse and Karim, 2007). The density of hydrogen (0.08375 kg/m^3) is considerably smaller than that of air (1.23 kg/m^3), and therefore the validity and accuracy of this assumption is questionable when the density ratio is very small (0.068 for hydrogen/air). It should be emphasized that our simulations match almost exactly with those of (Cisse and Karim, 2007) for other fuels with densities close to that of air, e.g., ethane with a density of 1.26 kg/m^3 that corresponds to a density ratio of close to unity (1.024 for ethane/air).

Figures 3.7 and 3.8 display the hydrogen concentrations at different locations and times for a partially open and a closed cylinder top, respectively. Similar to the open top case, complicated concentration contours dependent on both radial and axial position are again observed. It is found that the static pressure for the closed top case decreases near the axis (about 0.5 Pa) and hence hydrogen rises somewhat faster near the axis. Similar effect of pressure on hydrogen concentration was also reported in (Matsuura et al., 2008). For the case with the open top, the outside pressure (near the top) is equal to ambient pressure (1 atm), and the static pressure within the cylinder is always positive along the

axis. Consequently, hydrogen upward movement in air is relatively slower in comparison to the closed top case. As can be clearly visualized for the closed top geometry in Figure 3.8, hydrogen reaches the top near the cylinder centerline at about 2 s. For the cylinder with partially open top (Figure 3.7), the rate at which hydrogen rushes to the top is in between that of open and closed top, as expected.

Hydrogen mole fractions as a function of the normalized height at two particular locations (at the axis and at the wall) at different times for the closed top cylinder are plotted in Figure 3.9. Within about the first 1.5 s, hydrogen rises faster along the cylinder axis compared to the near wall locations when there is no opening at the top (negative pressure gradient). Hydrogen first reaches to the top in about 2 s near the cylinder axis with mole fractions of approximately 0.3 at almost all heights along the axis. At this time, only a small amount of hydrogen exists at 0.2 m height near the cylinder wall. Hydrogen concentrations usually vary more along the wall compared to the centerline at a fixed time. The general trends for the other two top conditions were similar. For the partially-open and open top cases, the maximum volumetric concentration of hydrogen within the cylinder drops down to about 16% after only a short period of 7 s.

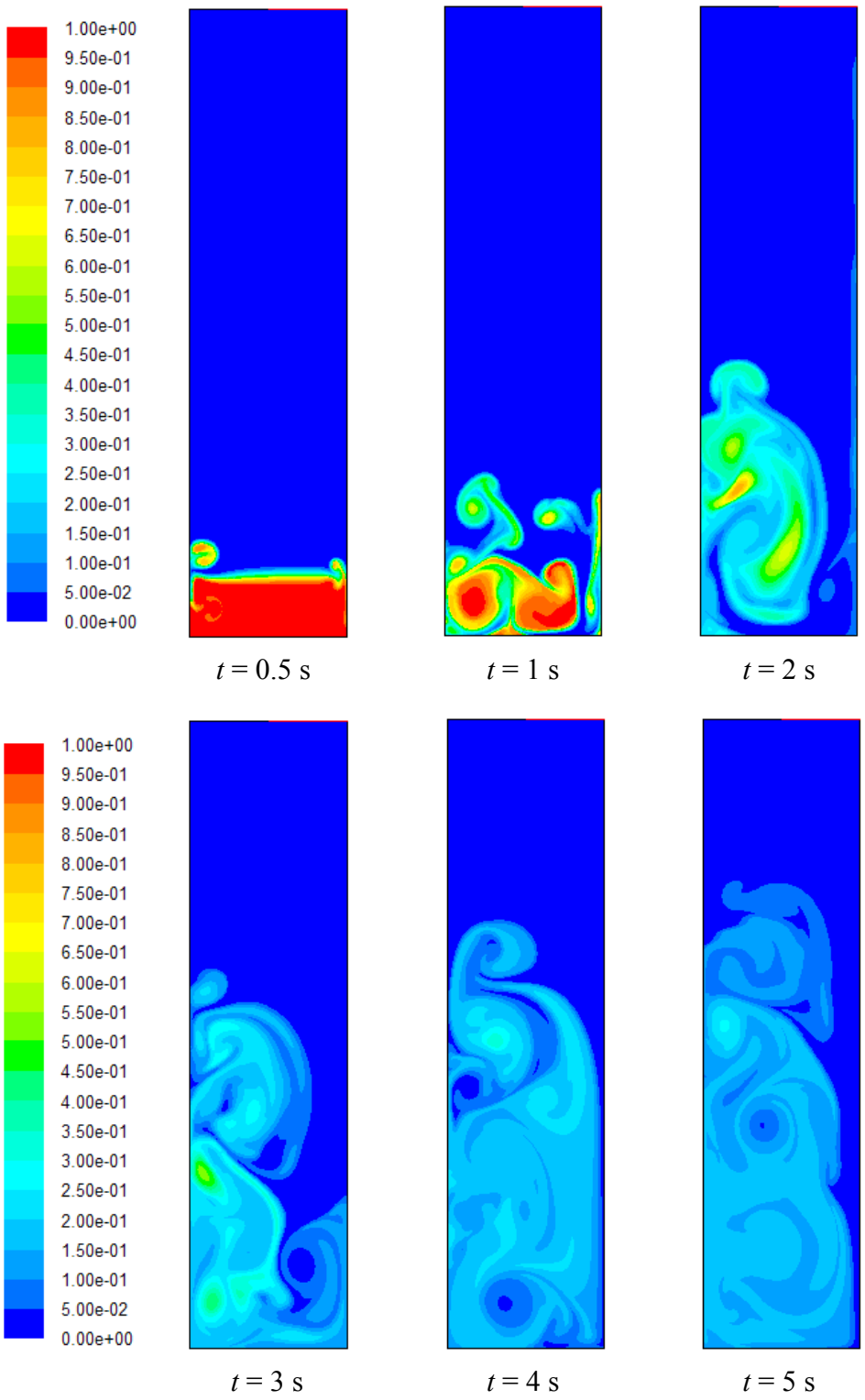

Figure 3.7. Hydrogen mole fraction contours for partially-open cylinder top at different times

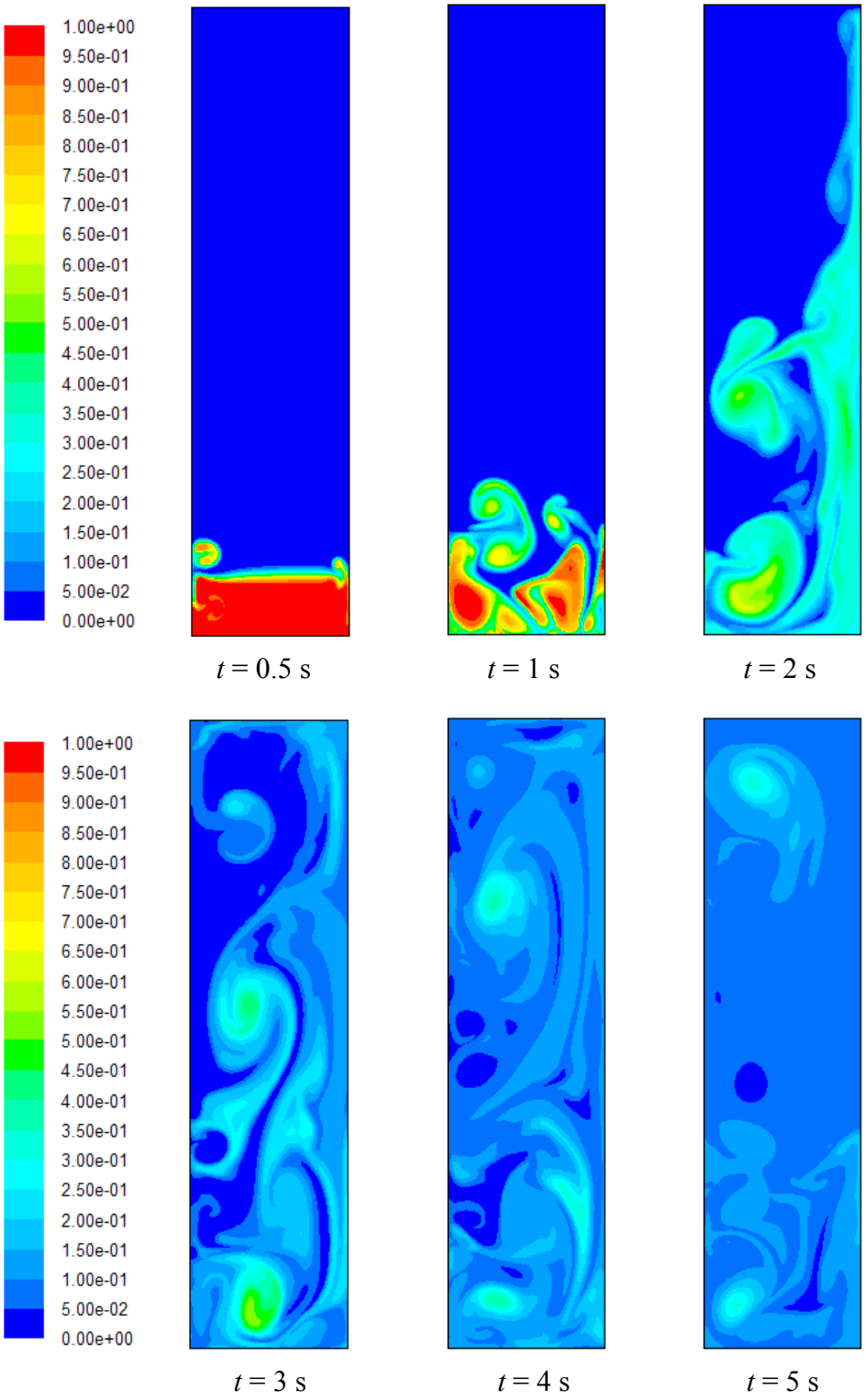

Figure 3.8. Hydrogen mole fraction contours for closed cylinder top at different times

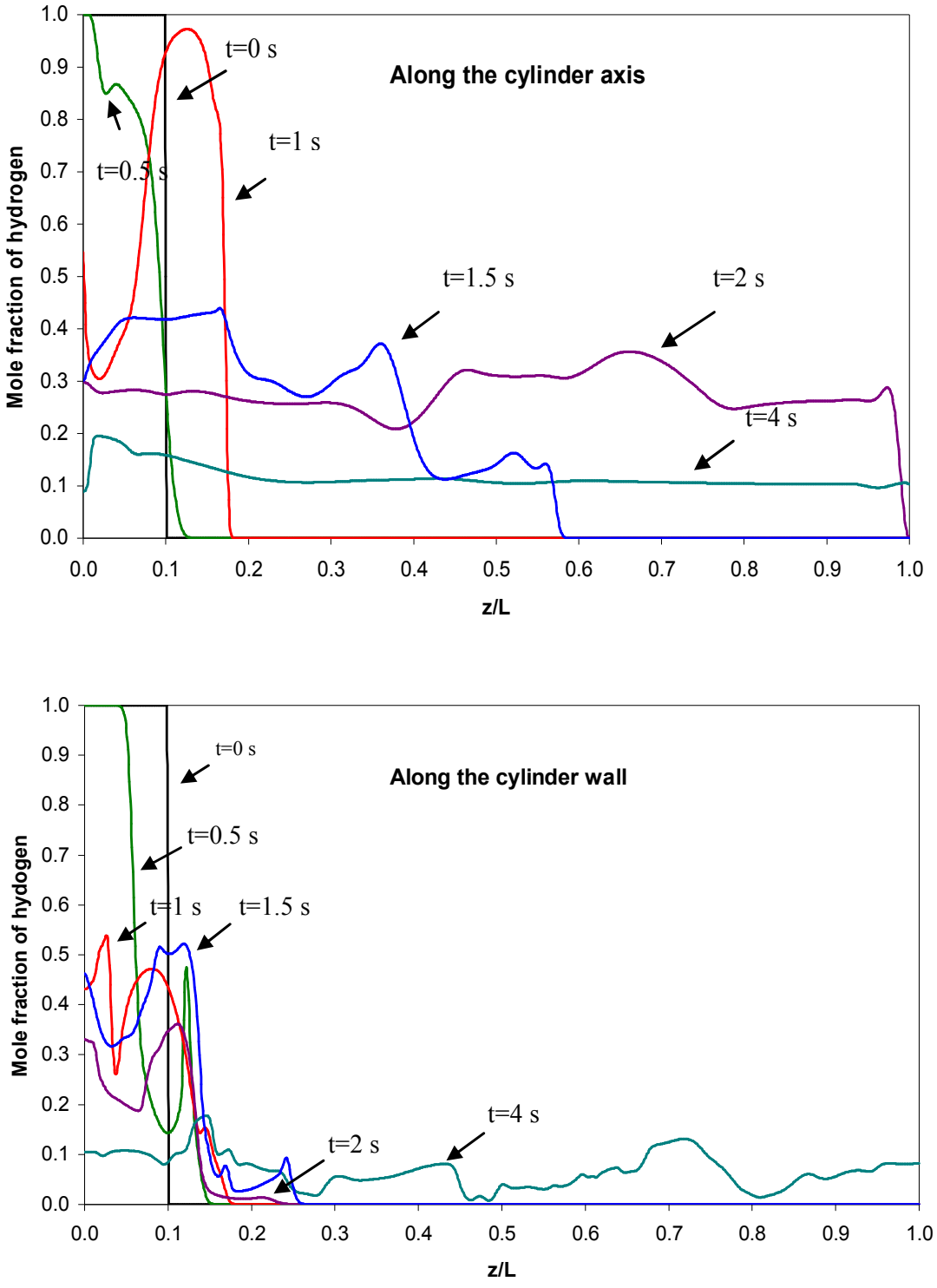

Figure 3.9. Mole fraction distributions near the axis and the wall for closed top at different times

3.4.2.2. Flammable regions. From the computed hydrogen concentration distributions for all three top conditions, important information related to fire detection and prevention can be obtained. For example, 1% hydrogen concentration by volume is usually sufficient to trigger many safety alarms in transportation and stationary applications, while a range of 4-75% hydrogen by volume potentially creates a flammable mixture with a fire safety risk. Accordingly, constant 1% hydrogen mole fraction contours and flammability envelopes are explored for all the three cases considered. The transient formation and growth of 1% hydrogen concentration and flammable regions within the cylinder are demonstrated at two typical times of t = 2 s and t = 3 s, respectively, in Figure 3.10. Islands of non-flammable conditions within the vessel are obvious with unsteady and non-uniform concentration distributions across the cylinder. The hydrogen concentration reaches 1% near the axis of the cylinder exit in about 2 s after its release for the semi-open and closed top conditions. As explained before, hydrogen rises faster when the vessel is completely closed with no interactions with the outside atmosphere. Despite a small amount of hydrogen release (10% by volume), flammable zones quickly cover a large portion of the container because of the relatively wide flammability limits. For the closed top case, hydrogen is distributed more uniformly throughout the vessel after a few seconds when the mass transfer due to diffusion will again play a more dominant role.

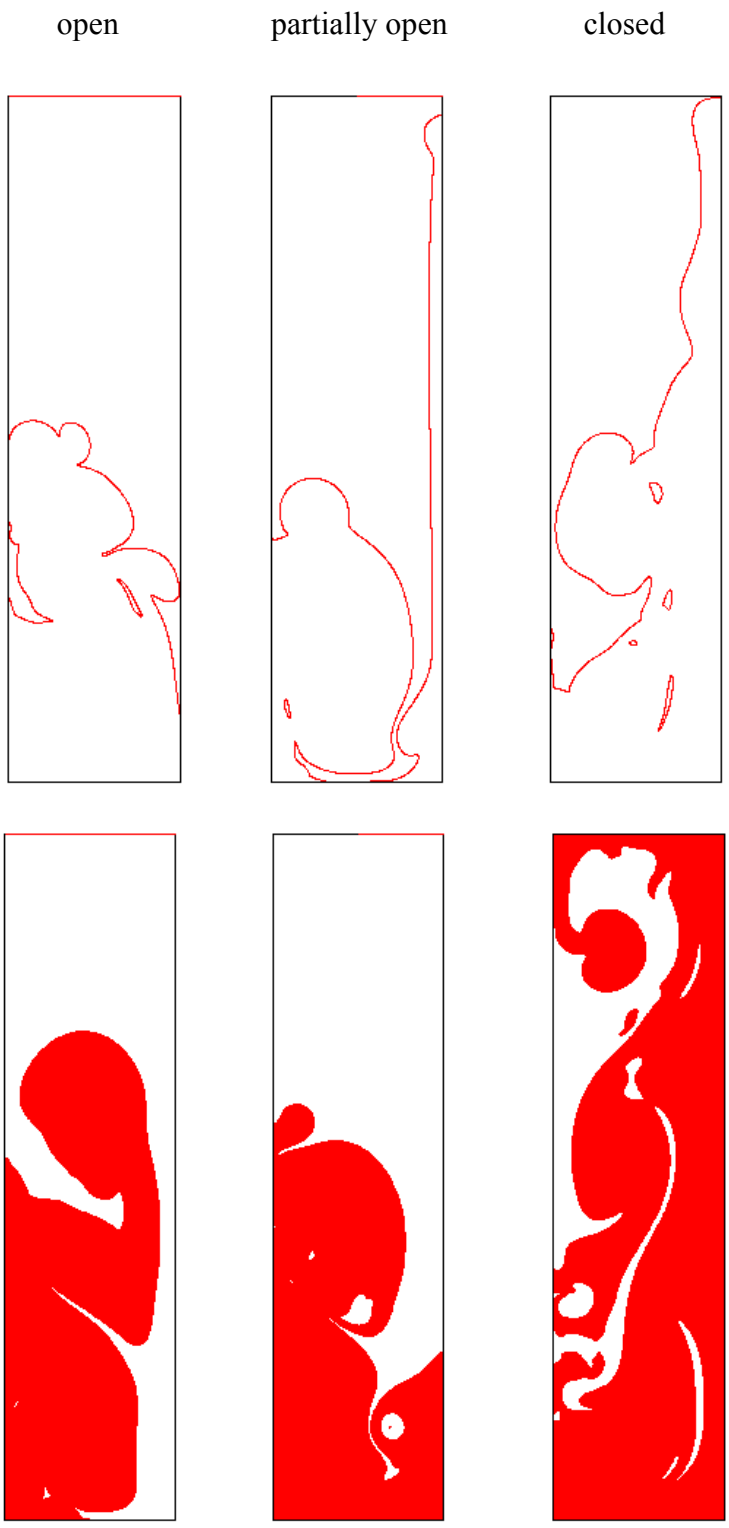

Figure 3.10. Constant 1% hydrogen mole fraction (above) and flammability envelope (below) for the three cylinder top conditions considered at t = 2 s and 3 s, respectively

The above results have various safety implications in practical applications involving the accidental releases of hydrogen gas. The simple axisymmetric cylinder geometry with three different top conditions considered here presents a basic model that may help explore more complicated features of real structures, especially the transient hydrogen behavior immediately after an accidental release. Some examples include hydrogen rises (and other relatively light gases) in air in open atmosphere, road tunnels, ventilated garages, and storage enclosures. The present computations quantify how fast hydrogen arrives at the top of a unit-length container and forms flammable mixtures at different axial and radial locations, even in the absence of the momentum of a jet. For the open and partially-open top configurations, the first emergence of hydrogen out of the cylinder into the open atmosphere in a few seconds is relevant to the estimation of evacuation times in larger size compartments. For the closed top condition, hydrogen fills up the container with dangerous flammable mixtures again within a very short period of time, emphasizing the importance of proper ventilation and/or sufficient storage volume during the design of hydrogen systems. From a detection perspective, it may be better to install hydrogen sensors near the geometrical symmetry where hydrogen may rise faster. Naturally, extremely quick upward movement of hydrogen dictates the required response time from detection units. The observation that the hydrogen reaches the cylinder top fastest for the closed top configuration (almost twice faster compared to the open top condition) suggests a potentially more effective hydrogen removal system: instead of having a continuous ventilation at the top of an enclosure (e.g., garage), install a safety alarm near symmetry axis that triggers not only the sound but also the ventilation opening.

3.4.2.3 Flow patterns. In order to demonstrate the flow dynamics of the hydrogen dispersion in air, the computed velocity vectors (colored by velocity magnitude, m/s) are displayed in Figure 3.11 for the open top case at a time of 2 s after the hydrogen release near the bottom is initiated. As discussed before, hydrogen moves up at a faster rate near the axis than near the wall for the closed top cylinder. This slowing down of velocity near the wall is due to the no-slip condition with the effects of viscous forces. A complex flow field can be seen from this typical figure with significant spatial variations in the velocity magnitudes and directions at a fixed time. The presence of flow circulation is associated with the concentration contours that depend on both the axial and radial positions and the small pockets of higher concentrations (as shown in Figures 3.6-3.8).

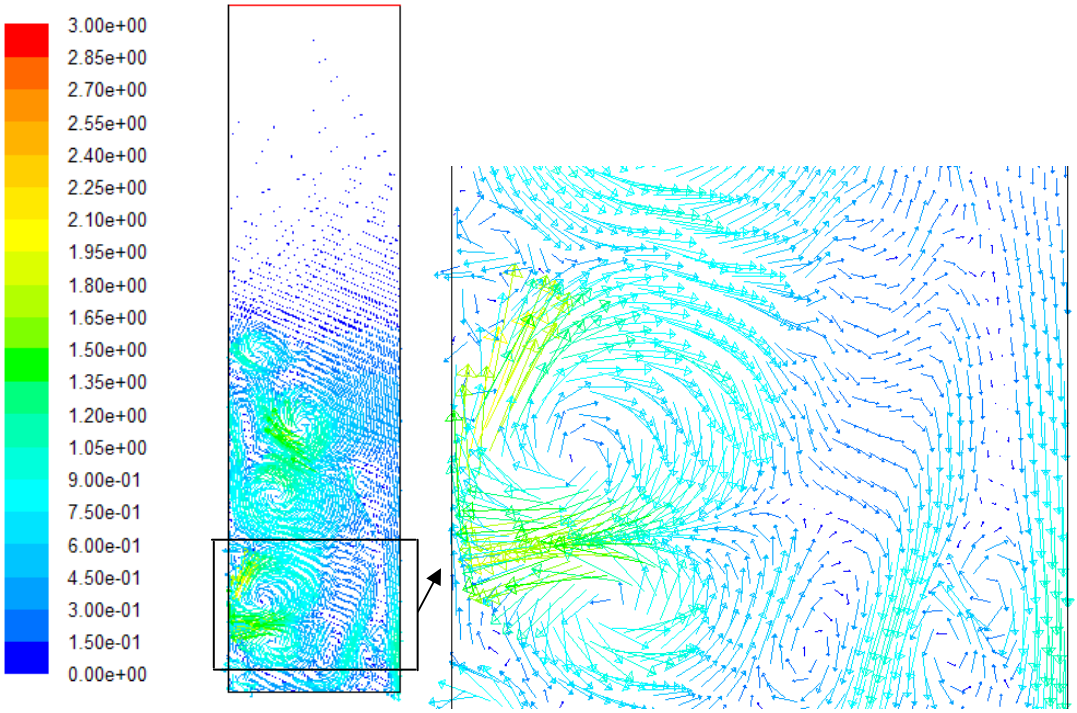

Figure 3.11. Velocity vectors colored by velocity magnitude (m/s) for the open top case at $t = 2$ s (with enlarged view)

3.4.3 Comparisons of Transient Mixing Behavior of Different Fuels. For the open top case, transient mixing behavior and spatial distributions of fuel in the overlaying air are also studied for methane-air and ethylene-air and compared with that of the hydrogen-air. The results at t = 2 s are shown in Figure 3.12. As the fuel density increases and gets close to the air density (Table 3.1), the upward movement of the fuel slows down. When the fuel density is similar to air density, mixing process is extremely slow, and the spatial distributions and hence the resulting flammable envelopes are significantly different compared to hydrogen-air. As can seen in Figure 3.12 for ethylene, which has a nearly identical density to air, the dispersion can be treated as almost one dimensional with nearly negligible radial and axial mixing.

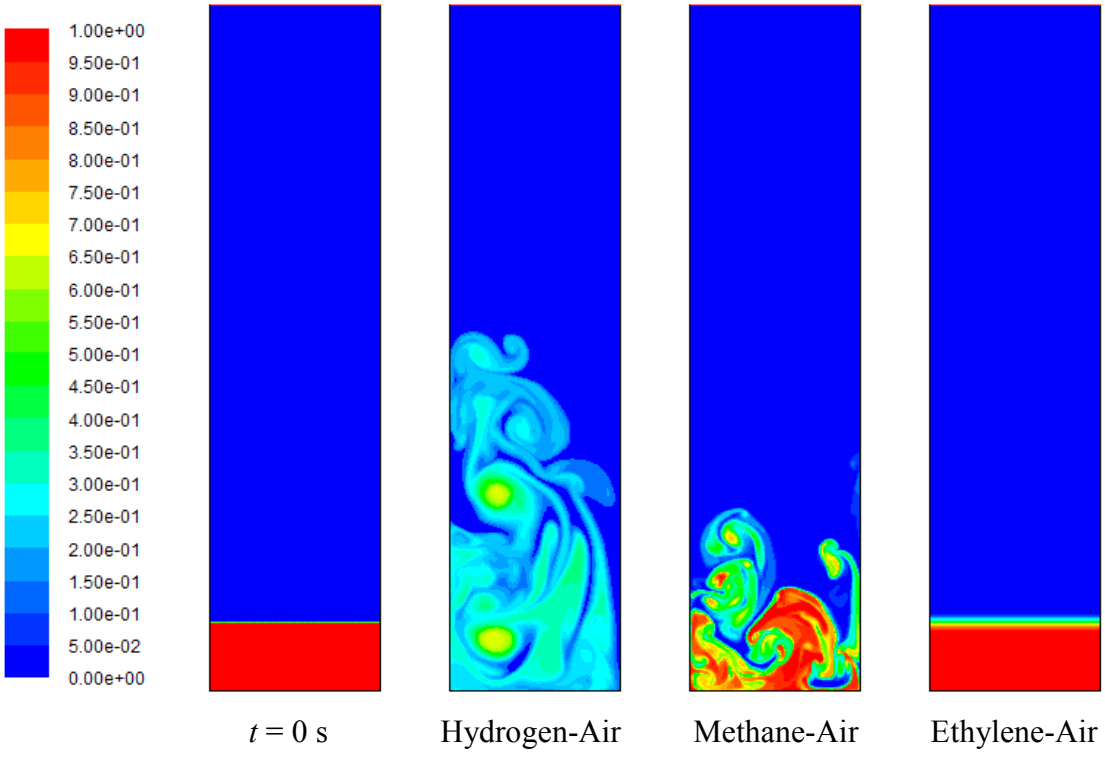

Figure 3.12. Mole fraction contours for the open top case at t = 2 s for hydrogen-air, methane-air and ethylene-air

Table 3.1. Comparisons of fuel densities at standard conditions

	Hydrogen	Methane	Ethylene
Fuel density (kg/m^3)	0.085	0.680	1.178
Fuel density relative to air density (1.202 kg/m^3)	0.071	0.566	0.980

3.4.4. Hydrogen Over Air. To evaluate the relative effects of buoyancy and diffusion on the mixing of hydrogen and air, another configuration in which hydrogen is initially above the air in the closed cylinder is also considered. This is equivalent to reversing the direction of gravitational force in the previous case discussed before or viewing the problem upside down. The unsteady mixing characteristics of this hydrogen-over-air case are shown in Figure 3.13. The penetration of the hydrogen concentration to the lower portions of the container is very slow with small axial concentration gradients developing near the interface of both fluids and very little dependence on radial location. This slow and one-dimensional dispersion is in clear contrast to the earlier case where the air is on top of the hydrogen. Consequently, when the density ratio of gases is very small, the mixing process is driven mostly by molecular diffusion if the lighter gas is on top. Such cases with negligible influence of buoyancy can be practically represented by a quasi-steady and 1-D approximation.

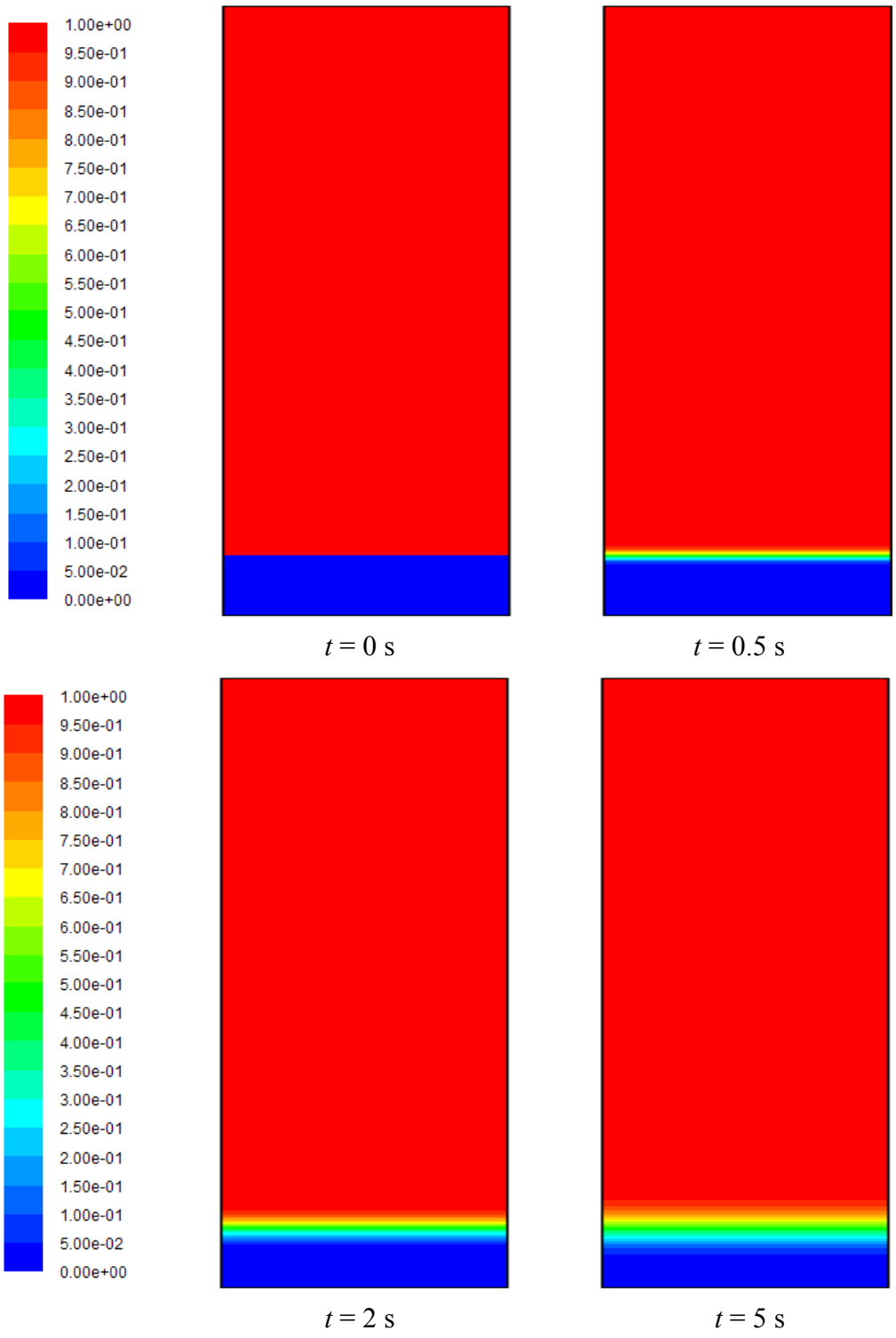

Figure 3.13. Hydrogen mole fraction contours for hydrogen over the air case at different times

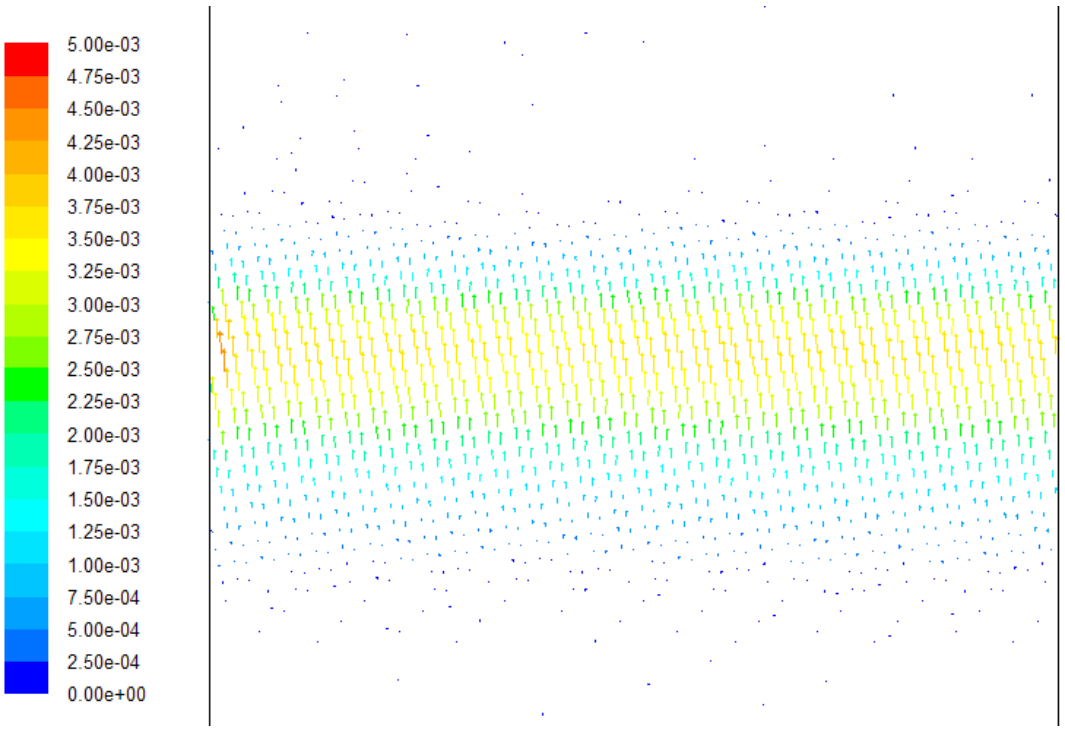

Figure 3.14. Velocity vectors for the hydrogen over air case (magnified near the interface) at t = 3 s

A typical velocity field is illustrated in Figure 3.14 near the interface of hydrogen and air after 3 s hydrogen at the top of the cylinder is released into the air underneath. As can be seen, the velocity vectors near the interface of two fluids are very small and perfectly aligned in the vertical direction. These results confirm that buoyancy is typically the controlling parameter for the previous cases where the air is initially above the hydrogen.

3.4.5. Small Hydrogen Leaks at the Container Bottom. The above computations involve cases where either natural convection or molecular diffusion is important. A more realistic scenario in practical applications is the unintentional small

hydrogen leak in which the momentum of the flow out of a storage tank becomes relevant as an additional forced-convection effect. Accordingly, for the same vertical closed cylinder geometry, two new cases with small continuous hydrogen jets issued at the bottom center are also investigated: (a) 2-mm-diameter hole with a hydrogen exit velocity of about 50 m/s, and (b) 10-mm-diameter hole with a hydrogen exit velocity of about 0.5 m/s. Non-dimensional parameters corresponding to these flow conditions are: (a) Reynolds number of Re = 1000 and a Richardson number of $Ri = 10^{-4}$ at the exit of the first leak with the larger velocity, and (b) Re = 50 and Ri = 5 at the exit of the second jet with the larger leak diameter. As a result, both leaks are laminar at the jet exits while the flow is changed from a momentum-dominated one in the first jet to another in which buoyancy is more important compared to the jet inertia in the second jet.

Hydrogen mole fraction contours at different time steps for the first jet with smaller leak diameter and higher velocity is shown in Figure 3.15. Hydrogen concentration is confined to a very small region near the cylinder centerline until it hits the closed top with the jet momentum and buoyancy working together in the same direction of the flow. The first arrival of hydrogen at the cylinder top is less than 1 s, after which a stagnation point is formed that causes radial flow movement and concentration distribution (see t = 5 s). With no escape route in this enclosure, hydrogen then flows downwards and starts occupying the entire cross section of the cylinder at a very slow rate, also generally described in (Swain et al., 2003). While there are some variations in the radial direction, the concentration contours become nearly parallel with the emergence of uniform distributions.

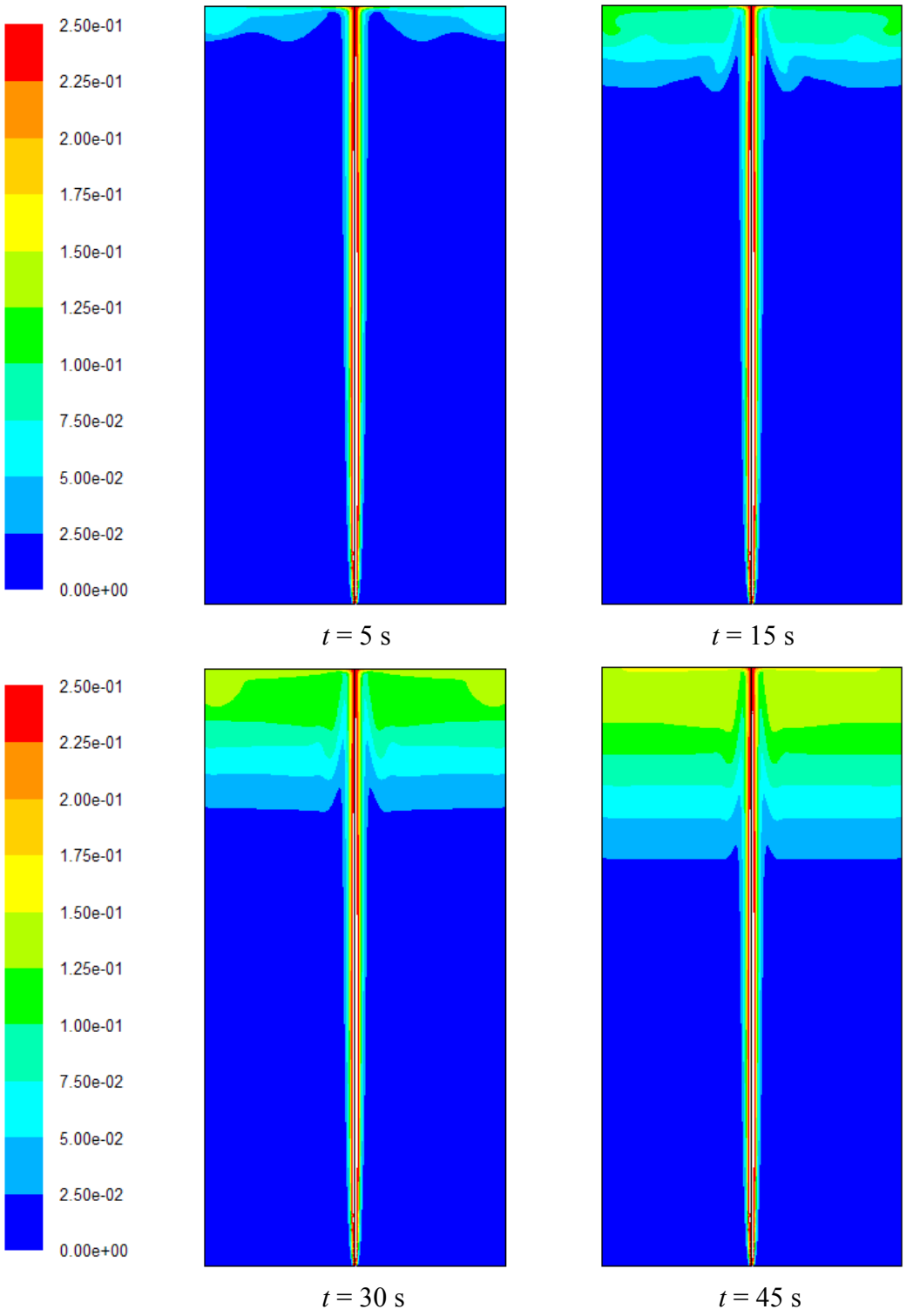

Figure 3.15. Hydrogen mole fraction contours at different times for a 2-mm-diameter leak at the cylinder bottom with *Re* = 1000

These trends are consistent with the flow field in Figure 3.16, which illustrates the magnitudes and directions of gas velocities near the bottom and the top of the cylinder at 30 s. The velocity vectors in the enlarged view of the cylinder corner are mostly aligned in the vertical direction as hydrogen begins to slowly move down. This is in contrast to the velocity field in Figure 3.11 but similar to the one in Figure 3.14, indicating that the molecular diffusion takes over the mixing process once the jet momentum is lost to the top wall and the flow turns in the same direction of the gravitational force. These observations are again a result of the fact that hydrogen has a very low density compared to that of air.

The flammable mixtures are restricted to a very narrow region along the axis at all times and to the complete cylinder cross section as hydrogen accumulates near the top. The flammable regions increase in a one-dimensional manner as time goes by. Similar results were reported for the transient behavior of hydrogen and the process of accumulation (Matsuura et al., 2008; Barley et al., 2007). For the present conditions, only about 25% of the cylinder in the upper axial locations is filled with a flammable mixture of hydrogen and air 45 seconds after the hydrogen is issued into the container while the remaining lower portions are mostly pure air. The development of flammable zones can be seen from Figure 3.17 to be even slower for the second jet with a larger diameter and lower jet exit velocity. For this case, the mass flow rate of hydrogen entering the container is 0.0033 g/s, four times less than the value for the first jet, while the jet exit momentum is 400 times less. Accordingly, almost the entire container volume, except a very thin region along its axis, stays non-flammable with hydrogen concentrations smaller than 5% until about 120 s. The increase in cylinder pressure is generally

negligible (less than 0.05 Pa) with a small change (around 0.5 Pa) at the point where the jet impinges on the top wall.

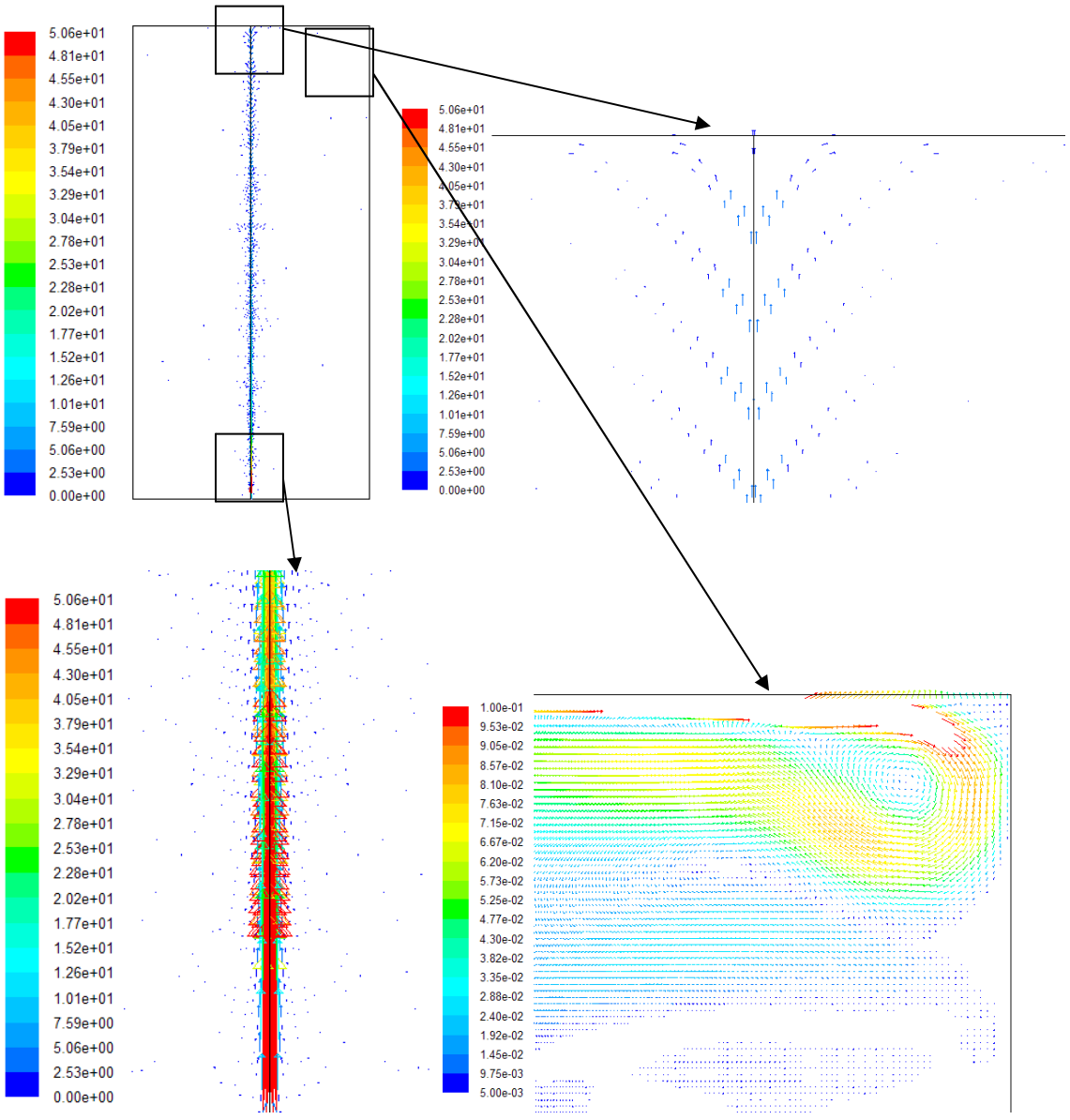

Figure 3.16. Velocity vectors colored by velocity magnitude (m/s) for the leak at the cylinder bottom with Re = 1000 at t = 30 s (with enlarged view near the bottom and the top of the cylinder)

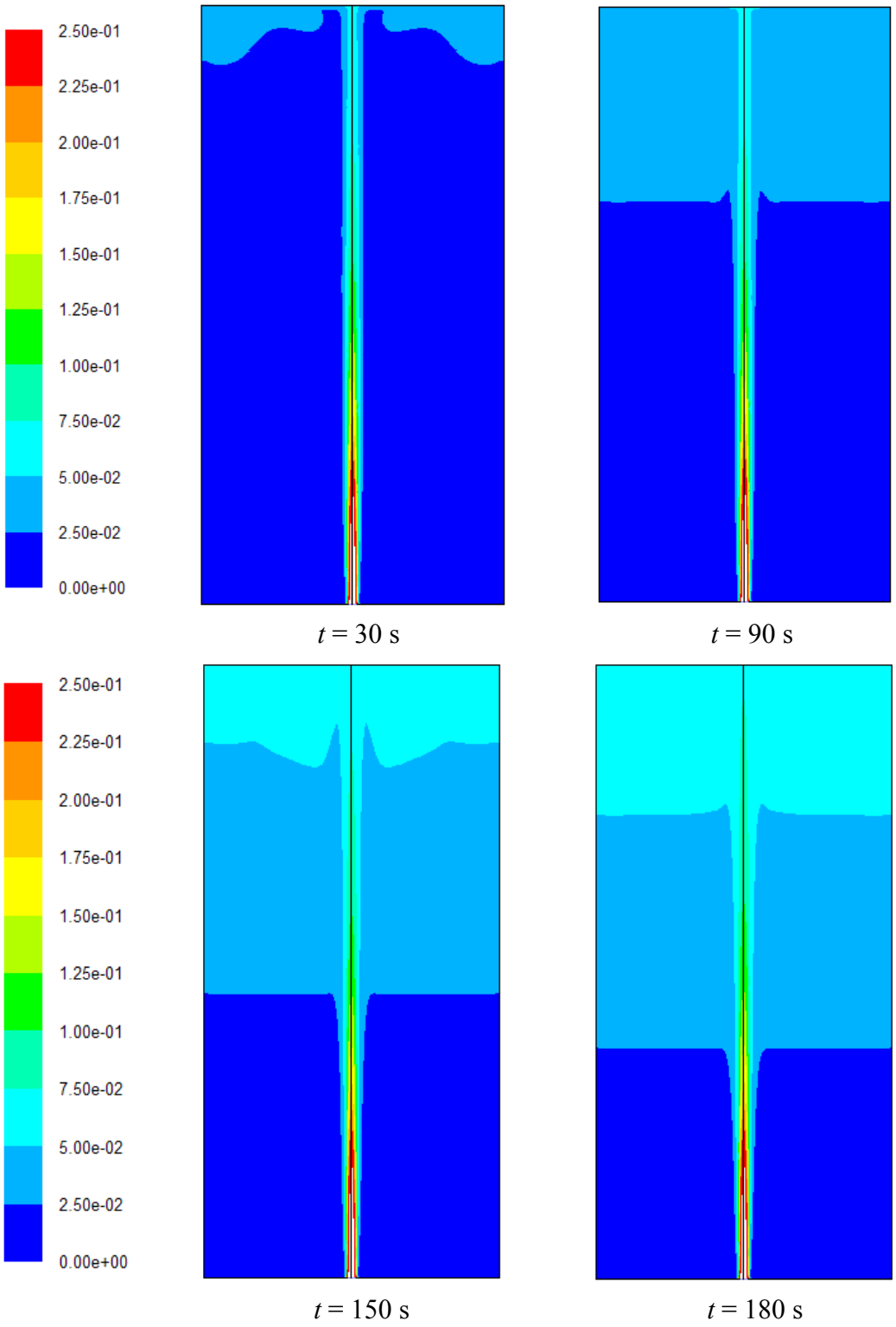

Figure 3.17. Hydrogen mole fraction contours at different times for 10-mm-diameter leak at the cylinder bottom with $Re = 50$

These results confirm the common consensus that, for testing hydrogen leak in a closed room, the gas detector should be placed near the top of the room where there is more probability of flammable hydrogen to accumulate. For reducing fire and explosion hazards in more complex geometries, adequate natural or forced ventilation should especially be provided in these areas. More importantly, the present computations quantify the escape time for occupants in accidental releases of hydrogen within enclosures while there is a dependence of container volume, leak size and flow rate, and geometry. About 45 s and 180 s after the initiations of the two small leaks considered here, only less than a quarter of the container near the top contains flammable hydrogen/air mixture. This implies that the occupants during a possible hydrogen accidental release in an enclosed area may have substantially more time, typically on the order of a minute (depends on the geometry), to escape underneath the gas accumulation near the ceiling. In contrast, a traditional fuel leak accumulates near the lower escape routes with a gas density similar to that of air and forms flammable mixtures typically within a few seconds and hence less time to escape.

3.4.6. Reverse Hydrogen Leak at the Container Top. The small hydrogen leaks at the cylinder bottom consist of conditions in which both buoyancy and jet momentum help hydrogen rise faster. The transient process of hydrogen behavior and accumulation depends on the relative position of leak with respect to the enclosure. Here, an extreme case in which hydrogen jet is at the cylinder top is considered. In particular, the 2-mm-diameter leak with Re = 1000 that is reported in Figure 3.15 is issued downwards from the top this time. Figure 3.18 shows the computed hydrogen flammable regions for these conditions. For this case when the jet momentum is initially in the opposite direction of

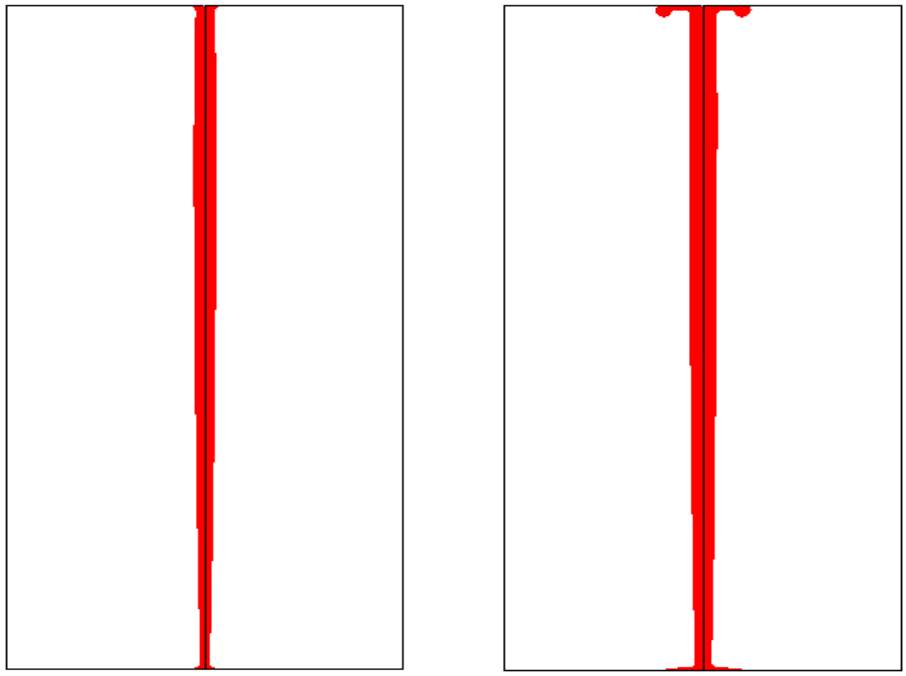

$t = 0.5$ s

$t = 1$ s

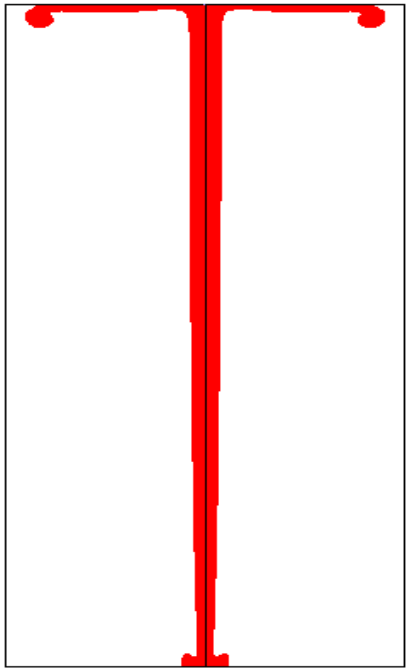

$t = 3$ s

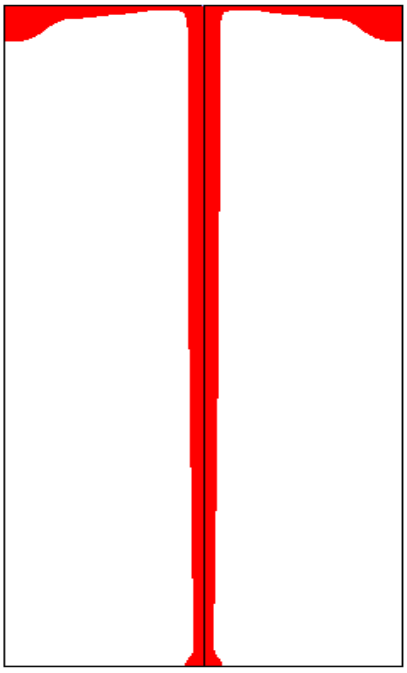

$t = 5$ s

Figure 3.18. Hydrogen flammability envelope at different times for a 2-mm-diameter leak at the cylinder top with $Re = 1000$

buoyancy force, the flammable regions beyond the symmetry line still begin to form near the enclosure top after about 1 s. The hydrogen concentration stays below the lower flammability limit of 4% in most of the cylinder volume except a limited region near the axis and the top. These results demonstrate that the hydrogen comes back up fast along the release in the vertical direction even if the leak is downwards, still causing the accumulation to occur near the higher container regions.

3.5. SUMMARY AND CONCLUSIONS

A comprehensive understanding of the transient behavior of hydrogen mixing and the associated flammability limits in air at short times is essential to support the fire safety and prevention guidelines. The present study focuses on the fundamental features of hydrogen transient dispersion for different cases within a unit-length vertical cylinder that can be used as a benchmark problem for simulating more complicated and practical hydrogen release scenarios with complex geometries. The computational parameters are varied so that the flow conditions are controlled by either buoyancy or molecular diffusion or jet momentum.

When hydrogen disperses into the overlaying air, the mixing process is dominated by buoyancy due to the low density of hydrogen, and the concentration distribution strongly depends on both radial and axial location. If hydrogen is over the air, the mixing process is generally by slow molecular diffusion due to local concentration difference with very little dependence on radial location.

When the mixing is buoyancy controlled, hydrogen rapidly moves up. For the closed top container, hydrogen moves twice faster near the axis compared to the open top

case due to decrease in pressure along the axis when the cylinder is completely closed. This observation suggests to install a safety alarm near symmetry axis that triggers not only the sound but also the ventilation opening instead of a continuous ventilation at the top of an enclosure (e.g., garage).

When investigating hydrogen leakage from the cylinder bottom into the same configuration, the flow conditions are varied from a momentum-dominated one to another in which buoyancy is relatively more important compared to the jet inertia. With no escape route in this enclosure, after hitting the container top, hydrogen flows downwards and starts occupying the entire cross section of the cylinder in a one-dimensional manner at a very slow rate. With times on the order of a minute after the initiations of small jet leaks, only less than a quarter of the container near the top contains flammable hydrogen-air mixture. This implies that the occupants during a possible hydrogen accidental release in an enclosed area may have substantially more time unlike other traditional fuel leaks that would accumulate near the lower escape routes because of relatively high density and less buoyancy.

When the leak is downward at the top of the container (jet momentum and buoyancy force are in the opposite directions), the flammable regions beyond the symmetry line still begin to form near the enclosure top. Hydrogen comes back up fast along the release in the vertical direction, still causing the accumulation to occur near the higher container regions. These results show that, for testing hydrogen leak in a closed room, the gas detector should be placed near the top of the room where there is more probability of flammable hydrogen accumulating.

4. HIGH-PRESSURE HYDROGEN LEAK FROM A STORAGE TANK

4.1. INTRODUCTION

In general, leaks can be categorized as buoyancy-driven (small leaks) or momentum-driven (large leaks). In Section 3, the transient hydrogen mixing and flammability in air in simple geometries for small buoyancy-dominated leaks have been investigated. Because of its low density, hydrogen is often compressed to high pressures for storage in hydrogen fueling stations, hydrogen-powered vehicles, and other industrial applications. While there exist many studies in the literature on small hydrogen leaks, very few studies are available on the unsteady fluid dynamics behavior of momentum-dominated hydrogen leak from a high-pressure storage tank (Schefer et al., 2007) that is important for the safety risks associated with catastrophic failures. Those limited studies have mainly focused on approximate methods to investigate the fluid dynamics of such high-velocity leaks. Thus, the present work focuses on a high-pressure hydrogen leak from a storage cylinder in a typical mobile hydrogen unit (MHU) used in hydrogen fueling stations. There are two objectives of this study. First, the applicability of the widely-used effective diameter approach developed for high-pressure gas leaks to hydrogen safety analysis will be assessed. Second, the transient mixing behavior of a high-pressure hydrogen leak into air and the resulting flow field in the MHU will be investigated. This analysis will be helpful in evaluating the ventilation design of mobile hydrogen units and other hydrogen fueling stations in the extreme cases of catastrophic failures of hydrogen storage tanks/valves due to unexpected accidents.

4.2. UNDEREXPANDED FREE JET

When a high-pressure leak occurs, the exit flow chokes at the sonic velocity if the pressure ratio across the leak is greater than the critical pressure ratio (the pressure ratio which will accelerate the flow to a velocity equal to the local velocity of sound, approximately 1.89 for hydrogen). At pressure ratios higher than this critical value, the exit velocity remains sonic, when Mach number is unity, $M = 1$ (Schefer et al., 2006; Schefer et al., 2007). For such a supercritical release, the flow leaves the exit to form an underexpanded jet as shown in Figure 4.1. The sonic flow at the exit of the leak is accelerated to supersonic speeds by the Prandtl-Meyer expansion fans. As the flow proceeds downstream, the atmospheric constant-pressure boundary redirects the discrete expansion waves towards the centerline as a series of compression waves. These compression waves coalesce to form an oblique shock known as the barrel shock as shown in the figure. This barrel shock, which separates the inner jet core from the outer sheath of supersonic fluid, terminates at the Mach disk (Ewan and Moodie, 1986; Woodmansee and Lucht, 1999; McDaniel et al., 2002). As seen in Figure 4.1, Mach disk is a normal and slightly curved shock, and the downstream condition after the Mach disk is subsonic. It is worth to note that such an underexpanded free jet is also used to produce a rarefied, hypersonic flow for a model test section to perform tests on the reaction control system (RCS) that provides the flight control of an aerospace vehicle to maintain its trajectory (McDaniel et al., 2002).

Numerical solution of the underexpanded region near the leak is computationally intensive because it requires very fine mesh densities (Houf et al., 2009). To overcome this difficulty of numerically solving the details of the underexpanded jet, alternative

approaches have been suggested by Schefer et al. (2007), Ewan and Moodie (1986), Birch et al. (1984), Birch et al. (1987), and Winters and Evans (2006) by considering the same mass flow rate of the leak that would be released from a larger effective diameter at ambient conditions. These approaches avoid the calculation of supersonic expansion between the sonic condition at the jet opening and the eventual subsonic flow downstream in the ambient. The schematic of the effective diameter approach is illustrated in Figure 4.2.

The applicability of the effective diameter approach for hydrogen safety analysis is not available in literature. In this study, two most commonly-used effective diameter approaches suggested by Birch et al. (Birch et al., 1987) and Winters et al. (Winters and Evans, 2006) were compared with the complete detailed underexpanded jet analysis for a high-pressure steady-state hydrogen free jet releasing into ambient air. The high-pressure leak considered here was from a tank with a stagnation pressure of 485 bar (7034 psi), a stagnation temperature of 283 K, and an actual leak diameter of 0.0127 m (0.5 inches).

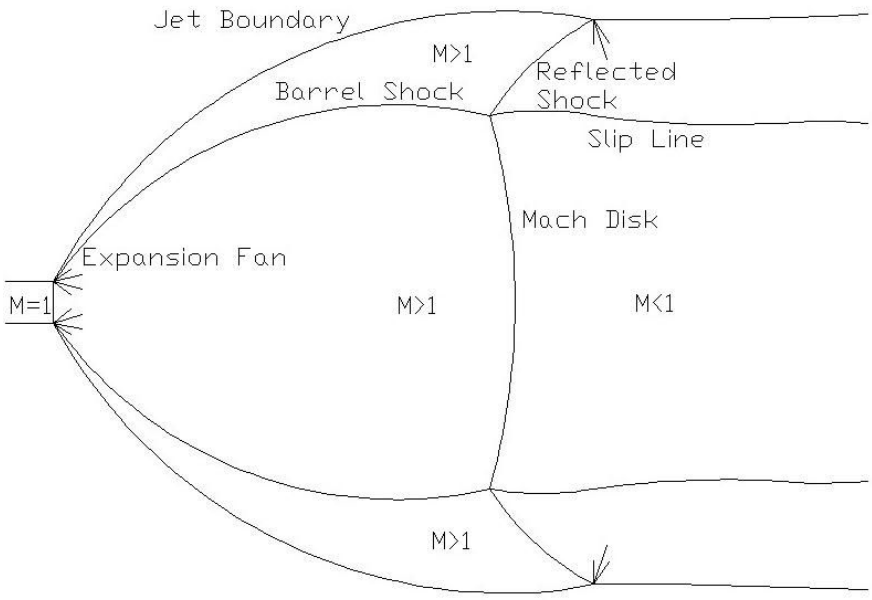

Figure 4.1. Schematic of an underexpanded jet (McDaniel et al., 2002)

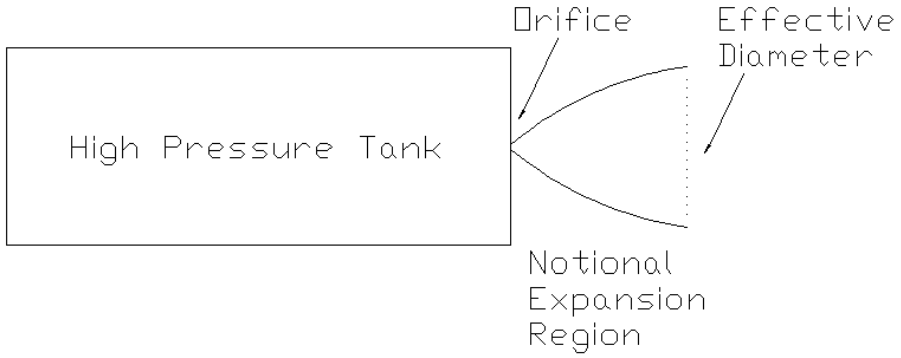

Figure 4.2. Schematic of the effective diameter approach

4.2.1 Geometry and Computational Model. An axis-symmetrical domain of 1.27 m (50 inches) length and 0.635 m (25 inches) radius was considered to study the fluid dynamics behavior of the underexpanded free jet in detail. The ambient conditions were 1.01 bar and 298 K. Steady-state equations for the conservation of mass, momentum, and energy as well as the non-reacting transport equations (two species, hydrogen and air) were solved using a commercial CFD software (ANSYS FLUENT, 2010). The two-equation standard $k-\varepsilon$ turbulence model (Launder and Spalding, 1972; Woodmansee and Lucht, 1999; ANSYS FLUENT, 2010) was used to account for the turbulent flow conditions. Mass flow inlet boundary condition was used for the inlet while pressure outlet (open to the ambient) boundary condition was used around the circumference and at the open end. Second order upwind discretization was employed to obtain better accuracy. Grid independent study was completed to ensure that the results were independent of grid size.

4.2.2. Results and Discussion. The steady-state results for the above-mentioned leak condition using detailed underexpanded jet analysis and two effective diameter approaches are presented and discussed in the following. Birch et al. approach employs an effective diameter of 0.1334 m (5.25 inches) with a Mach number of 1.8 whereas Winters at al. approach employs an effective diameter of 0.3355 m (13.21 inches) with a Mach number of 0.389 at the leak location instead of the actual leak diameter of 0.0127 m (0.5 inches) with sonic condition (M = 1) as used in the detailed analysis. It is important to note that both the effective diameter approaches assume the larger effective diameter to be at the actual leak location instead of a small distance (ten to twenty times the actual leak diameter) downstream (Winters and Evans, 2006).

Figure 4.3 shows the Mach number contours on the same scale of 0 to 9 for all three figures. The underexpanded jet analysis indicated the formation of Mach disk (seen clearly in the enlarged view) similar to the schematic shown in Figure 4.1. The Mach number of the flow increases smoothly from $M = 1$ at the exit to $M = 8.79$ just before the Mach disk and became subsonic downstream. Since Birch et al. and Winters et al. effective diameter approaches use a larger diameter than the actual leak diameter, their flows had much lower velocities as seen in Figure 4.3. The Mach number variations along the axis and along the radial direction at an axial location of 1.27 m (50 inches) are shown in Figure 4.4. The sudden drop in Mach number from $M = 8.79$ to $M = 0.3$ due to the Mach disk occurred at an axial distance of approximately 0.18 m from the leak location for the present underexpanded jet analysis. The Mach number along the axis was almost constant when an effective diameter was used, $M = 1.8$ and $M = 0.4$ for Birch et al. and Winters et al. effective approaches, respectively. At locations away from the axis, the drop in Mach number could also be seen in Figure 4.4. Because of the presence of the inner jet core and the outer sheath of supersonic fluid (also seen in Figure 4.3), the underexpanded jet analysis yielded a small increase in Mach number and then a gradual decrease as moved away from the axis. Using the effective diameter approaches, the Mach number gradually decreased to 0 from their respective values at the axial location ($M = 1.8$ and $M = 0.4$ for Birch et al. and Winters et al., respectively).

Present Study (2010), detailed underexpanded jet analysis

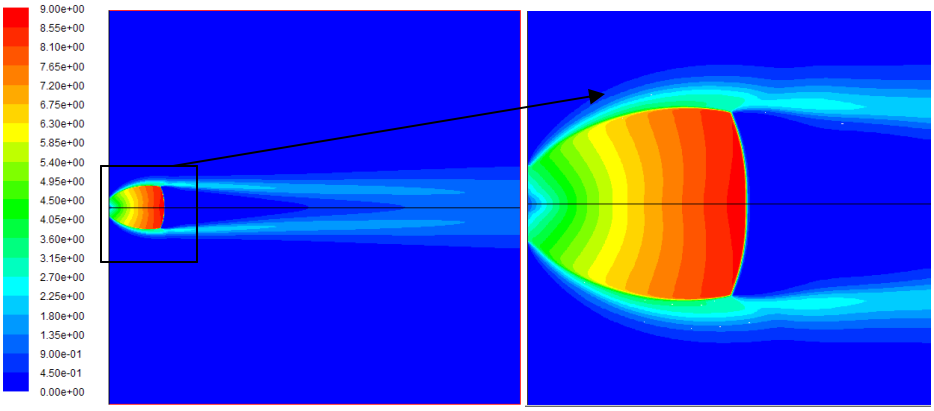

Birch et al. (1987), effective diameter approach

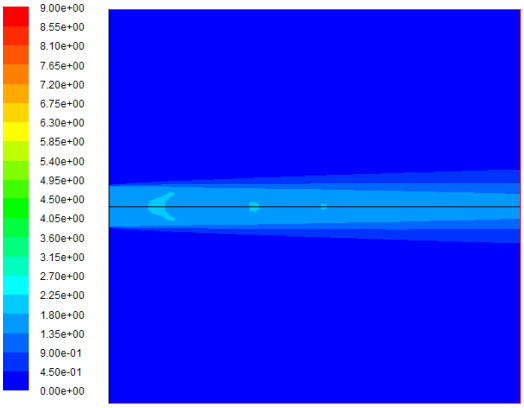

Winters et al. (2006), effective diameter approach

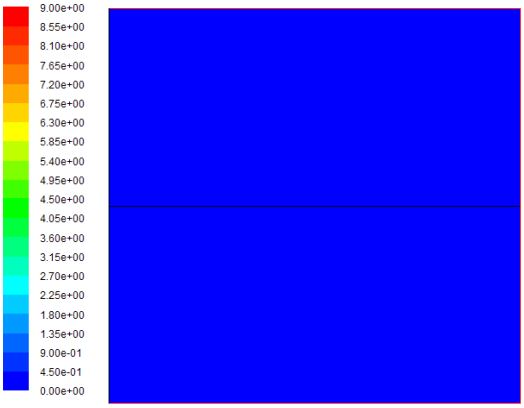

Figure 4.3. Mach number contours using various approaches

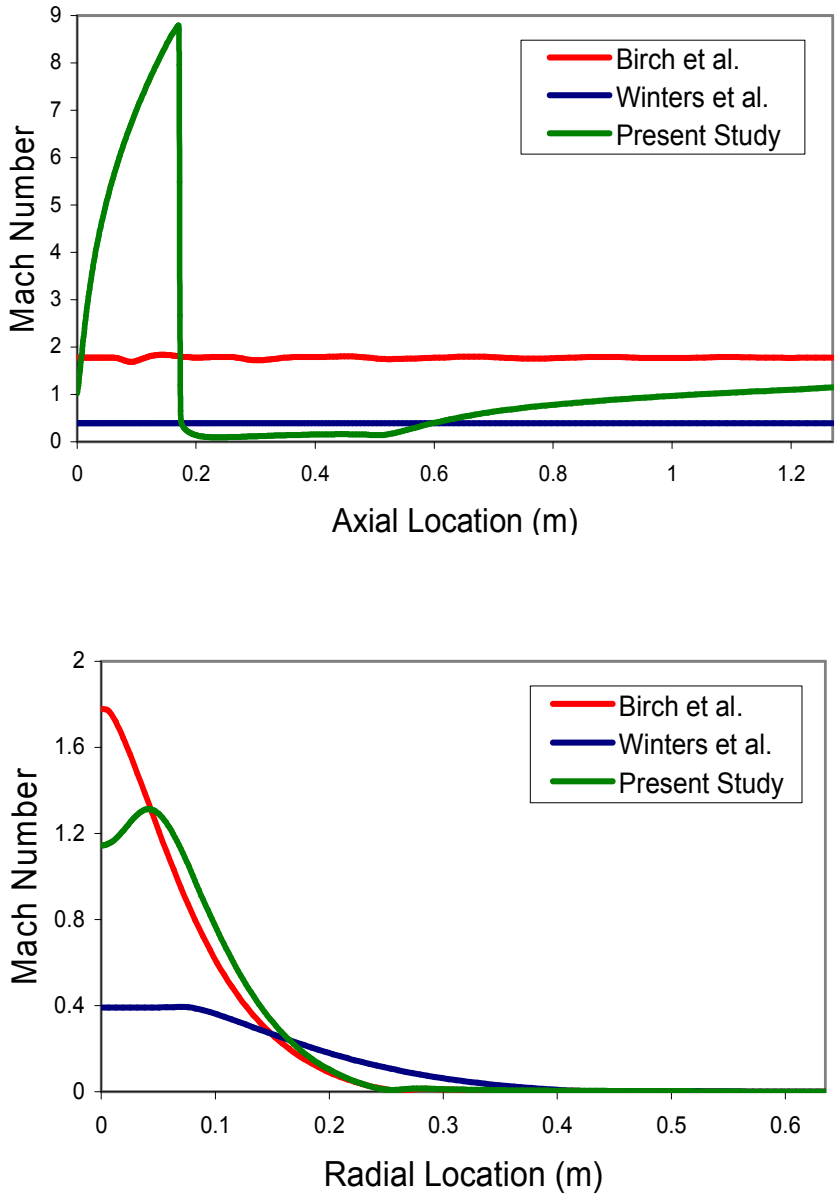

Figure 4.4. Mach number variations using various approaches along the axis (above) and along the radial direction (below) at an axial location of 1.27 m

Figures 4.5 and 4.6 show the hydrogen mole fraction contours and their variations along the axis and radial direction. For all three cases, the mole fraction of hydrogen along the axis was 1. The decay of the hydrogen mole fraction using the current

underexpanded jet analysis was consistent with the formation of the Mach disk. It is important to note that it took about 0.5 m along the radial direction at an axial location of 1.27 m (50 inches) for the hydrogen mole fraction to drop to zero using Winters et al. approach but only 0.3 m using Birch et al. approach and the present underexpanded jet analysis.

With a total or stagnation temperature of 283 K in the tank, the static temperature or critical temperature at the leak location was 234.89 K using compressible flow equations (Anderson, 2003). Figures 4.7 and 4.8 show the static temperature contours and their variations along the axis and radial location in the flow. The current underexpanded jet analysis considered here was able to capture the low static temperature conditions of approximately 20 K just before the Mach disk (due to very high Mach number) and the sudden increase in temperature up to 283 K just after the Mach disk and then a gradual decay. Such low temperatures could help condense a very small portion of the fluid near the Mach disk, but as will be discussed later in the section, when a more practical scenario is considered, the lowest temperatures near the Mach disk are higher than that of the steady-state free jet case. On the other hand, the static temperature values along the axis were found to be approximately constant at 275 K and 212 K for Winters et al. and Birch et al. effective approaches, respectively. As radially moved away from the axis, the temperature gradually increased to ambient conditions as shown in Figure 4.8.

Present Study (2010), detailed underexpanded jet analysis

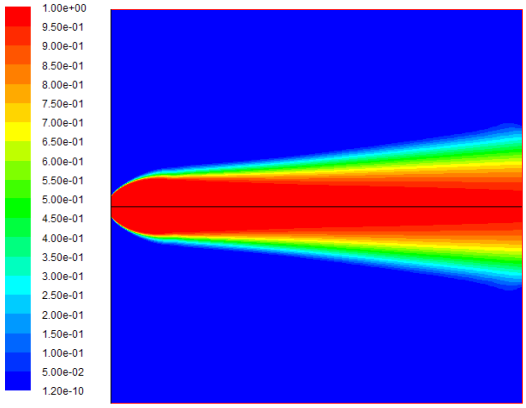

Birch et al. (1987), effective diameter approach

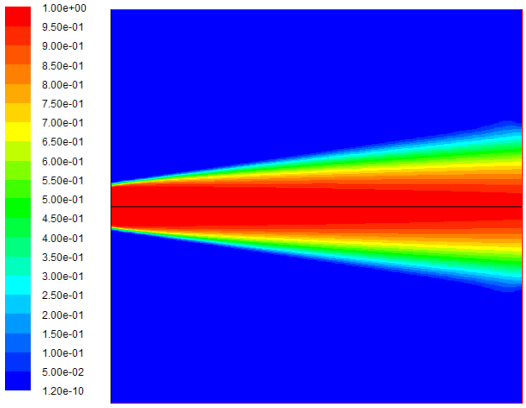

Winters et al. (2006), effective diameter approach

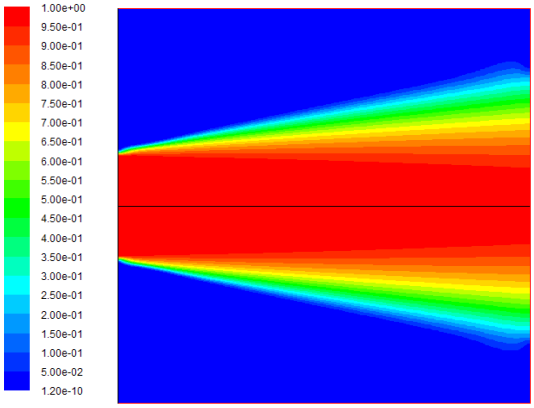

Figure 4.5. Hydrogen mole fraction contours using various approaches

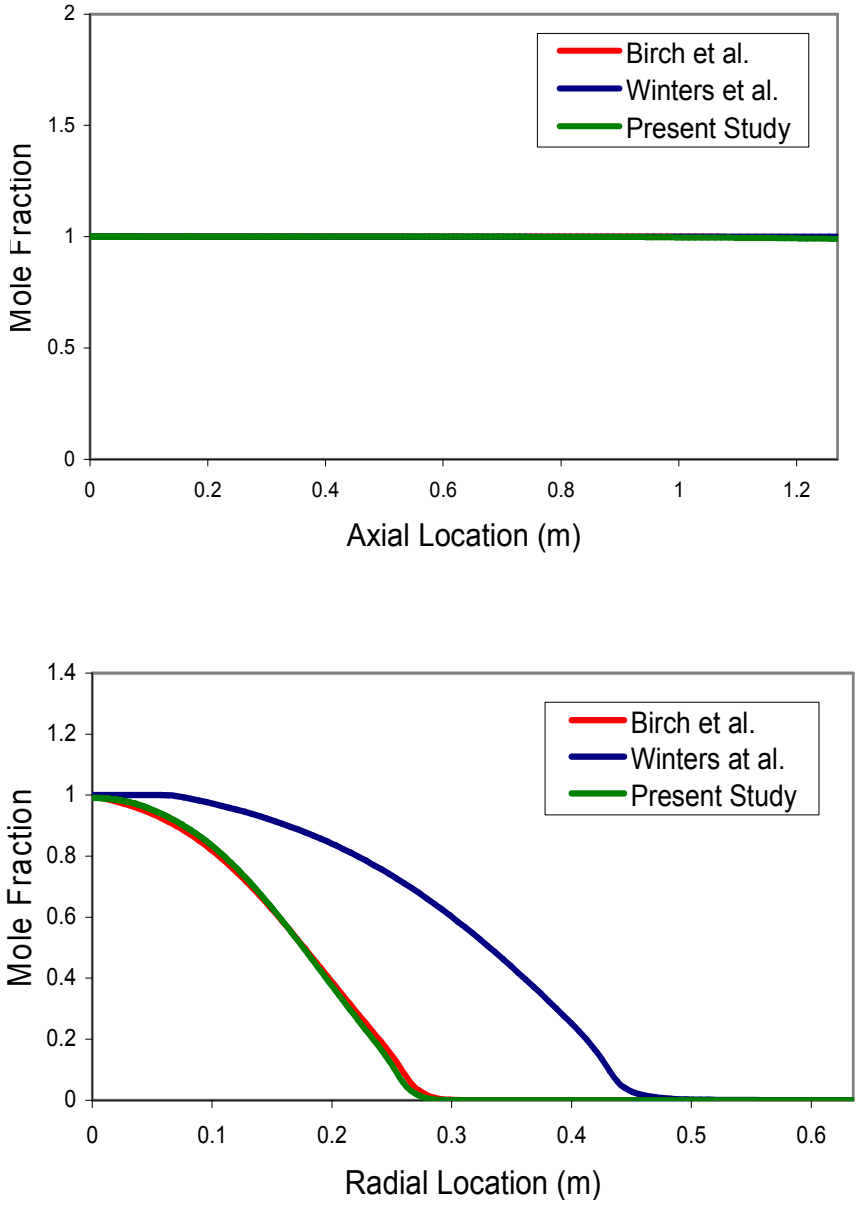

Figure 4.6. Hydrogen mole fraction variations using various approaches along the axis (above) and along the radial direction (below) at an axial location of 1.27 m

Present Study (2010), detailed underexpanded jet analysis

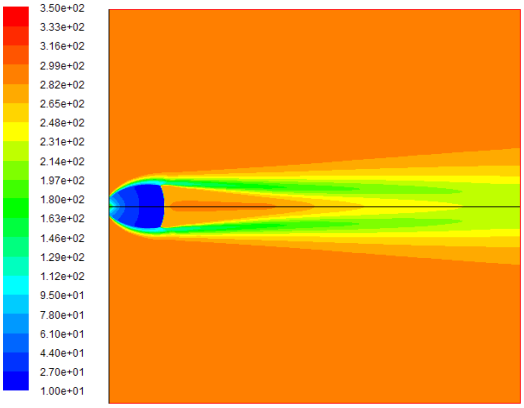

Birch et al. (1987), effective diameter approach

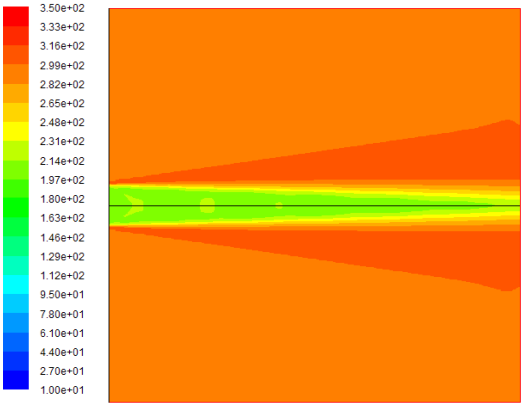

Winters et al. (2006), effective diameter approach

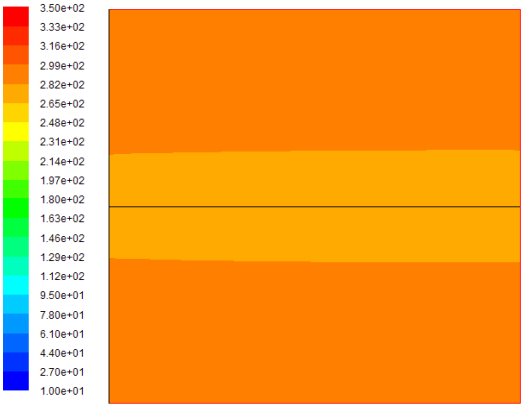

Figure 4.7. Static temperature contours using various approaches

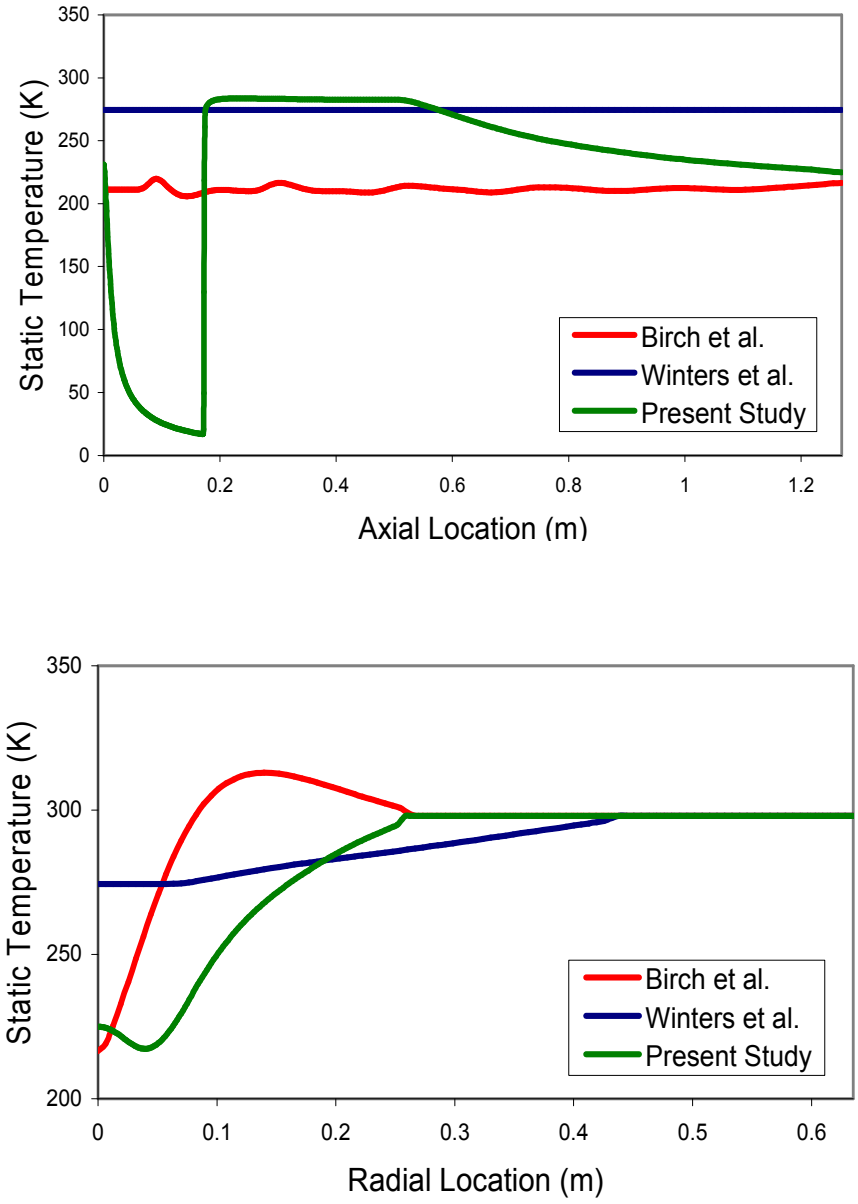

Figure 4.8. Static temperature variations using various approaches along the axis (above) and along the radial direction (below) at an axial location of 1.27 m

This analysis shows that the Birch et al. effective diameter approach could yield reasonable predictions for steady-state free jet analysis where the flow properties very close to leak (near field) are not important. This is because Birch et al. approach suggests a smaller diameter and larger leak velocity than the Winters et al. approach. In addition to assuming the same mass flow rate of the leak through the effective diameter at ambient pressures, Winters et al. analysis also included the formation of a shock to make sure the leak is subsonic for much easier numerical computations. However, any effective diameter approach should be employed only if it is a free steady-state jet and becomes questionable if the flow is unsteady or if there is a cross flow or an obstacle such that the flowfield gets disturbed (Birch et al., 1987; Winters and Evans, 2006, Houf et al., 2009).

4.2.3. Grid Independence of Computations. To ensure the present results were grid independent, three different grids with 60000 cells, 65142 cells and 73143 cells were considered, and the plots of Mach number and mole fraction using the detailed underexpanded analysis along the radial direction at an axial location of 1.27 m (50 inches) are shown in Figure 4.9. Accordingly, the results presented in this Section are for the grid with 73143 cells and second order upwind discretization.

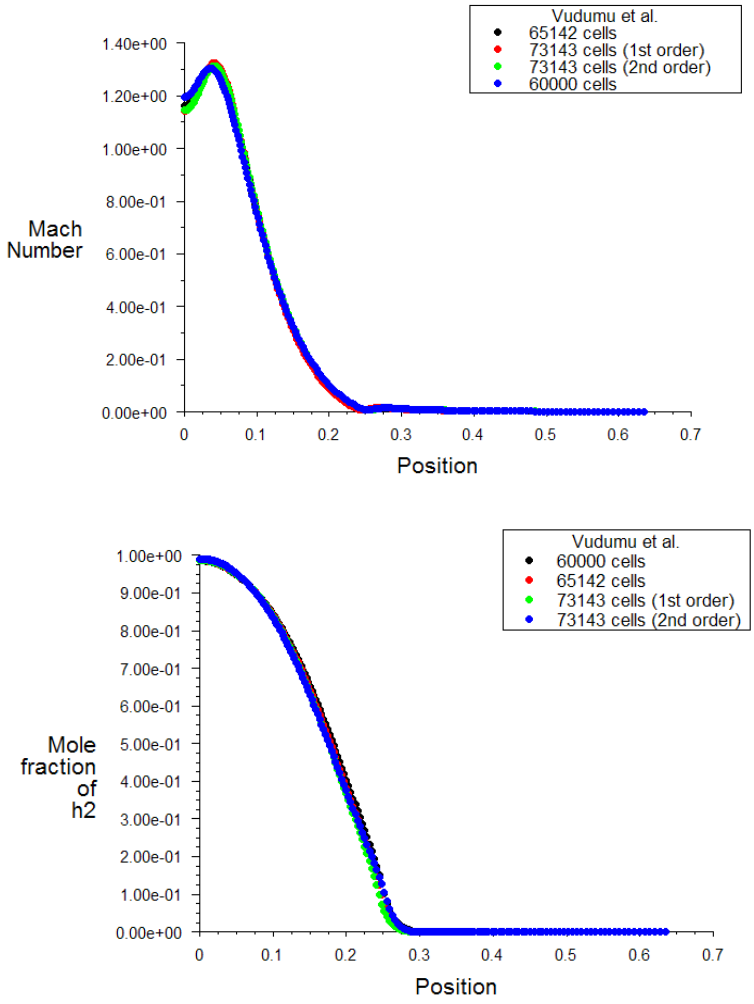

Figure 4.9. Plots of grid independent study for Mach number and mole fraction using the detailed underexpanded analysis along the radial direction at an axial location of 1.27 m

4.3. HIGH-PRESSURE UNSTEADY HYDROGEN LEAK FROM A STORAGE CYLINDER IN A MOBILE HYDROGEN UNIT (MHU)

The transient mixing behavior and the flow field of a high-pressure hydrogen leak in air in a typical mobile hydrogen unit (MHU) is studied next. Because this is more practical scenario with a leak occurring in a confined space, the effective diameter approaches as explained in the previous section are not valid and therefore the detailed underexpanded jet analysis is performed here. Two cases are considered with this

analysis: (a) constant mass-flow-rate leak (b) varying mass-flow-rate leak by taking into account the tank conditions during the blowdown process. After all the hydrogen content from the high-pressure cylinder is released into the MHU (release phase), the time required for the MHU to get replenished with fresh ambient air (purging) due to the ventilation system of the MHU is also investigated (subsequent diffusion phase).

4.3.1. Geometry and Computational Model. A typical mobile hydrogen unit (MHU) consists of a fuel processor to produce hydrogen using steam-methane reforming, a hydrogen purifier, a high-pressure compressor, and two to three hydrogen storage tanks capable of storing about 18 kg of hydrogen with an exhaust fan at the top of the entire enclosure for ventilation. A computational domain of dimensions $4.2\times2.4\times2.4$ m^3 ($165\times96\times96$ $inch^3$) with one high-pressure cylinder (diameter = 0.6 m = 22 inches) was considered as shown in Figure 4.10 in order to represent a typical MHU. An exhaust opening (open to ambient - natural convection) of 0.3×0.3 m^2 (12×12 $inch^2$) was provided at the top wall, 1.27 m (50 inches) away from the leak location. All the sides of the MHU were solid walls at 298 K. The leak diameter was 0.0127 m (0.5 inches) and the tank was initially at 485 bar (7034 psi) stagnation pressure and 283 K stagnation temperature. These conditions simulated a potential accidental scenario in which there was a catastrophic failure of a pressure relief device (PRD) or a sudden small crack in the storage vessel.

For the above conditions, the unsteady governing equations for the conservation of mass, momentum and energy as well as the non-reacting transport equations (two species, hydrogen and air) were solved with the standard $k-\varepsilon$ turbulence model. A careful approach to modeling was necessary because the flow was unsteady, three

dimensional, compressible, and highly turbulent. In addition to these complications, hydrogen diffusion was extremely fast and sonic velocity existed at the leak location. To overcome the numerical difficulty of a very high initial mass flow rate, a relatively small initial time step of 0.0001 s was employed here.

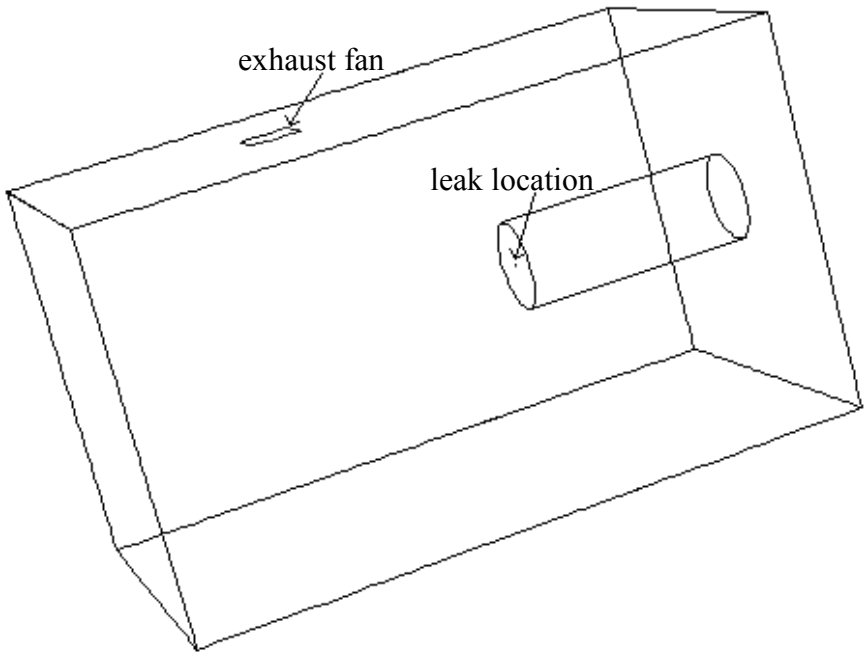

Figure 4.10. Schematic of the domain considered to study high-pressure leaks in a mobile hydrogen unit (MHU)

4.3.2. Results and Discussion - Constant Mass-Flow-Rate Leak. For a tank with stagnation conditions of 485 bar and 283 K, a leak diameter of 0.0127 m (0.5 inches) gave an initial mass flow rate of 3.884 kg/s at the orifice. For the first case, the flow rate of the leak was kept constant at this value in order to simplify the highly-complex flow conditions, and the results are presented in this Section.

Mach number contours at t = 0.1 s from the underexpanded jet analysis at the midplane of the MHU are shown in Figure 4.11. For a qualitative comparison, the results that would be obtained by using Birch et al. effective diameter approach are also shown in Figure 4.11. Note, however, that the validity of any effective approach may be questionable in closed areas where the jet hits with a wall a very short time after its releases. The formation of Mach disk could be observed in the figure (underexpanded jet analysis), but due to the presence of wall at the other end and more than ambient pressures in the MHU (confined space), the maximum Mach number was approximately 6, which was smaller than the value of about 9 obtained for a steady-state free jet shown in Figure 4.3.

Figure 4.12 shows the static temperature contours at t = 0.1 s. With the present underexpanded jet analysis, it was found that major portion of the MHU was at 310 K but the temperature near the orifice in the underexpanded region dropped to about 50 K (due to very high Mach number). The effective diameter approach, however, was unable to predict this sudden temperature drop.

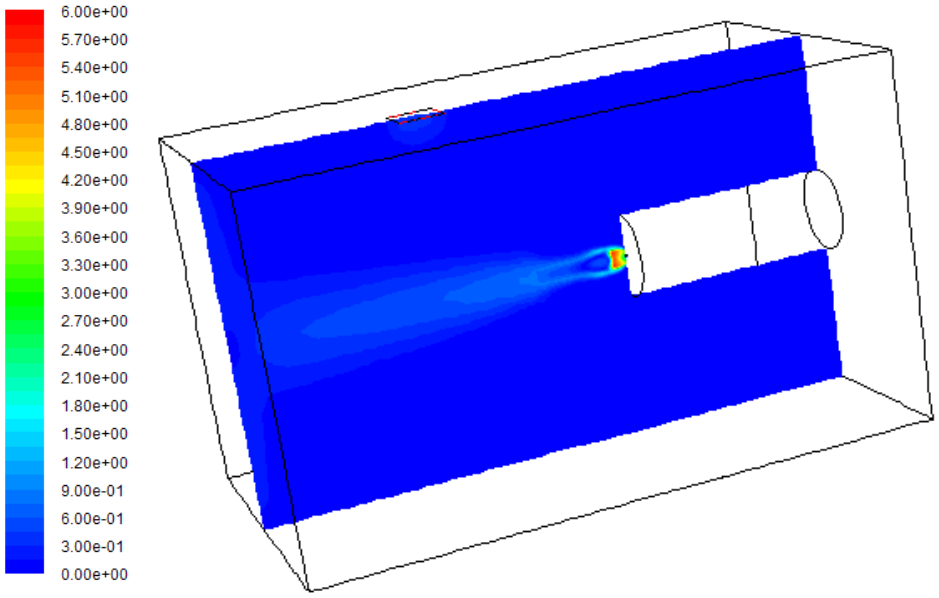

underexpanded jet analysis

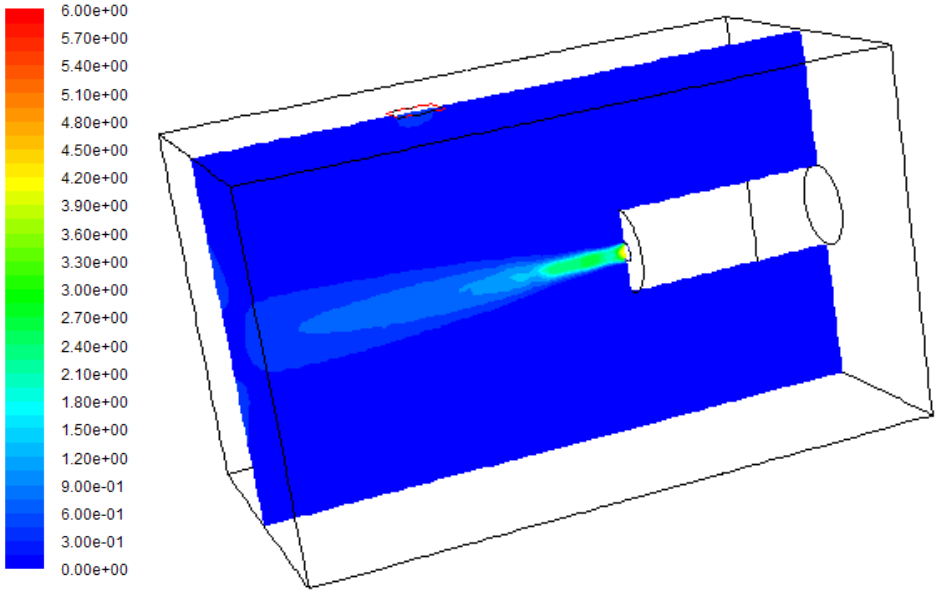

effective diameter approach

Figure 4.11. Mach number contours at t = 0.1 s at the MHU midplane from (a) the underexpanded jet analysis, and (b) the effective diameter approach

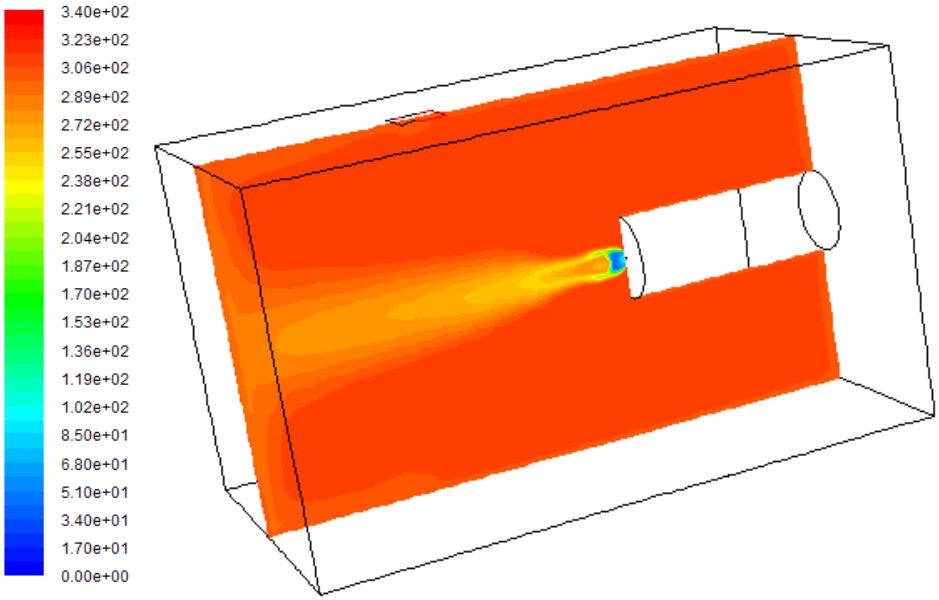

underexpanded jet analysis

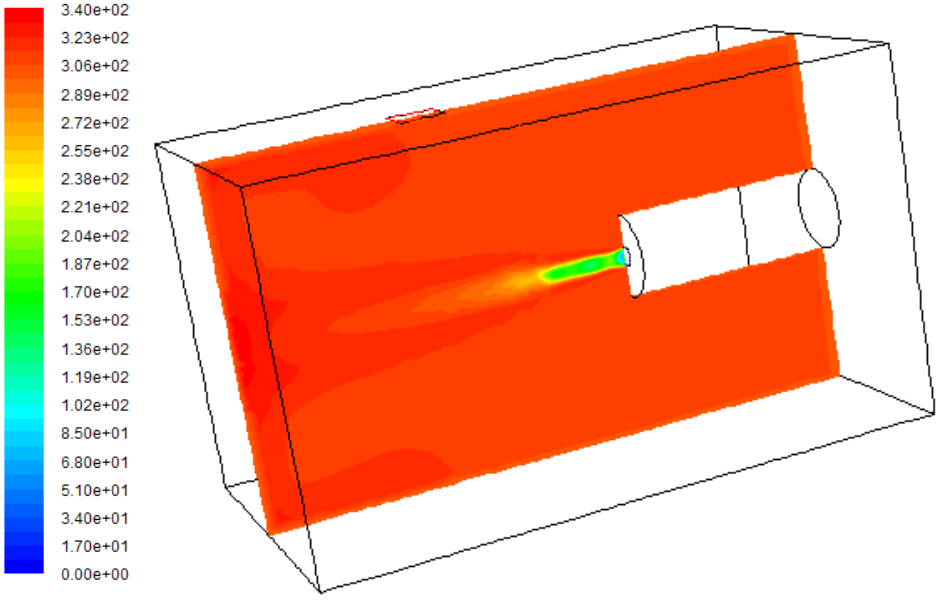

effective diameter approach

Figure 4.12. Static temperature contours at $t = 0.1$ s at the MHU midplane from (a) the underexpanded jet analysis, and (b) the effective diameter approach

Hydrogen mole fraction contours at different time steps using the present underexpanded jet analysis at the midplane of the MHU are shown in Figure 4.13. All the contours in Figure 4.13 are on the same scale of 0 to 1 with blue color representing 0% hydrogen and red color representing 100% hydrogen. Since the mass flow rate of the leak was very high (3.884 kg/s), the leak was momentum dominated with negligible buoyancy effects. It was found that the jet hit the wall, which was 2.72 m (107 inches) away, in approximately 0.02 s, and the hydrogen dispersed almost equally in both the upward and downward directions which would not be the case for a buoyancy-dominated slow leak as presented in Section 3. Hydrogen first arrived at the exhaust location in approximately 0.1 s. At initial times until t = 0.1 s, most of the space in the MHU except in the region in front of the leak had no hydrogen but only air (hydrogen mole fraction = 0). As time proceeded, because the flow rate of the leak was much higher than the flow rate at which hydrogen could escape through the exhaust opening, hydrogen started to accumulate in the MHU as shown in Figure 4.13 at 0.5 s and later. Major portion of the MHU (except the region in front of the leak) has 50%, 75%, and 88% hydrogen concentration at 0.5 s, 1 s, and 1.6 s, respectively. As expected, the region in front of the leak had the highest hydrogen concentration. At a constant mass flow rate of 3.884 kg/s, it would take approximately 1.6 s for the tank containing 6.2 kg of hydrogen to evacuate.

The Mach number contours of the hydrogen leak at different time steps are shown in Figure 4.14. After the jet hit the wall in front of it in 0.02 s, the Mach number contours did not change with time due to the constant leak rate. The maximum Mach number was approximately 6 in the underexpanded region (very close to leak) and 0.05 at far-field locations in the MHU with small effects of jet momentum.

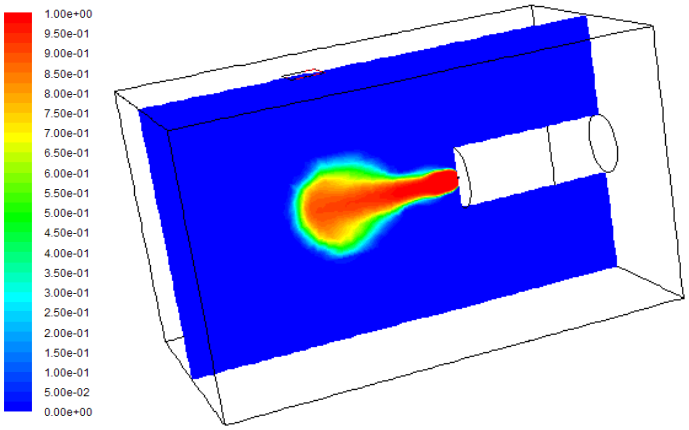

$t = 0.01$ s

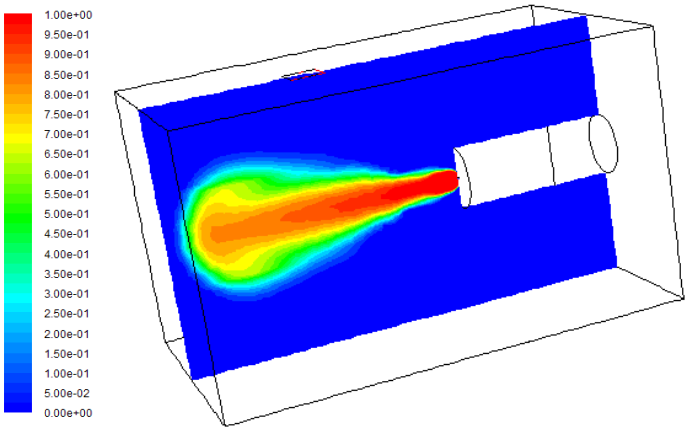

$t = 0.02$ s

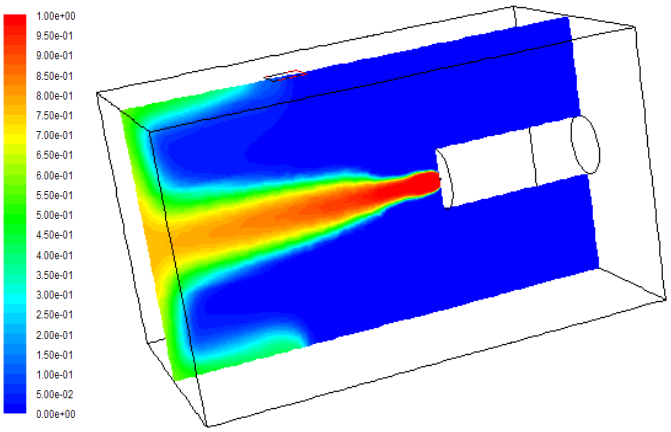

$t = 0.1$ s

Figure 4.13. Hydrogen mole fraction contours at different time steps using the underexpanded jet analysis at the midplane of the MHU for constant mass flow rate

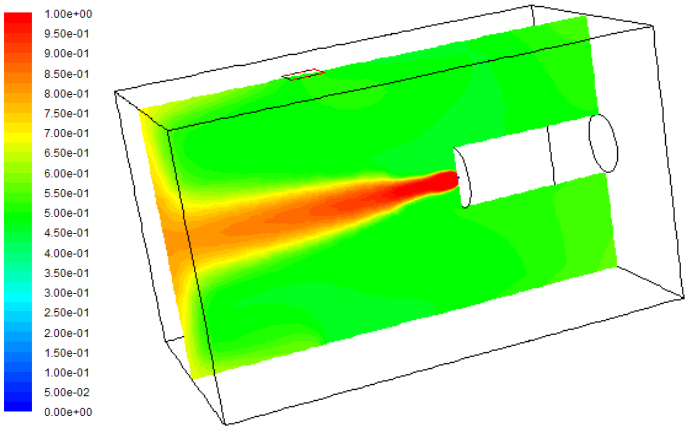

$t = 0.5$ s

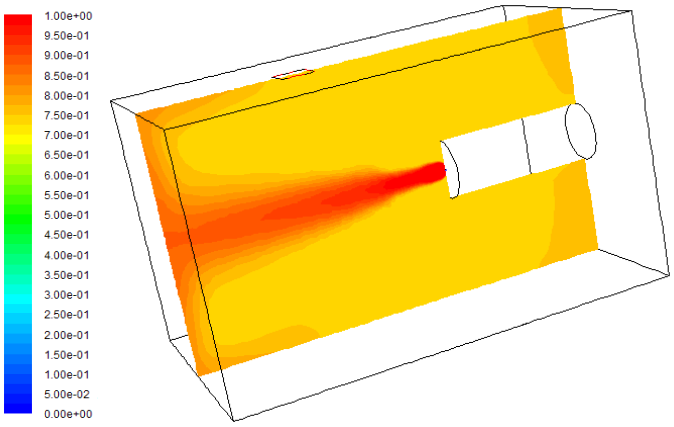

$t = 1$ s

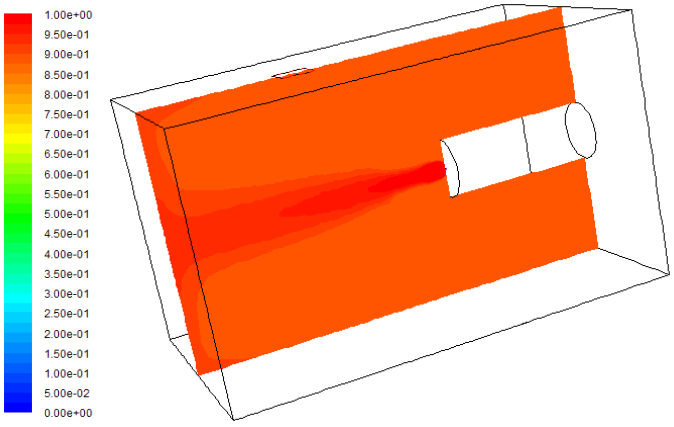

$t = 1.6$ s

Figure 4.13. Hydrogen mole fraction contours at different time steps using the underexpanded jet analysis at the midplane of the MHU for constant mass flow rate (cont.)

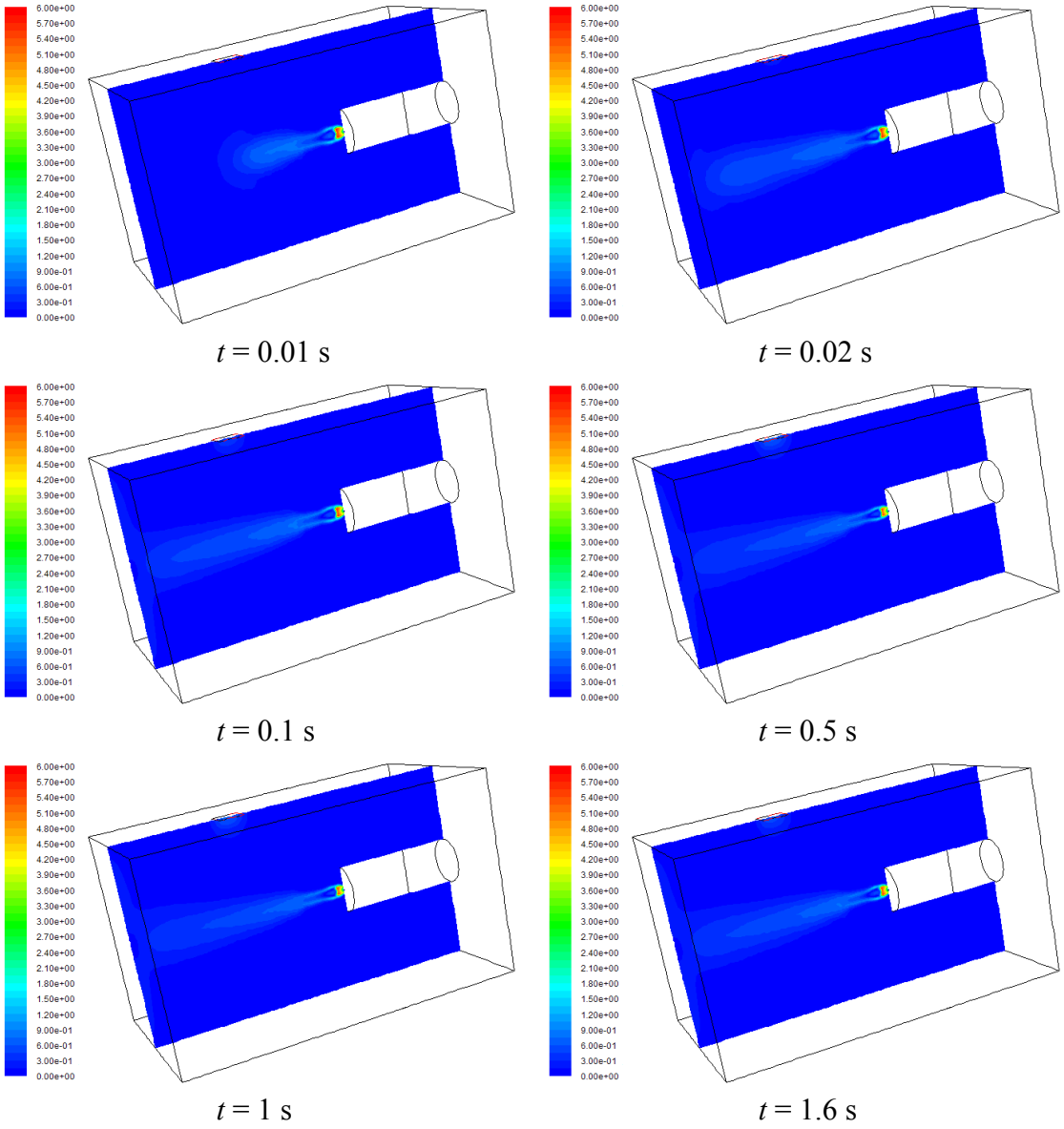

Figure 4.14. Mach number contours at different time steps using the complete underexpanded jet analysis at the midplane of the MHU for constant mass flow rate

4.3.3. Results and Discussion – Varying Mass-Flow-Rate Leak. When hydrogen leaks from a tank, since there is a fixed amount of hydrogen in the tank, the mass of hydrogen leaving the tank and the pressure in the tank decrease with time. To account for this blowdown process, the boundary conditions at the leak location (orifice) must be changed accordingly.

Initially at time t = 0 s, the tank contained 6.2 kg of hydrogen at 485 bar and 283 K with an initial mass flow rate of 3.884 kg/s. After a small time step, mass of hydrogen left in the cylinder, the new tank pressure and density, and hence the new leak rate needed to be calculated using the standard isentropic flow relations (Anderson, 2003). This process was repeated until the pressure in the cylinder dropped to 1.89 (critical pressure ratio) times the ambient pressure. During the blowdown, the stagnation temperature was assumed to be constant (Tchouvelev et al., 2007; Schefer et al., 2010).

To accomodate the varying mass flow rate and pressure at the leak location (boundary condition), two user defined functions (UDF) were written in C programming language and incorporated into the CFD software. Figure 4.15 shows the stagnation and static pressure variations at the leak location with time. The stagnation pressure decreased quite rapidly, intitally due to the high flow rate of hydrogen and then more moderately due to the depletion of hydrogen in the storage cylinder. The variation of leak mass flow rate with time is displayed in Figure 4.16. It takes 10.5 s for the cylinder to completely blowdown for the above-mentioned initial conditions.

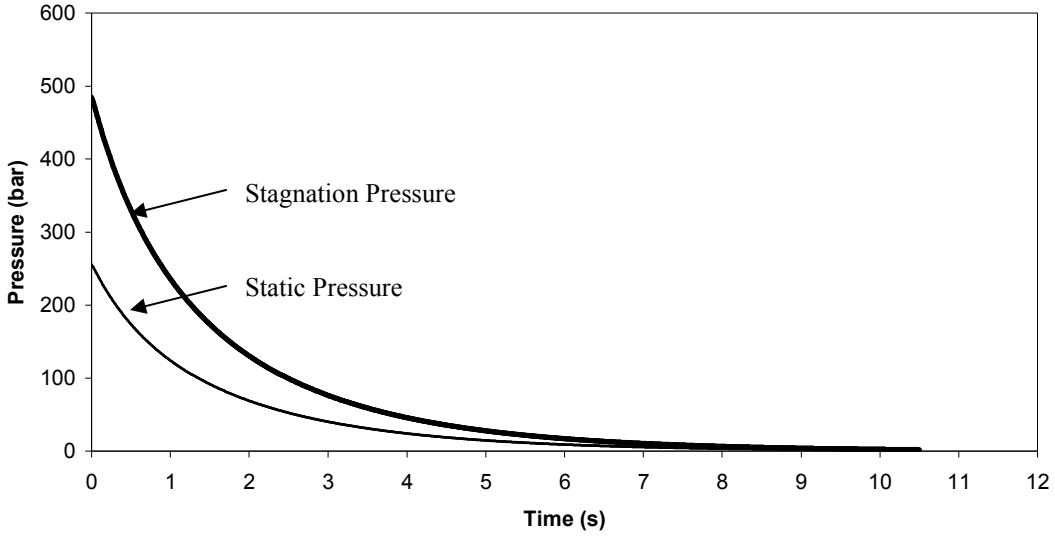

Figure 4.15. Variations of stagnation and static pressures with time during the blowdown

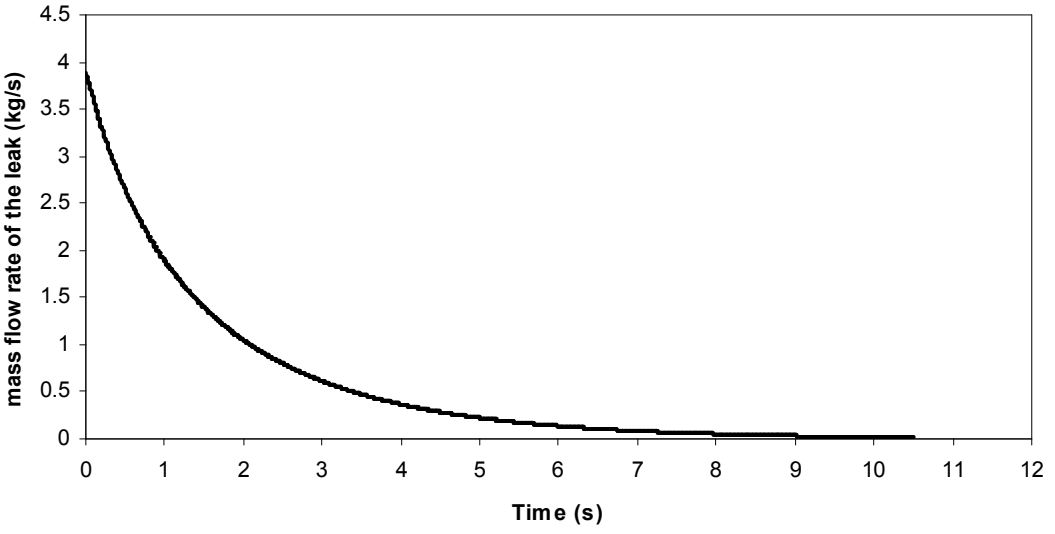

Figure 4.16. Variation of mass flow rate with time during the blowdown process

Hydrogen mole fraction contours at different time steps using the underexpanded jet analysis for the varying leak mass flow rate case are shown in Figure 4.17. The results were generally similar to the constant mass-flow-rate case but, since the total mass leaked at a certain time interval was less, there was less amount of hydrogen leaked into the MHU. In 0.5 s, the total amounts of hydrogen leaked were 1.615 kg and 1.942 kg for the varying mass-flow-rate case and constant mass–flow-rate case, respectively. Major portion of the MHU (except the region in front of the leak) had 44%, 65% and 75% hydrogen concentrations at 0.5 s, 1 s, and 1.6 s, respectively.

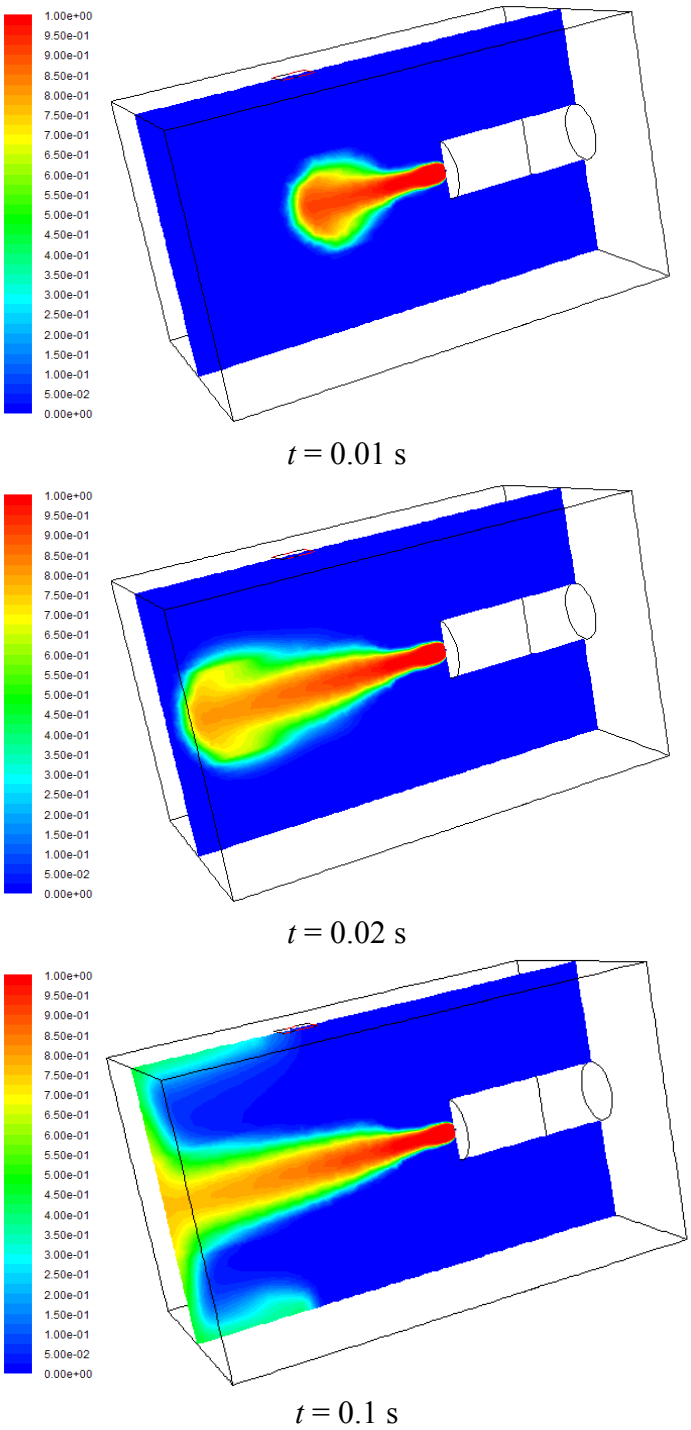

Figure 4.17. Hydrogen mole fraction contours at different time steps using the underexpanded jet analysis at the midplane of the MHU for varying mass flow rate

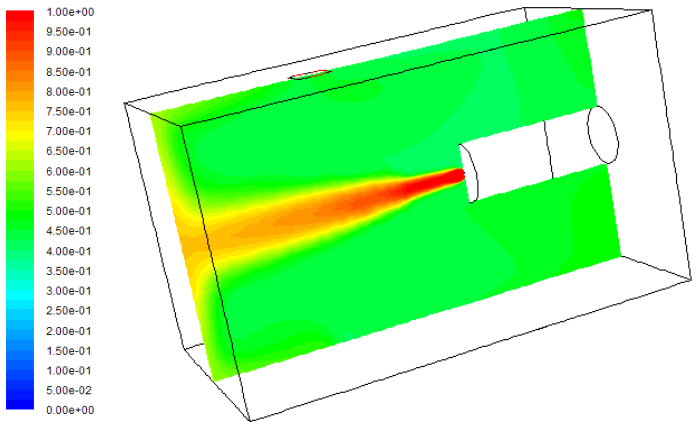

$t = 0.5$ s

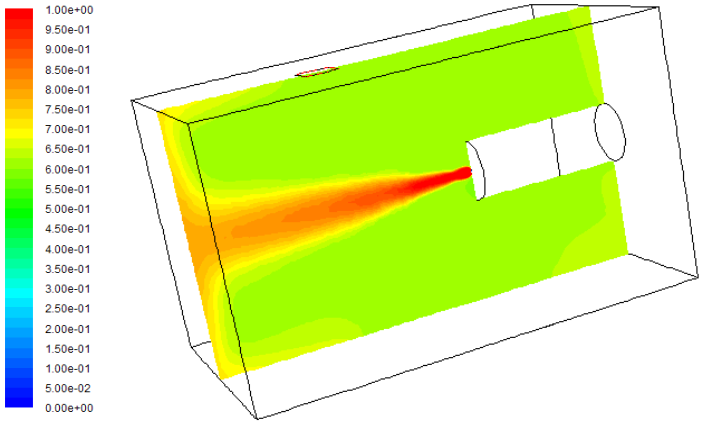

$t = 1$ s

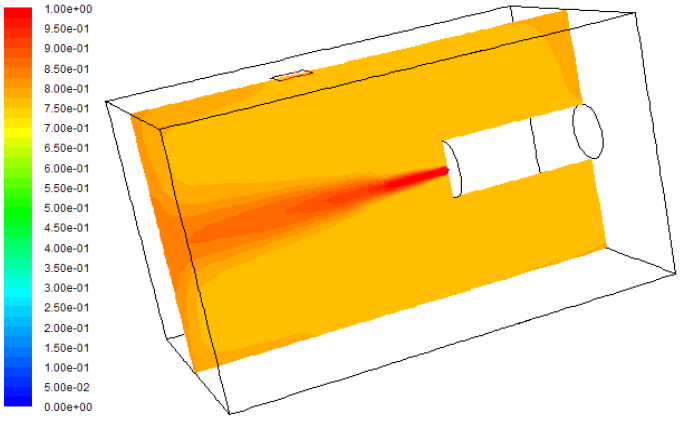

$t = 1.6$ s

Figure 4.17. Hydrogen mole fraction contours at different time steps using the underexpanded jet analysis at the midplane of the MHU for varying mass flow rate (cont.)

4.3.4. Results and Discussion – Diffusion Phase. After all the hydrogen content from the high-pressure cylinder was released into the MHU (release phase), the computational results were also obtained for the subsequent diffusion phase during which the MHU was replenished with fresh ambient air.

A typical MHU, or any similar space such as a car garage, is not air tight and will contain several small ambient air leakages into the unit (Lacome et al., 2007; Gupta et al., 2009; Prasad et al., 2009). According to ASHRAE, the ventilation requirement for such large configurations related to transportation applications is 3 ACH (air changes per hour) (Emmerich et al., 2003; Swain and Shriber, 1998). Accordingly, in the present study, idealized ambient air ventilation of 0.025 kg/s from an opening of 0.0075 m^2 (4×3 $inch^2$) was considered to meet the above-mentioned minimum ventilation requirements. Similar approach was also used by other studies for safety analysis of hydrogen leaks in confined spaces (Venetsanos et al., 2009; Prasad et al., 2009; Swain and Shriber, 1998).

Figure 4.18 shows the hydrogen mole fraction contours in the MHU during the diffusion phase after the complete blowdown of the hydrogen tank. Because there was no high-pressure leak in this second phase, and ambient air was assumed to enter from an idealized opening on the right wall at the bottom, nearly uniform mole fraction contours in the vertical direction were initially observed. Hydrogen, being much lighter than air, collected at the top and escaped out of the MHU through the exhaust opening. As time proceeded, the concentration of hydrogen dropped and reached a safe level (below 4%) in approximately 30 minutes. The knowledge of this time scale, which also depends on the actual ventilation of the MHU, is important for the firefighters or safety personnel to wait before entering the MHU after a catastrophic failure of the high-pressure cylinder.

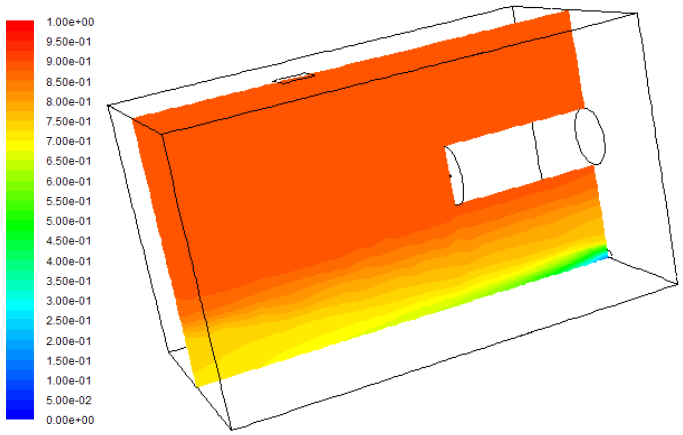

t = 1 min

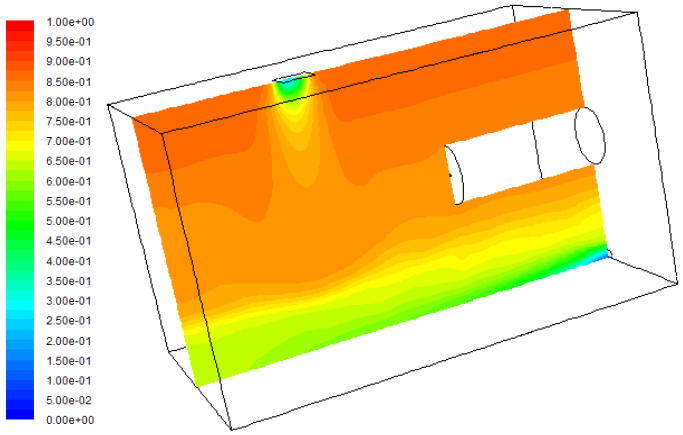

t = 2 min

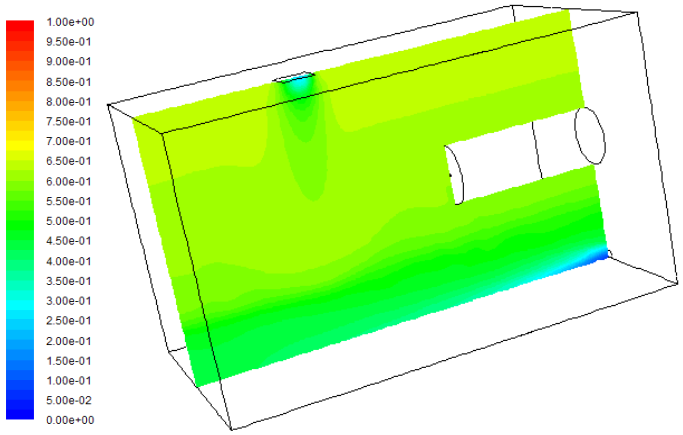

t = 5 min

Figure 4.18. Hydrogen mole fraction contours at different time steps during the diffusion phase

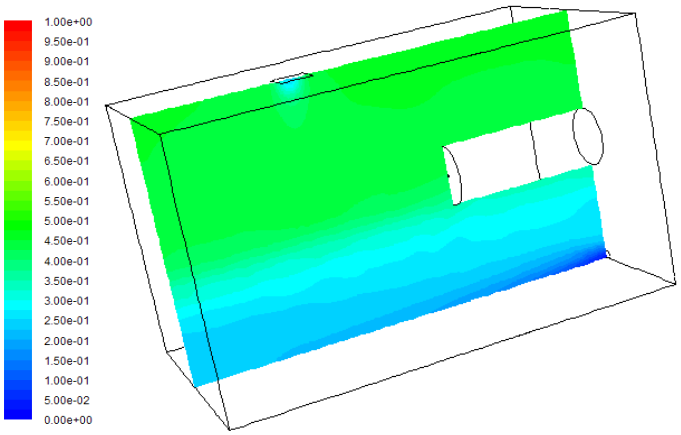

t = 10 min

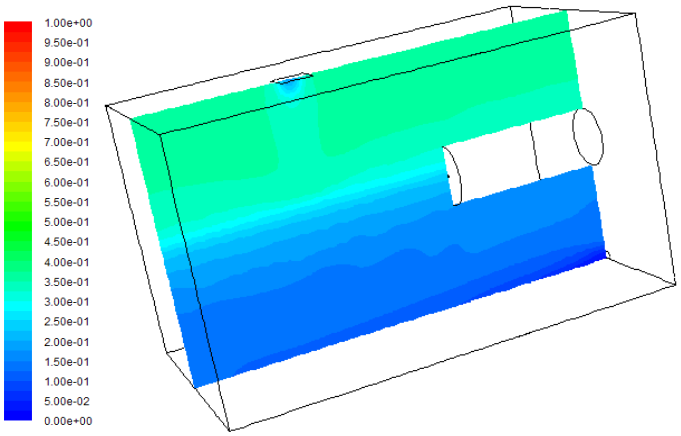

t = 15 min

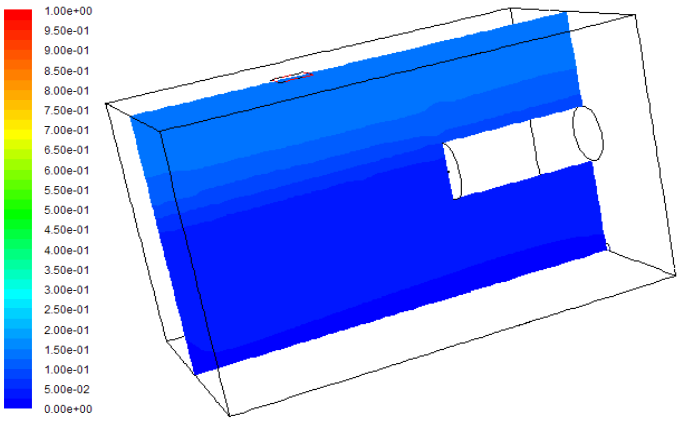

t = 30 min

Figure 4.18. Hydrogen mole fraction contours at different time steps during the diffusion phase (cont.)

4.4. SUMMARY AND CONCLUSIONS

When a high-pressure leak occurs, the exit flow chokes at the sonic velocity if the pressure ratio across the leak is greater than the critical pressure ratio (approximately 1.89 for hydrogen). For such a supercritical release, the flow leaves the exit to form an underexpanded jet. The flow at the exit of the leak is accelerated to supersonic speeds by the Prandtl-Meyer expansion fans until it forms a normal curved shock - Mach disk. To overcome the difficulty of numerically solving the details of the underexpanded jet, alternative approaches with an effective diameter have been suggested in literature. In this study, the applicability of two widely used effective diameter approaches has been studied for representing the high-pressure leaks from hydrogen storage tanks. It was found that one of these effective diameter approaches could yield reasonable predictions for steady-state free jet analysis where the flow properties very close to leak (near field) were not important. However, the effective diameter approach should be employed only if it is a free steady-state jet because it becomes questionable if the flow is unsteady or if there is a cross flow or an obstacle such that the flowfield gets disturbed.

With the complete underexpanded jet analysis, a 0.0127 m diameter high-pressure hydrogen leak from a storage tank containing 6.2 kg of hydrogen at 485 bar and 283 K was investigated. This scenario represents a potential accidental scenario in which there is a catastrophic failure of a pressure relief device (PRD) or a sudden small crack in the storage vessel in a typical mobile hydrogen unit (MHU) used in hydrogen fueling stations. The transient mixing behavior of hydrogen in air and the corresponding flow velocities were computed for two cases, constant leak rate and decaying leak rate to account for the fixed mass of the hydrogen in the cylinder. It was found the maximum

Mach number in the underexpanded region was 6, and the temperature dropped to 50 K in this region. The high-pressure jet hit the wall, which was 2.72 m away, in approximately 0.02 s, and the hydrogen dispersed almost equally in both the upward and downward directions which would not be the case for a buoyancy-dominated slow leak, as presented in the Section 3. Hydrogen first arrived at the exhaust location of the MHU in approximately 0.1 s. As time proceeded, hydrogen started to accumulate almost uniformly in the MHU except in the region in front of the leak. Major portion of the MHU (except the region in front of the leak) had 50%, 75% and 88% hydrogen concentration at 0.5 s, 1 s, and 1.6 s, respectively, when the leak flow rate was constant at 3.884 kg/s. The hydrogen concentrations were 44%, 65% and, 75% at 0.5 s, 1 s, and 1.6 s, respectively when the flow rate of the leak was decaying according the changing tank conditions during the blowdown process.

After all the hydrogen content from the high-pressure cylinder was released into the MHU, the results were also obtained for the subsequent diffusion phase during which the MHU was replenished with fresh ambient. It was found that for a typical MHU ventilation system considered here, it took approximately 30 minutes for the concentration to drop below the lower flammability limit.

5. COMPUTATIONAL MODELING, VALIDATION, AND UTILIZATION FOR PREDICTING THE PERFORMANCE, COMBUSTION AND EMISSION CHARACTERISTICS OF HYDROGEN IC ENGINES

5.1. INTRODUCTION

Internal combustion engines fueled by hydrogen have the potential for higher power and efficiency with lower emissions when compared to gasoline. In Sections 3 and 4, unignited hydrogen leaks were studied for various flow regimes to asses the safety issues when hydrogen is used in transportation applications. In this section, the performance, combustion and emission characteristics of a hydrogen-fueled engine when used in a vehicle are presented.

As mentioned in Section 1, when compared to gasoline, hydrogen has a higher heating value, higher flame speed, wider flammability limits and lower minimum ignition energy, these properties make hydrogen a favorable fuel to be used in engines (Negurescu et al., 2006; Li and Karim, 2004). In addition, hydrogen can be produced from renewable sources and its combustion does not produce any green house gases unlike other traditional fuels. The existing engine design methods and manufacturing plants can be fitted with minor modifications to produce hydrogen engines in the near term while other technologies, such as fuel cells, demand a complete re-design of vehicles in the long term. Consequently, hydrogen engines can also act as a transitional technology to fuel cell and hybrid vehicles during the development of a hydrogen economy (White et al., 2006; Verhelst et al., 2006).

Hydrogen IC engines have the potential for high power because of more energy per unit mass and high flame speed, high efficiency because of high flame speed that causes high rate of pressure rise in the cylinder and hence near constant-volume

combustion, and near-zero emissions, except NO_x at higher loads, because of the absence of carbon in the fuel molecular structure. Hydrogen can be operated with wide open throttle due to extremely wide flammability limits, which, unlike gasoline engines, decrease the cycle-by-cycle variations even with very lean mixtures, (Negurescu et al., 2006; White et al., 2006; Verhelst and Sierens, 2001; Subramanian et al., 2005; Verhelst et al., 2009). Because of its distinct properties described above, hydrogen can also be used as a single component fuel or in a multi-component fuel to improve combustion of other fuels like gasoline, methane, alcohols, LPG, biogas, and diesel (Verhelst et al., 2009; Hu et al., 2009; Das, 2002).

Hydrogen IC engines have also technical challenges that need to be overcome. Increasing the equivalence ratio for a higher power demand increases NO_x emissions, which are higher than those from a regular gasoline engine for the same conditions, limits the use of hydrogen fuel to low power density engines (Whit et al., 2006; Subramanian et al., 2005; Verhelst et al., 2008). Due to hydrogen's lower minimum ignition energy, any hot spot in the combustion chamber might become a source of ignition, potentially resulting in pre-ignition/backfire (Negurescu et al., 2006; White et al., 2006; Verhelst et al., 2006). The high rate of combustion could cause very high rate of pressure rise and uncontrolled abnormal combustion resulting in engine knock (Negurescu et al., 2006; Subramanian et al., 2005).

To realize maximum advantages of hydrogen with the above-mentioned distinctive properties, detailed research is required for the development of fuel-specific combustion and emission models. Advanced control methods and operating strategies to reduce NO_x emissions at high loads are also needed. These efforts have the potential of

producing more efficient and lower emission hydrogen engines that surpass the current fossil-fuel burning IC engines.

While there are many experimental and numerical studies on the characteristics of hydrogen-fueled spark-ignition engines (Negurescu et al., 2006; Subramanian et al., 2005; Das, 2002; Verhelst et al., 2008; Polasek et al., 2002; Shudo and Suzuki, 2002; Heffel, 2003; Jorach et al., 1997), very few have used computational tools that could be extended later for investigating advanced combustion modes, emission control technologies, and new efficiency increasing opportunities with a second law analysis.

Although multi-dimensional models are necessary to understand the details of in-cylinder combustion conditions, they are computationally demanding. Simpler one-dimensional models are desirable for fast computations with reasonable accuracy for practical design, control and optimization purposes. Such engine simulations also provide cost-effective technical tools that considerably shorten the development time from conceptual ideas to actual products. This is especially important for non-conventional emerging engine technologies that are in the initial stages of development and commercialization. Hence, there is a crucial need to develop, validate and utilize simple yet predictive models for hydrogen engines.

Among many others, one of the leading one-dimensional engine simulation software is GT-POWER by Gamma Technologies Inc. (2006). After extensive development and validation for conventional gasoline and diesel engines, it has become industry-standard engine simulation software for relatively fast but reasonably accurate essential predictions. While these computational models have been widely used in the literature for hydrocarbon-fueled engines, only a limited number of studies are available

on its application in predicting the performance of hydrogen-fueled engines. Noteworthy is the study by Polasek et al. (2002) who compared their experiments on a hydrogen engine with a model developed in GT-POWER. However, they used a non-predictive model by fitting the coefficients in the Wiebe function to their experimental data for obtaining the combustion burn rate/heat release rate. Accordingly, their approach is engine specific and may not be applied to other hydrogen engines. Furthermore, many past simulations of hydrogen engines, including (Polasek et al., 2002), were based on sub-models that have specifically been developed for hydrocarbon fuels. One important example is that hydrogen has a much higher flame speed compared to gasoline at a fixed equivalence ratio. Therefore, distinctive properties of hydrogen must be accounted for using new sub-models.

5.2. OBJECTIVES

The objective of the present study is to develop a hydrogen fuel-specific predictive one-dimensional engine model based on two-zone combustion methodology, validate it against independent experimental data for widespread implementation, and demonstrate its utilization for finding operating conditions for higher performance and lower emissions. Specifically, an accurate hydrogen flame speed sub-model is to be incorporated into the GT-POWER software so that the fuel-specific properties can be properly accounted for and therefore the computational predictions can be significantly improved. Additionally, a predictive turbulent combustion model is to be adopted so that the combustion burn rate sub-model and therefore the engine performance and emission characteristics do not require experimentally-prescribed parameters (Gamma

Technologies, 2006). This will yield a computational tool that can directly predict different operating conditions, allowing it to be potentially used for any hydrogen engine. A well-documented experimental study (Subramanian et al., 2005) on a spark-ignition port-injected IC engine fueled by gaseous hydrogen is identified for comparing against the simulations and therefore assessing the accuracy and suitability of the computational predictions. A proportional-integral-derivative (PID) controller is then added to the present model for adjusting exhaust gas recirculation (EGR) and quantifying the accompanying reductions in NO_x emissions. Since GT-POWER is already established for predicting gasoline and diesel engines, the results presented here are expected to contribute to the improved design and analysis of hydrogen IC engines in the automotive industry and therefore a faster and smoother transition to emerging cleaner and more efficient engines.

5.3. MODELING

5.3.1. Engine Operating Conditions. The operating conditions of the hydrogen IC engine modeled and simulated in this investigation were chosen similar to the independent study by Subramanian et al. (2005) because their reported test conditions and experimental data were well-documented. The specifications of the spark-ignition hydrogen engine from (Subramanian et al., 2005) used in this computational study are given in Table 5.1. The single-cylinder research engine was operated at wide open throttle (no throttle restriction), and the equivalence ratio (hence the power output) was varied by changing the amount of gaseous hydrogen injected into the intake port. The simulations were optimized for minimum advance for best torque (MBT) for each case,

similar to the experimental study (Subramanian et al., 2005) that was used here for comparing against the present computations. Adiabatic flame temperature of hydrogen (2318 K) is slightly lower than that of gasoline (2470 K) but the rapid combustion allows very little heat loss to the surroundings and hence high instantaneous local temperatures are produced. Also, the high auto-ignition temperature of hydrogen allows larger compression ratios to be explored in a hydrogen engine compared to a conventional one (Verhelst et al., 2006). Again following (Subramanian et al., 2005), a compression ratio of 9:1 was used at 2500 rpm.

Table 5.1. Engine specifications

Type	Four-stoke, single-cylinder, spark-ignited, naturally-aspirated, port-fuel-injected engine
Fuel	Hydrogen
Number of cylinders	One
Bore × Stroke	85 × 95 mm
Displacement volume	530 cm^3
Compression ratio	9:1
Engine speed	2500 rpm

Due to the low density of hydrogen, the power densities of port-fuel-injected hydrogen engines may be diminished relative to gasoline-fueled engines (Verhelst et al., 2008). One option is to inject hydrogen fuel directly into the cylinder at very high pressures (Polasek et al., 2002), but it would be practically difficult for the injector to survive such an extreme thermal environment of combustion chamber over a prolonged operation period. In addition, due to the relatively short fuel/air mixing time in a direct injection engine, the mixture can be non-homogenous. Studies have suggested that this

could lead to higher NO_x emissions relative to the non-direct injection systems (Jorach et al., 1997). A port-fuel-injected system would also require little modifications to the combustion chamber design during transitional period from gasoline to hydrogen engines (Verhelst et al., 2008). As a result, a port-fuel-injected engine was used in (Subramanian et al., 2005) and therefore in the present study.

5.3.2. Governing Equations. In the present computations, the entire system was divided into many discrete volumes that were connected by boundaries. The scalar quantities such as pressure, temperature, density, internal energy, enthalpy, species concentration were assumed to be uniform over each volume and were calculated for the center of the volume. The vector variables such as mass flux, velocity, mass fraction flux were calculated at each boundary.

Simultaneous equations of continuity, momentum and energy as shown in Equations 1, 2 and 3 were solved with all the quantities averaged across the flow direction (one-dimensional). Continuity and energy equations yielded the mass and energy for the next time step, and density was calculated with a known volume. The solver was iterated for temperature and pressure until they satisfied the gas density and energy that were already calculated.

$$\frac{dm}{dt} = \sum_{boundaries} \dot{m} \tag{1}$$

$$\frac{d\dot{m}}{dt} = \frac{dPA + \sum_{boundaries} \left(\dot{m} u \right) - 4C_f \times \frac{\rho u |u|}{2} \frac{dxA}{D} - C_p \left(\frac{1}{2} \rho u |u| \right) A}{dx} \tag{2}$$

$$\frac{d(me)}{dt} = P\frac{dV}{dt} + \sum_{boundaries}\left(\dot{m}H\right) - hA_s\left(T_{fluid} - T_{wall}\right) \quad (3)$$

5.3.3 Combustion Model. A two-zone combustion methodology, dividing cylinder into an unburned zone and a burned zone, was employed to model combustion with the assumptions and details explained in the following. At the start of combustion, all the cylinder contents were in the unburned zone. At each subsequent time step, a mixture of fuel and air was transferred from the unburned zone to the burned zone. The burn rate was directly predicted from flame speed correlation (predictive combustion) instead of imposing an experimentally-fitted Wiebe function (non-predictive combustion). If a non-predictive approach were used, the prescribed burn rate would have been the same irrespective of the cylinder conditions. While the unburned mixture of fuel and air was entrained into the flame front at a rate proportional to the flame speed (Equation 4), the burn rate became proportional to the amount of unburned mixture behind the flame front (Equation 5). Thus, the present predictive approach took into account the operating conditions such as cylinder geometry, spark timing, air motion, and fuel properties.

$$\frac{dm_e}{dt} = \rho_u A_e (S_T + S_L) \quad (4)$$

$$\frac{dm_b}{dt} = \left(\frac{m_e - m_b}{\tau}\right) \quad (5)$$

Once the unburned fuel and the associated air were transferred from the unburned zone to the burned zone, a chemical equilibrium was carried out for the entire burned zone. This calculation considered all the atoms of each species (C, H, O, N) present in the burned zone at that time and calculated the equilibrium concentration of combustion products (N_2, O_2, H_2O, H_2, NO, NO_2). The species concentrations depended on the burned zone temperature and, to a lesser degree, pressure. With the new composition of burned zone, the internal energies of each species and the complete zone were computed. By energy conservation equations given in Equations 6 and 7, the new unburned and burned zone temperatures were also obtained.

Unburned zone,
$$\frac{dm_u e_u}{dt} = -P\frac{dV_u}{dt} - Q_u - \left(\frac{dm_f}{dt}h_f + \frac{dm_a}{dt}h_a\right) \quad (6)$$

Burned zone,
$$\frac{dm_b e_b}{dt} = -P\frac{dV_b}{dt} - Q_b + \left(\frac{dm_f}{dt}h_f + \frac{dm_a}{dt}h_a\right) \quad (7)$$

To account for the distinctive properties of hydrogen, especially the higher flame speed, hydrogen fuel-specific flame speed model needed to be incorporated into the computations. Changes in the flame speed correlation were necessary because the flame speed model offered in GT-POWER is only sufficient for several hydrocarbons. It is worth noting that, even for methane, the equations and constants do not accurately correlate with the data over the entire range of temperature and pressure relevant to engine operation (Heywood, 1988). Consequently, a new correlation for flame speed applicable for hydrogen combustion was adopted in the present study (Equation 8) based on the equations and the comprehensive literature review done by Knop et al. (2008).

Using this fuel-specific model, the variations of hydrogen and gasoline flame speeds with respect to equivalence ratio are illustrated in Figure 5.1, which clearly demonstrates that hydrogen has a very high flame speed compared to gasoline.

$$S_L = S_{LO}\left(\frac{T_u}{T_o}\right)^{\alpha}\left(\frac{P}{P_o}\right)^{\beta}\left(1-2.06X_{dil}{}^{0.77}\right) \tag{8}$$

where, $S_{LO} = B_m - B_\phi(\phi-\phi_m)^2$

B_m = maximum laminar speed = 2.82 m/s

ϕ_m = equivalence ratio at maximum speed = 1.5

B_ϕ = laminar speed roll-off value = -0.5209 m/s

α, β = constants, function of equivalence ratio

$\alpha = 2.18 - 0.8(\phi - 1)$, $\beta = -0.16 + 0.22(\phi - 1)$

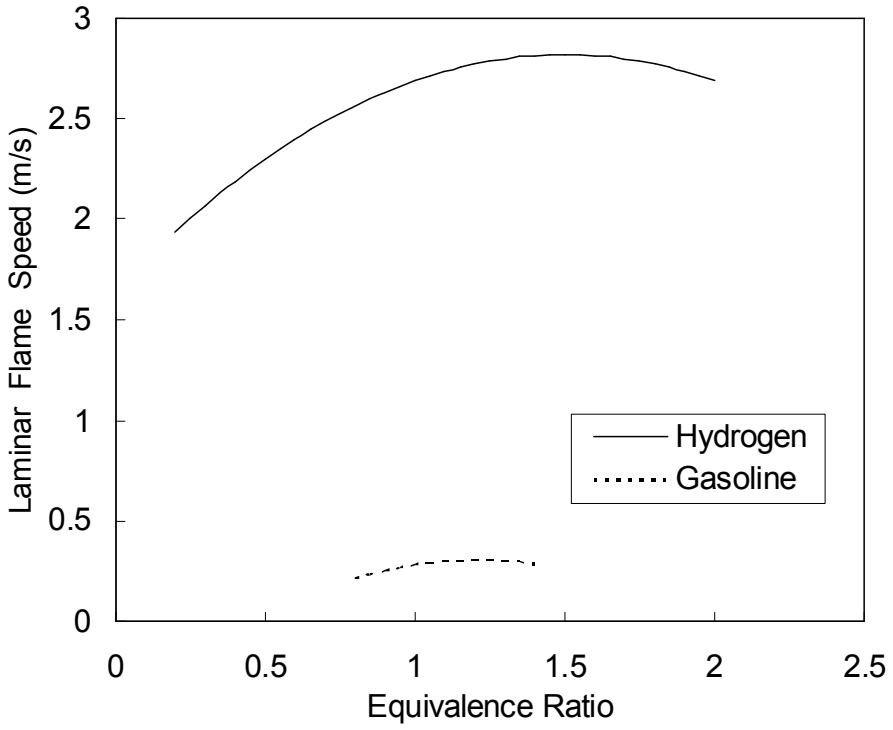

Figure 5.1. Laminar flame speeds of hydrogen and gasoline at various equivalence ratios

The emissions of oxides of nitrogen (NO and NO_2 = NO_x) were predicted based on the three step extended Zeldovich mechanism (given below). In principle, nitrogen oxides (NO_x) are the only harmful engine-out emissions but the burning of lubricating oil in the combustion chamber produces carbon oxides (CO_x) and hydrocarbons (HC) at near-zero levels (White et al., 2006). As reflected in the Zeldovich mechanism, production of NO_x in an engine mainly depends on the combustion temperature and the oxygen availability.

Extended Zeldovich mechanism:

N_2 oxidation rate equation,

$O + N_2 \Leftrightarrow NO + N$ with rate constant $k_1 = 7.60 \times 10^{10} \times e^{-\frac{38000}{T_b}}$

N oxidation rate equation,

$N + O_2 \Leftrightarrow NO + O$ with rate constant $k_2 = 6.40 \times 10^{6} \times T_b \times e^{-\frac{3150}{T_b}}$

OH oxidation rate equation,

$N + OH \Leftrightarrow NO + H$ with rate constant $k_3 = 4.10 \times 10^{10}$

where, T_b is the burned sub-zone temperature

Recirculating a portion of the exhaust gases back into the intake manifold, which is called exhaust gas recirculation (EGR), is a convenient way to displace excess air, at the same time to increase the specific heat capacity of the mixture in the cylinder, and hence to lower in-cylinder temperatures for the same amount of heat addition (White et al., 2006; Verhelst et al., 2008). This will reduce NO_x emissions, the possibility of pre-

ignition, knock, and backfire. Past studies have also shown that EGR is an effective way to reduce NO_x emissions in hydrogen-fueled IC engines (Das, 2002; Verhelst et al., 2008; Heffel, 2003). In order to vary EGR level and quantify its effect on exhaust emissions, the present model was supplemented with a proportional-integral-derivative (PID) controller, which will be discussed more later on in the Section.

5.4. RESULTS AND DISCUSSION

5.4.1. Comparison of Hydrogen and Gasoline IC Engines. Before a comparison to experimental data, the computational model for hydrogen engine was first compared to the one for a gasoline engine with the same geometry and operating conditions given in Table 5.1. This exercise is useful to understand the general features of a hydrogen engine relative to a traditional engine. Cylinder pressure variations with crank angle as well as with relative cylinder volume are shown in Figure 5.2 for an equivalence ratio of 0.9 for both types of engines. As expected, in comparison to the gasoline engine, hydrogen engine has a higher rate of pressure rise and a higher maximum pressure in the cylinder due to a significantly higher burning speed. For the conditions considered here, the peak pressure in the hydrogen engine was 45 bars at 14 degrees crank angle compared to 38 bars at 28 degrees in the gasoline engine. The *P*-*V* diagram also demonstrates that the heat addition process in the hydrogen engine takes place at nearly constant volume similar to the Otto cycle due to much faster combustion.

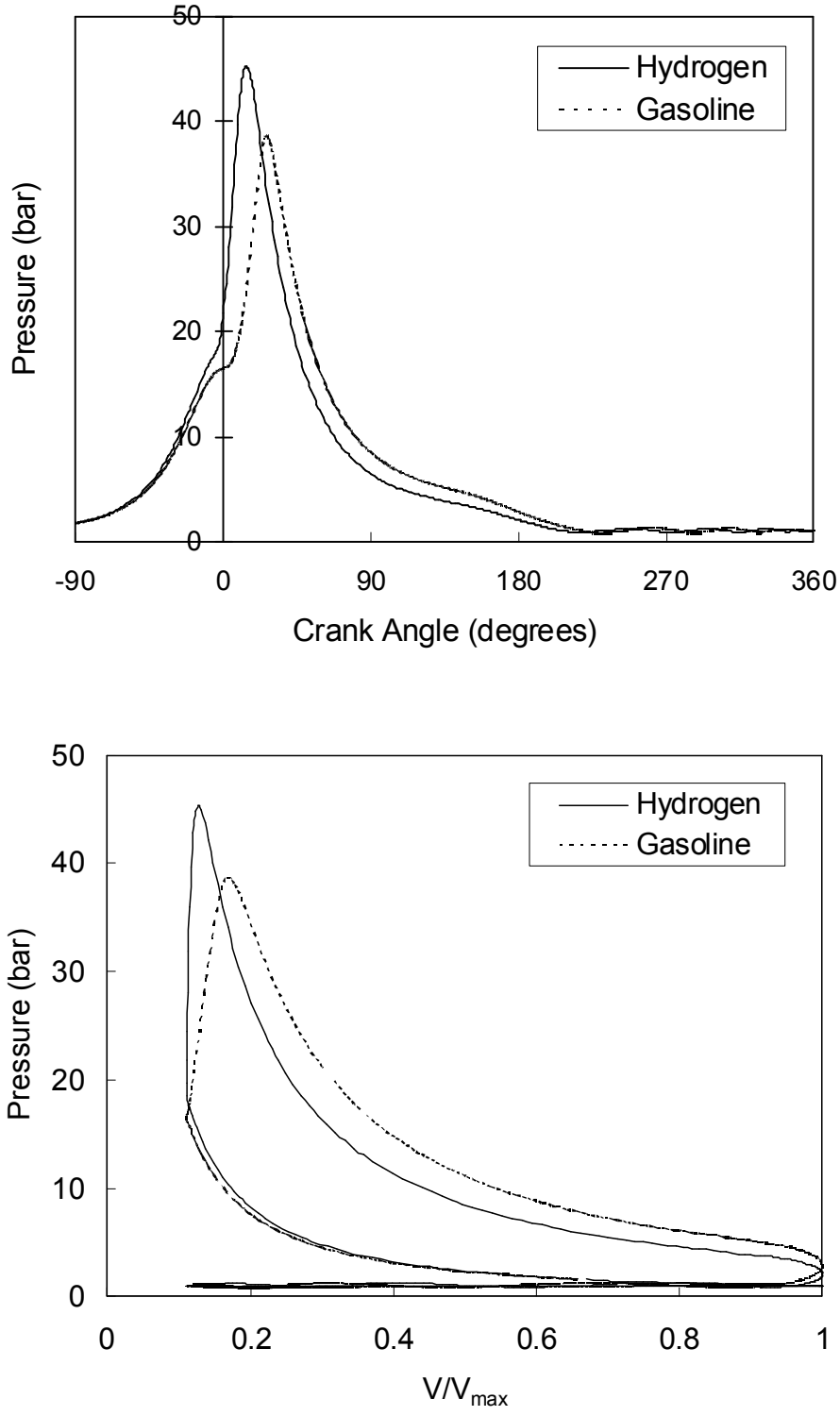

Figure 5.2. Pressure vs. crank angle and pressure vs. volume diagrams for hydrogen- and gasoline-fueled spark-ignition engines

Table 5.3 compares two other relevant parameters, the ignition delay (crank angle degrees for the first 2% of the total heat release) and combustion duration (crank angle degrees for 0%-90% of the total heat release), for the hydrogen and gasoline engines under the identical operating conditions mentioned above. In terms of crank angle, the ignition delay and combustion duration of the hydrogen engine were approximately 50% lower than those of the gasoline engine. The faster ignition and shorter combustion duration were responsible for the optimal spark timing (MBT) to be close to the top dead center (8 degrees before TDC).

Table 5.2. Computed combustion properties of hydrogen in comparisons to those of gasoline for the same engine operating conditions

Fuel	Ignition delay (for the first 2% of the total heat release)	Burn duration (for 0-90% of the total heat release)
Hydrogen	6 degrees crank angle	22.4 degrees crank angle
Gasoline	13.6 degrees crank angle	36.4 degrees crank angle

5.4.2. Model Validation – Comparison of Simulations to Experiments. As discussed in the combustion modeling section, the burn rate in this study was computed based on the flame speed instead of fitting a Wiebe function to the experimental data (Polasek et al., 2002). This fundamental approach can therefore predict the combustion burn rate in any hydrogen engine because it accounts for the changes in engine conditions. The predicted heat release rates are compared to the measured values reported

by (Subramanian et al., 2005) in Figure 5.3 as a function of crank angle for the maximum equivalence ratio of 0.84. The experiments indicated that faster burning speed of hydrogen caused relatively high rate of heat release in a small time interval. Specifically, the heat release became noticeable about 3 degrees before the TDC, reached a peak value of about 84 J/degrees at 10 degrees after TDC, and nearly diminished around 15 degrees. Aside from a small delay at the end of the combustion, the simulations were in excellent agreement with the experiments, correctly predicting the start of the combustion as well as the value and the timing of the peak heat release rate.

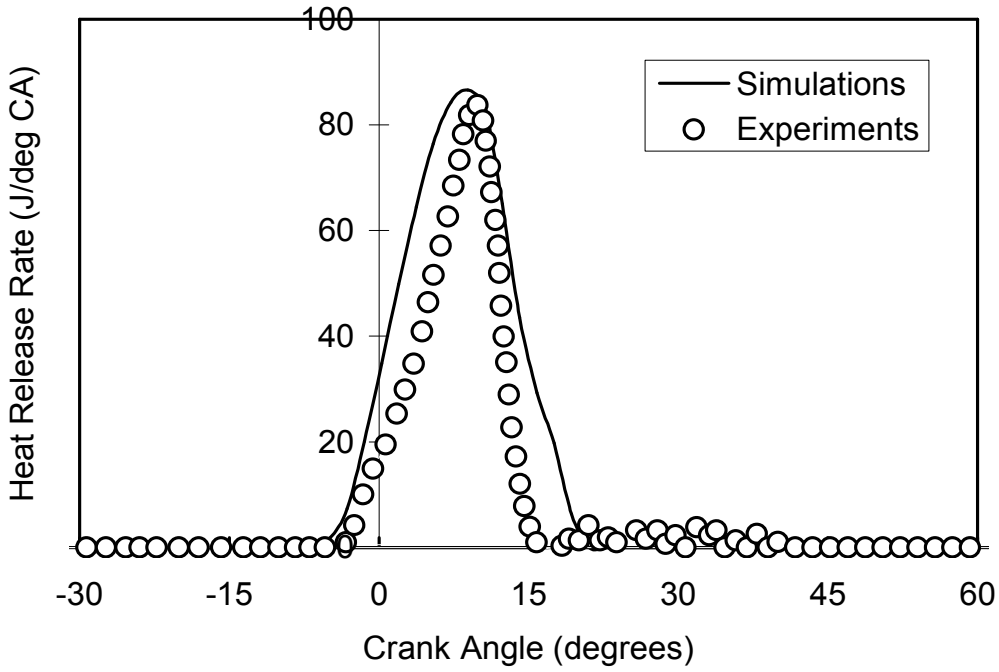

Figure 5.3. Predicted heat release rates and comparison to experimental data for the hydrogen engine simulated in this study

The variation of brake power with equivalence ratio for the hydrogen engine under investigation is shown in Figure 5.4. As the equivalence ratio (or the amount of fuel injected) was increased, the power generated by the engine increased. The simulations again captured this trend and agreed well with the experimental data as the difference was less than 8% at higher equivalence ratios and less than 15% at lower equivalence ratios. The latter observation was attributed to the very small brake powers produced at such extremely fuel-lean mixtures. The brake power was 7.4 kW at an equivalence ratio of 0.84, which was the maximum value considered during the experiments (Subramanian et al., 2005) due to the limitation of backfiring.

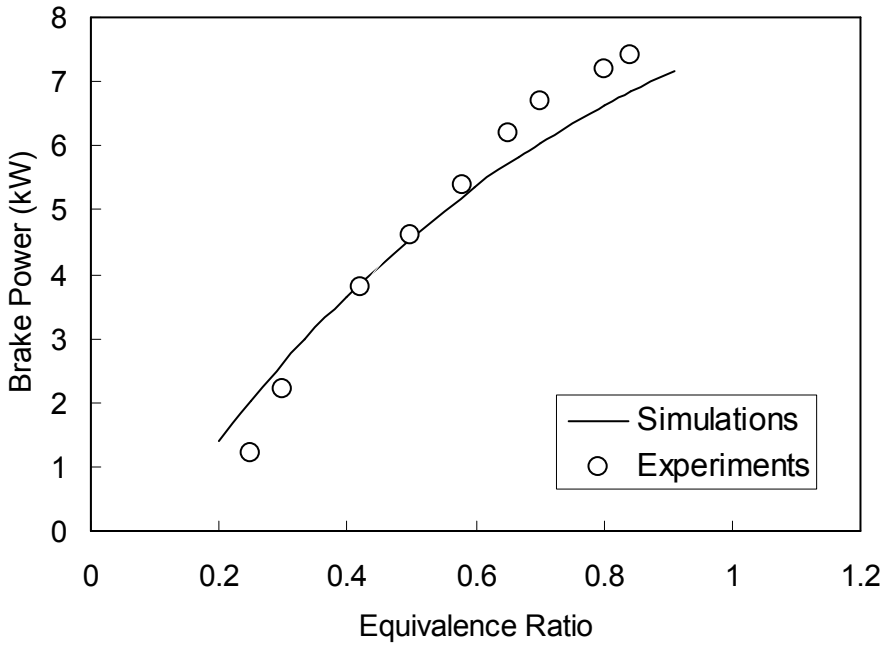

Figure 5.4. Comparison of predicted and measured brake powers as a function of equivalence ratio

Figure 5.5 displays the change in the cylinder peak pressure with brake power (or equivalence ratio) and the comparison of simulations with measurements. The peak pressure was found to increase almost linearly with brake power. For the maximum brake power of 7.4 kW, the peak pressure was approximately 44 bars. As mentioned before, such relatively high peak pressures in the cylinder are due to the fast combustion process that causes high rate of pressure rise. The maximum rate of pressure rise was 2.2 bars per degree crank angle. The predicted peak pressures agreed well (within 10%) with the experiments at medium to high brake powers. There were again some differences at the two lowest brake powers of 1-2 kW for which the equivalence ratio of the hydrogen/air mixture in the cylinder was less than 0.3, corresponding to extremely lean conditions.

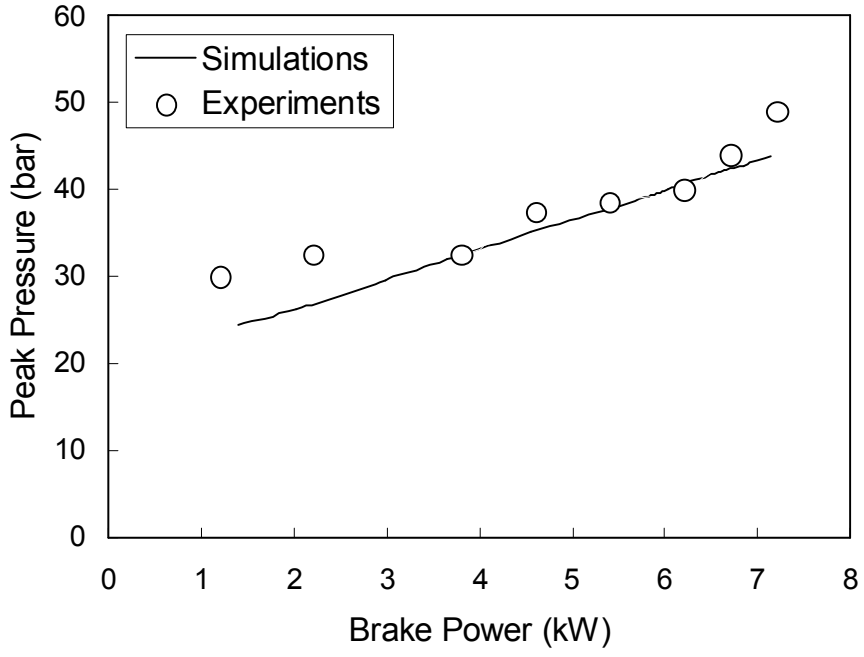

Figure 5.5 Comparison of predicted and measured peak in-cylinder pressures as a function of brake power

Brake thermal efficiency of the hydrogen engine was computed using the Chen-Flynn friction model (Heywood, 1988) shown in Equation 9. The variations of brake thermal efficiency with brake power are shown in Figure 5.6 for the simulations and the experiments, both of which resulted in an initial increase in efficiency with brake power followed by gradual leveling off. The maximum brake thermal efficiency was nearly 30% for the cylinder compression ratio of 9:1. Indicated thermal efficiency would be a more relevant comparison as this study was more concerned with the combustion process instead of the power transmission. Nevertheless, the experimental data of (Subramanian et al., 2005) were obtained for brake thermal efficiency (after friction) instead of indicated thermal efficiency (before friction).

$$FMEP = 0.7 + 0.008 \times P_{\max\_cylinder} + 0.12 \times Speed_{mean\_piston} + 0.0015 \times Speed^{2}_{mean\_piston} \qquad (9)$$

where, $FMEP$ = Friction Mean Effective Pressure

Because the friction conditions of the actual engine were unknown, it was necessary to adjust the constants in the friction model for a meaningful comparison. While this did not affect the overall computed trends, it somewhat reduced the magnitude of brake thermal efficiency at each brake power and resulted in good agreement between the simulations and measurements at all operating conditions. After this consideration, the maximum deviation of the computations from the experiments was less than 10%.

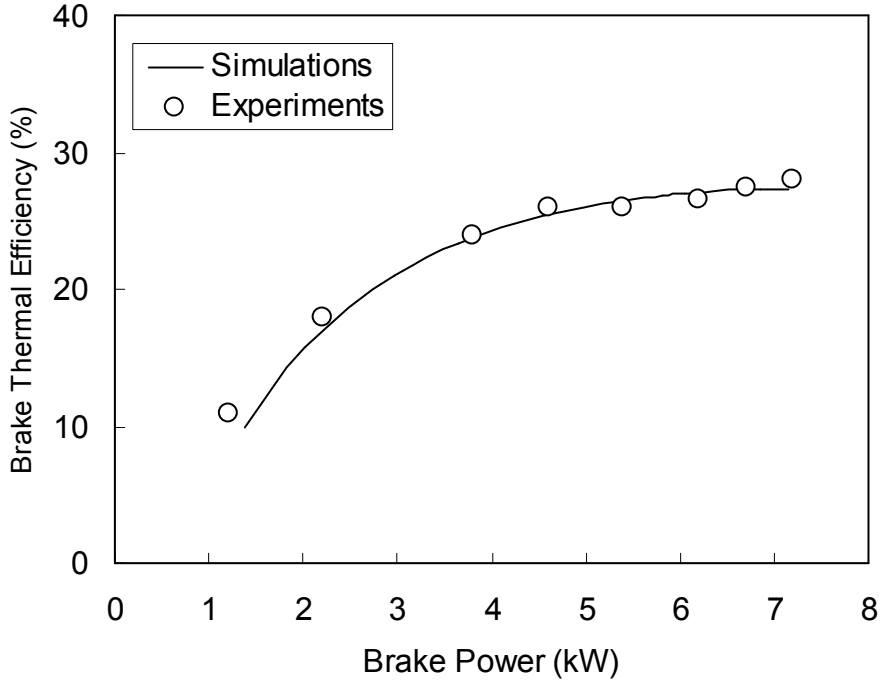

Figure 5.6. Comparison of predicted and measured brake thermal efficiencies as a function of brake power

In the present study, the standard Woschni's equation (Heywood, 1988) was used to predict the heat transfer between the combustion gases and the cylinder walls. Subramanian et al. (2005) also reported thermocouple measurements of exhaust gas temperatures. Unfortunately, they did not specify the location of the thermocouple along the length of the exhaust pipe and the pipe properties. On the other hand, the temperature of the gases at the end of the exhaust runner was obtained during the present simulations based on reasonable assumptions about the pipe properties and thermocouple location. The exhaust temperatures predicted in this manner relative to those measured are illustrated in Figure 5.7. The temperature of the gas stream flowing in the exhaust pipe increased from about 300 ºC to 500 ºC with increasing brake power or equivalence ratio.

In view of the fact there were some unknown experimental parameters that could not be exactly specified during the computations, the observed differences between the predicted and measured values were still satisfactory within these uncertainties.

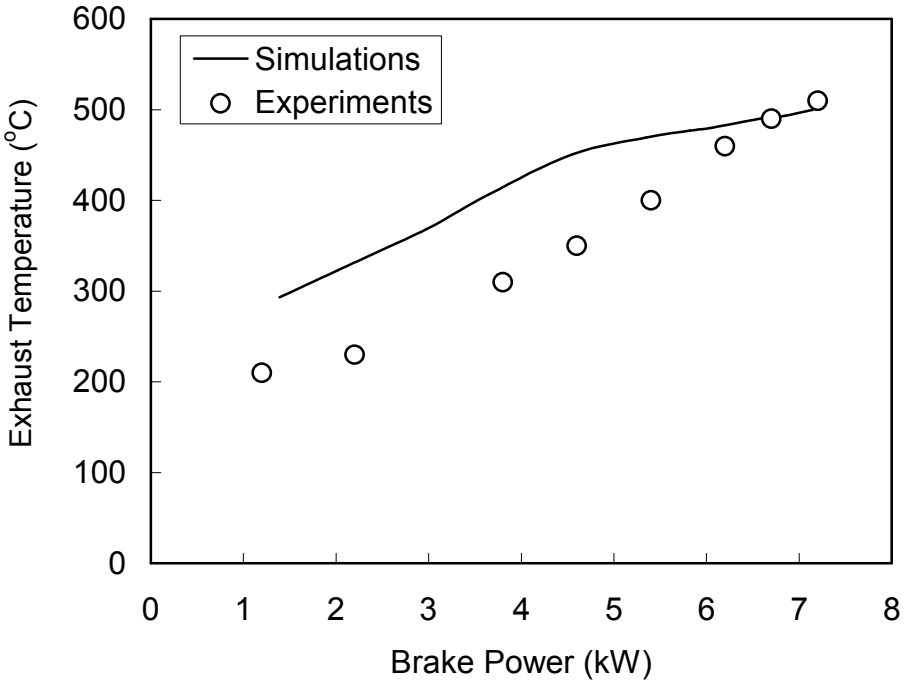

Figure 5.7. Comparison of predicted and measured exhaust gas temperatures as a function of brake power

NO_x emissions from the hydrogen engine are shown in Figure 5.8 as a function of brake power, which is directly tied to the equivalence ratio (Figure 5.4). Although the experiments (Subramanian et al., 2005) only reported NO while the simulations predicted both NO and NO_2, the rational for their comparison was based on the fact that a major portion (about 95%) of NO_x emissions involved NO. Because of its high sensitivity to the

temperature, NO_x formation was negligible below a break power of 4.5 kW or an equivalence ratio of 0.5. The rapid increase in NO_x after this operating condition limits the usage of hydrogen engines to low powers/equivalence ratios. Considering that the primary advantage of a hydrogen engine is near-zero emission, the brake power for the hydrogen engine considered here should be limited to 5 kW in order to keep NO_x concentration below 50 ppm, a typical value imposed by the strict emission standards (a gasoline engine will not be able to operate at such low emissions with out aftertreatment). Note, however, that the potential to expand the power band while maintaining low NO_x emissions still exists by considering other advanced methods (White et al., 2006).

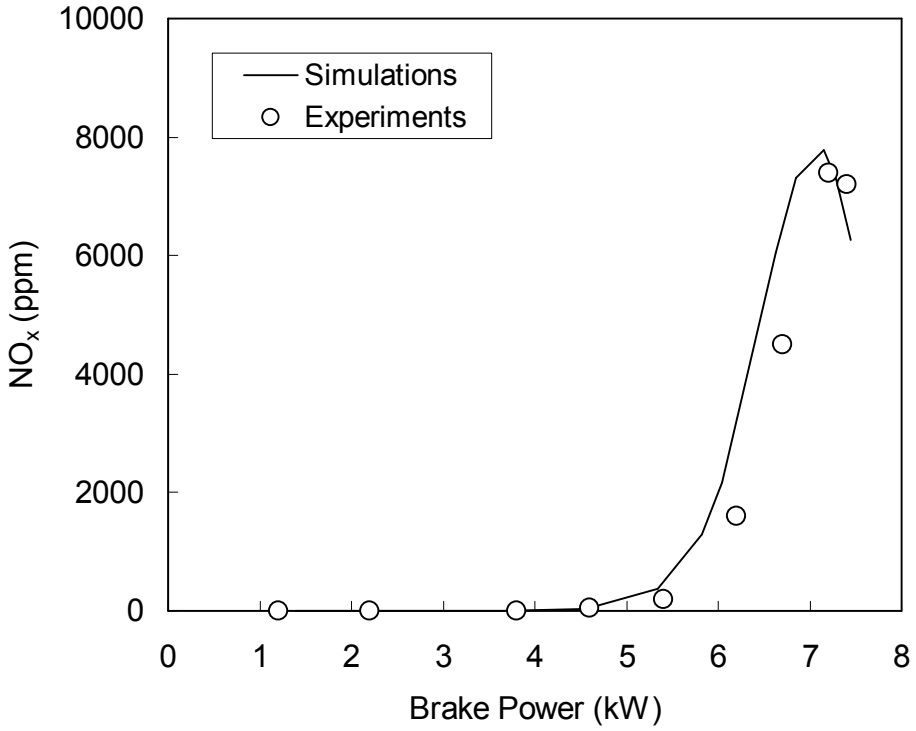

Figure 5.8. Comparison of predicted and measured NO_x emissions as a function of brake power

The measurements in Figure 5.8 revealed a maximum NO emission of 7000 ppm at a break power of about 7.4 kW (corresponding to an equivalence ratio of 0.84) and a slight decrease after this peak. The computations based on the extended Zeldovich mechanism followed the data closely. For example, the predicted maximum NO_x concentration was 7300 ppm, which deviates only 4% from the measured value. As the stoichiometric condition was approached, some of the formed NO_x dissociated due to a reduction in oxygen amount and an increase in free radicals at the highest combustion temperatures. The present simulations of NO_x emissions were in agreement not only with the experimental data of Subramanian et al. (2005) on a single hydrogen engine but also with the technical review of White et al. (2006), who compiled tailpipe emission data from several different studies.

5.4.3. Model Utilization – Effect of EGR on NO_x Emissions. After its development and validation, the computational model could be utilized for investigating various aspects of hydrogen-fueled engines. One possibility is to simulate burning of mixtures of hydrogen and another traditional fuel such as gasoline or natural gas in an IC engine (Bysveen, 2007). Another possibility is to computationally study the reduction in NO_x as a function of EGR level which will be briefly explored here.

Production of NO_x depends on the combustion temperature and the oxygen availability. Injecting a portion of the exhaust gases back to the intake manifold, called exhaust gas recirculation (EGR), displaces excess air, increases the specific heat capacity of the mixture, and lowers in-cylinder temperatures for the same amount of heat addition. This, in turn, reduces not only NO_x emissions but also the possibility of pre-ignition, knock and backfires. To induce variable EGR levels, the present hydrogen engine model

was modified as shown in Figure 5.9. A proportional-integral-derivative (PID) controller was used with a 15 mm-diameter throttle valve to control the amount of EGR through the EGR circuit. An appropriate control system was essential to supply the desired amount of diluent back into the cylinder.

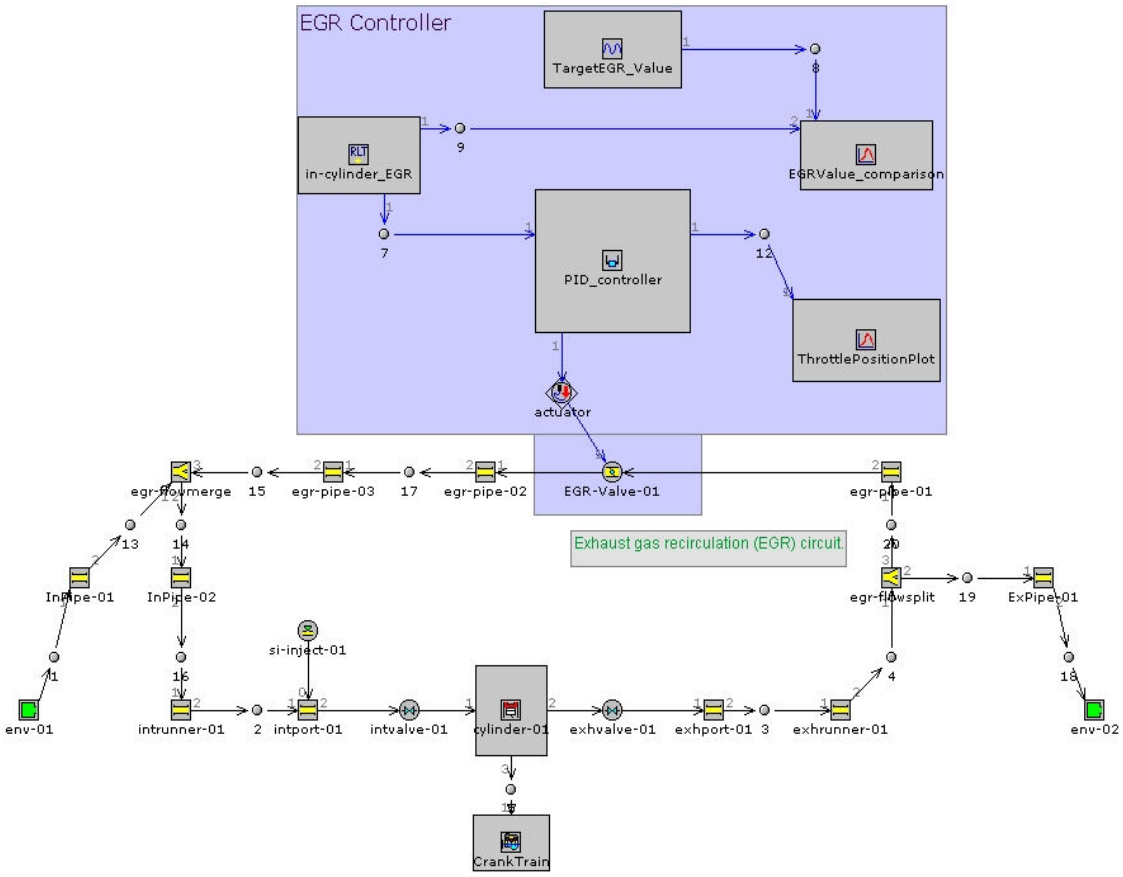

Figure 5.9. Hydrogen engine model modified with a PID controller to vary EGR level

The effect of EGR on NO_x emissions from the engine simulated in this investigation is quantified in Figure 5.10 at the maximum equivalence ratio (0.84)

considered. The computations revealed nearly linear decrease in NO_x concentrations from 7300 ppm to 800 ppm when the EGR level was increased from 0 to 16%. Overall, the predictions reasonably agreed with the experiments from another study (Subramanian, 2007) under nearly identical engine conditions. The nearly-linear decrease in the predicted amounts of NO_x with relatively low percentages of EGR is also consistent with the measured trends reported by Verhelst et al. (2006). Note that if the EGR level is increased further, it is expected that there will be less decrease in NO_x that may question implementation of EGR approximately above 30%. While the observed nearly an order of magnitude reduction in NO_x with only 16% EGR was significant, it also compromised the engine performance: At this maximum percentage of EGR considered here, the brake power, maximum pressure, and brake thermal efficiency decreased by 20%, 13%, and 13%, respectively. The application of post-combustion methods such as three-way catalytic converters (TWC) could further reduce the raw NO_x concentrations predicted above for achieving near zero exhaust-out emissions (Verhelst et al., 2006).

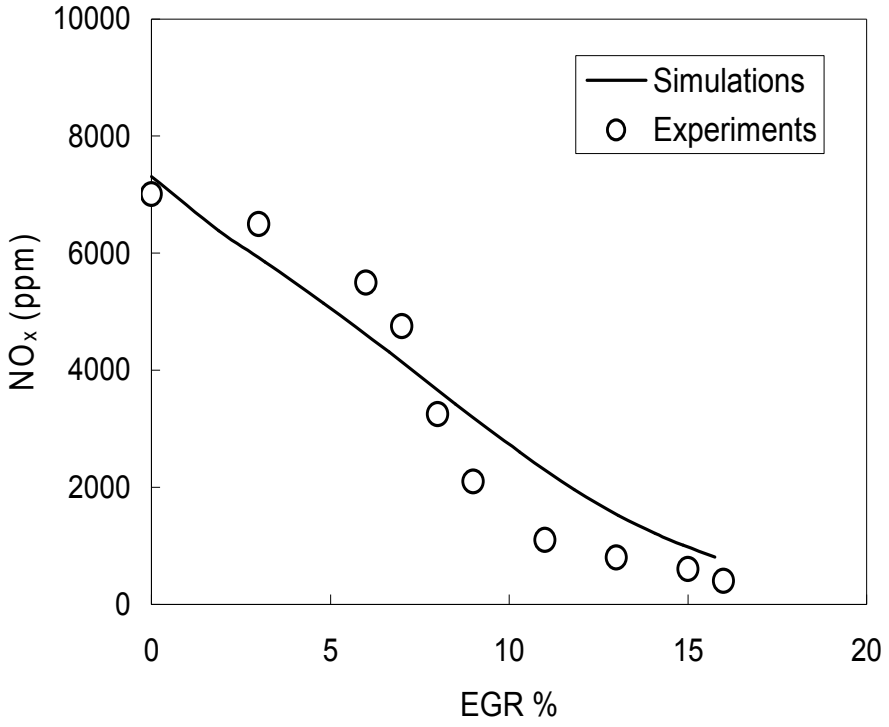

Figure 5.10. Variations of NO_x emissions with exhaust gas recirculation (EGR)

5.5. SUMMARY AND CONCLUSIONS

Hydrogen is a viable fuel for use in IC engines. The unique combustion characteristics of higher flame speed, wider flammability limits and easier ignition of hydrogen allow cleaner and more efficient engine operations at low engine loads but present difficulties at higher loads. In this study, engine simulations were employed to study the performance, combustion and emission characteristics of a hydrogen-fueled engine. In particular, hydrogen fuel-specific predictive sub-models were developed and incorporated into the one-dimensional simulations. Two significant improvements included a flame speed model that is exclusively accurate for hydrogen fuel/air mixtures and a predictive burn rate model that can be applied to any hydrogen engine. The

computational predictions were then compared to independent and well-documented experimental data from (Subramanian et al., 2005) in order to evaluate accuracy and suitability for widespread implementation.

The simulations generally agreed well (typically 10% difference) with the measurements under similar engine operational conditions, validating the predictive ability of the present model. In particular, the variations of peak in-cylinder pressure, heat release rate, brake power, brake thermal efficiency, exhaust temperature, and NO_x emissions were predicted close to the measured values within experimental and computational uncertainties. NO_x concentrations in the engine exhaust were negligible at lower equivalence ratios but they sharply increased after an equivalence ratio of 0.5, limiting the brake power of the hydrogen engine considered here to 5 kW.

After validation, the simulations were utilized to quantify the effect of exhaust gas recirculation (EGR) for lowering NO_x emissions by designing and adding a proportional-integral-derivative (PID) controller to the hydrogen engine model. Similar to the gasoline engines, EGR was found to be an effective method to reduce NO_x emissions in hydrogen engines. For example, a 16% EGR level at an equivalence ratio of 0.84 in the present hydrogen engine resulted in nearly an order of magnitude reduction in NO_x.

The results extended the use of GT-POWER software, which is already an industry-standard for designing gasoline and diesel engines, to hydrogen engines by properly accounting for the distinctive characteristics of hydrogen during simulations. This is expected to lead to improved designs of hydrogen engines, shorten the development time of alternative-fueled and hybrid vehicles in the automotive industry.

6. SUMMARY AND CONCLUSIONS

Hydrogen, as an energy carrier that can be produced from various renewable sources, is considered to be part of the sustainable solution portfolio to the increasing demands for clean and secure energy. Many technical barriers to the implementation of a hydrogen economy exist due to the lack of established scientific and technical knowledge that is needed to support the development of codes and standards for mitigation of potential fire and explosion hazards. To promote the use of safe hydrogen technologies, it is important to thoroughly understand the role of unique properties of hydrogen in various applications. In this study, effort has been made to first establish the lower flammability of hydrogen that is important for safety analysis, then, accidental hydrogen leaks for different flow regimes (small buoyancy-dominated and large momentum-dominated) were considered to investigate the transient mixing in air and the resulting formation of flammable envelopes. Additionally, the combustion, performance and emission characteristics of a hydrogen-powered internal combustion engine, which can serve as the transitional powertrain during the initial development of the hydrogen economy, were studied.

From an extensive literature search, it was found that the lower flammability limit, the concentration below which hydrogen-air mixture does not ignite, has remained as an empirical observation and dependent on the experimental setup used to observe it. Contradictory values of the flammability limit have been reported in the past, and the correlation between the flammability limits measured with various methods and the exact physical conditions that would occur in real accidents was not known. In this study, a simple but effective ideal experiment was developed to observe the lower flammability

limit of hydrogen in air that would be less dependent on the apparatus itself, and the result was supported with a theoretical analysis. After reducing the dependence on the apparatus as much as possible, it was found from both experiments and theoretical analysis that the lower flammability limit of hydrogen in air was 4.5%, a value close to what would be ideally observed in free space.

During the development of the above mentioned experiment, since hydrogen has very low density and high diffusion coefficient, preferential diffusion of hydrogen was found to have significant affect on the flammability of the hydrogen-air mixture. Consequently, a comprehensive study was conducted to analyze the fundamental features of hydrogen transient mixing and dispersion in air and the associated flammable envelopes within a unit-length vertical cylinder. The computational parameters were varied so that the flow conditions were controlled by either buoyancy or molecular diffusion or a small jet momentum. When hydrogen dispersed into the overlaying air, the mixing process was dominated by buoyancy due to the low density of hydrogen, and the concentration distribution was strongly dependent on both the radial and axial location. But if hydrogen was over the air, the mixing process was by slow molecular diffusion due to local concentration difference with very little dependence on radial location. When the mixing was buoyancy controlled, hydrogen rapidly moved up and for the closed top container, hydrogen moved twice faster near the axis compared to the open top case due to decrease in pressure along the axis when the cylinder was completely closed. This observation suggests the installation of safety alarms near symmetry axis which would trigger not only the sound but also the ventilation opening instead of a continuous ventilation at the top of an enclosure (e.g., garage).

When investigating small hydrogen leakages from the bottom into the completely closed container, hydrogen flowed downwards after hitting the container top and started occupying the entire cross section of the container in a one-dimensional manner at a very slow rate. With times on the order of a minute after the initiations of small jet leaks, only less than a quarter of the unit-length container near the top contained flammable hydrogen-air mixture. This implies that the occupants during a possible hydrogen accidental release in an enclosed area may have substantially more time unlike other traditional fuel leaks that would accumulate near the lower escape routes because of relatively high density and less buoyancy. If the leak was downward at the top of the container, the flammable regions beyond the symmetry line were still formed near the upper container regions. These results show that, for testing hydrogen leak in a closed room, the gas detector should be placed near the top of the room where there is more probability of flammable hydrogen accumulating.

If a high-pressure leak occurs, the exit flow chokes at the sonic velocity when the pressure ratio across the leak is greater than the critical pressure ratio (approximately 1.89 for hydrogen). For such a supercritical release, the flow leaves the exit to form an underexpanded jet. The flow at the exit of the leak is accelerated to supersonic speeds by the Prandtl-Meyer expansion fans until it forms a normal curved shock - Mach disk. To overcome the difficulty of numerically solving the details of the underexpanded jet, alternative approaches with an effective diameter have been suggested in literature. So initially, the applicability ranges of these widely-used effective diameter approaches for hydrogen safety analysis were assessed. It was found that these approaches are only valid for steady-state free jet analysis where the flow properties very close to leak (near field)

are not important but become questionable for more practical cases when the flow is unsteady or if there is a cross flow or an obstacle such that the flowfield gets disturbed.

With the complete underexpanded jet analysis, a 0.0127 m diameter high-pressure hydrogen leak from a storage tank containing 6.2 kg of hydrogen at 485 bar and 283 K was investigated. This scenario represents a potential accidental scenario in which there is a catastrophic failure of a pressure relief device (PRD) or a sudden small crack in the storage vessel in a typical mobile hydrogen unit (MHU) used in hydrogen fueling stations. It was found that the maximum Mach number in the underexpanded region was 6, and the temperature dropped to 50 K in this region. The high-pressure jet hit the wall, which was 2.72 m away, in approximately 0.02 s, and the hydrogen dispersed almost equally in both the upward and downward directions which would not be the case for a buoyancy-dominated slow leak. Hydrogen first arrived at the exhaust location of the MHU in approximately 0.1 s. As time proceeded, hydrogen started to accumulate almost uniformly (during the release phase) in the MHU except in the region in front of the leak. Major portion of the MHU (except the region in front of the leak) had 50%, 75% and 88% hydrogen concentration at 0.5 s, 1 s, and 1.6 s, respectively, when the leak flow rate was constant at 3.884 kg/s. The hydrogen concentrations were 44%, 65% and, 75% at 0.5 s, 1 s, and 1.6 s, respectively, when the flow rate of the leak was decaying according the changing tank conditions during the blowdown process. After all the hydrogen content from the high-pressure cylinder was released into the MHU, during the subsequent diffusion phase when the MHU gets replenished with fresh ambient air for a typical MHU ventilation system, it took approximately 30 minutes for the concentration to drop below the lower flammability limit.

The unique hydrogen combustion characteristics with a higher flame speed, wider flammability limits and higher energy content also made hydrogen as a viable fuel for clean and efficient operations of internal combustion engines. Hydrogen fuel-specific flame speed model and a predictive burn rate model that could be applied for any hydrogen engine were developed and incorporated into one-dimensional simulations. The computational predictions agreed well (less than 10% difference) with independent well-documented experimental data, validating the hydrogen engine model. It was found that the NO_x concentrations in the engine exhaust were negligible at lower equivalence ratios but they sharply increased after an equivalence ratio of 0.5, limiting the brake power of the hydrogen engine considered here to 5 kW. Similar to the gasoline engines, exhaust gas recirculation (EGR) was found to be an effective method to reduce NO_x emissions in hydrogen engines. To quantify, a proportional-integral-derivative (PID) controller was designed and used to control the amount of EGR injected into the intake manifold. A 16% EGR level at an equivalence ratio of 0.84 in the present hydrogen engine resulted in nearly an order of magnitude reduction in NO_x emissions.

The research results reported here will be important for understanding safety issues that need to be fully addressed by developing proper codes and standards that are critical for the design and operation of hydrogen-powered transportation vehicles and to provide improved designs of hydrogen engines that would shorten the development time of alternative-fueled and hybrid vehicles which are in the initial stages of development and commercialization.

RECOMMENDATIONS

Based on the current research, further work in the following areas is recommended for the widespread use of hydrogen technologies:

1. A similar fundamental understanding of ignited hydrogen leaks (small and large) and their interaction with other equipment around it. This study will also be important to help design hydrogen fueling stations and other infrastructure.

2. Development of easy to use simple analytical models for estimating the flammable hydrogen mixture and overpressures formed due to an explosion of a flammable volume in partially enclosed compartments (such as a garage).

3. Development of fast, reliable and affordable hydrogen gas and fire detection equipment.

4. Exploration of advanced combustion modes for utilization of hydrogen in engines, possibly direct injection of hydrogen into the cylinder, for higher power density, and a comprehensive second law analysis to find opportunities to further improve the engine efficiency.

5. Investigations on performance and emission characteristics of engines powered by fuel blends such as natural gas and hydrogen to accelerate the deployment of clean fuels in transportation applications.

6. Coordination with other research groups, NFPA, NIST and other national and international regulatory bodies working in this area to develop a comprehensive database and guidelines (based on sound scientific and technical knowledge) that is crucial for the development of the much-needed hydrogen safety codes and standards.

APPENDIX A.

ERROR ANALYSIS

When performing computations, it is essential that the numerical results satisfactorily converge, are grid independent, and compares with experimental data or analytical equations (Versteeg and Malalasekera, 2007; Chapra and Canale, 2005). Since the solution algorithms are iterative in nature, the residuals, which measure the overall conservation of flow properties, should be relatively small for an acceptable solution. Ideally, a very fine mesh should be used but this is computationally intensive. To eliminate errors due to grid coarseness, a grid-independent study should be carried out by successively refining the grid until key results no longer change. Accordingly, convergence study, grid-independence, and comparison with experimental data and analytical equations are performed during the course of the present study.

Figure A-1 shows the non-dimensional velocity and concentration decay profiles along the axis of a hydrogen unignited free jet that was simulated and compared with experimental data, analytical equations, and simulation results obtained from the literature. It was found that the current simulations shown by blue line were mostly within the minimum and maximum ranges reported by independent investigators in the past that are shown by red and green lines.

Figure A-2 shows the grid-independent study that was conducted for the high-pressure hydrogen leak. Mach number, mole fraction and static temperature plots obtained using the underexpanded jet analysis at a particular axial location along the radial direction of the leak are shown. These figures demonstrate that the present computations were grid independent after 73143 cells with a second order approach.

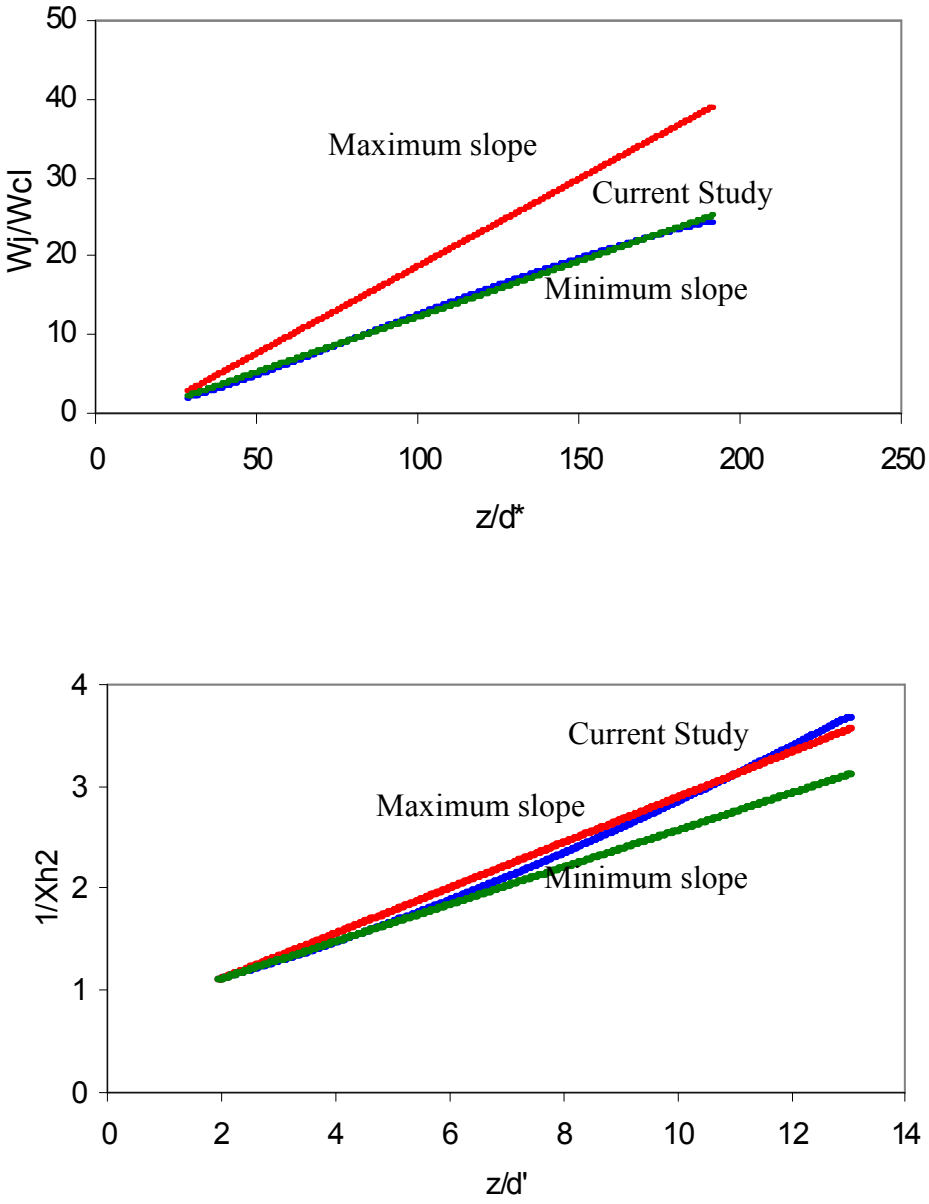

Figure A-1. Non-dimensional hydrogen jet velocity (above) and concentration (below) decay profiles along the axis for a hydrogen free jet

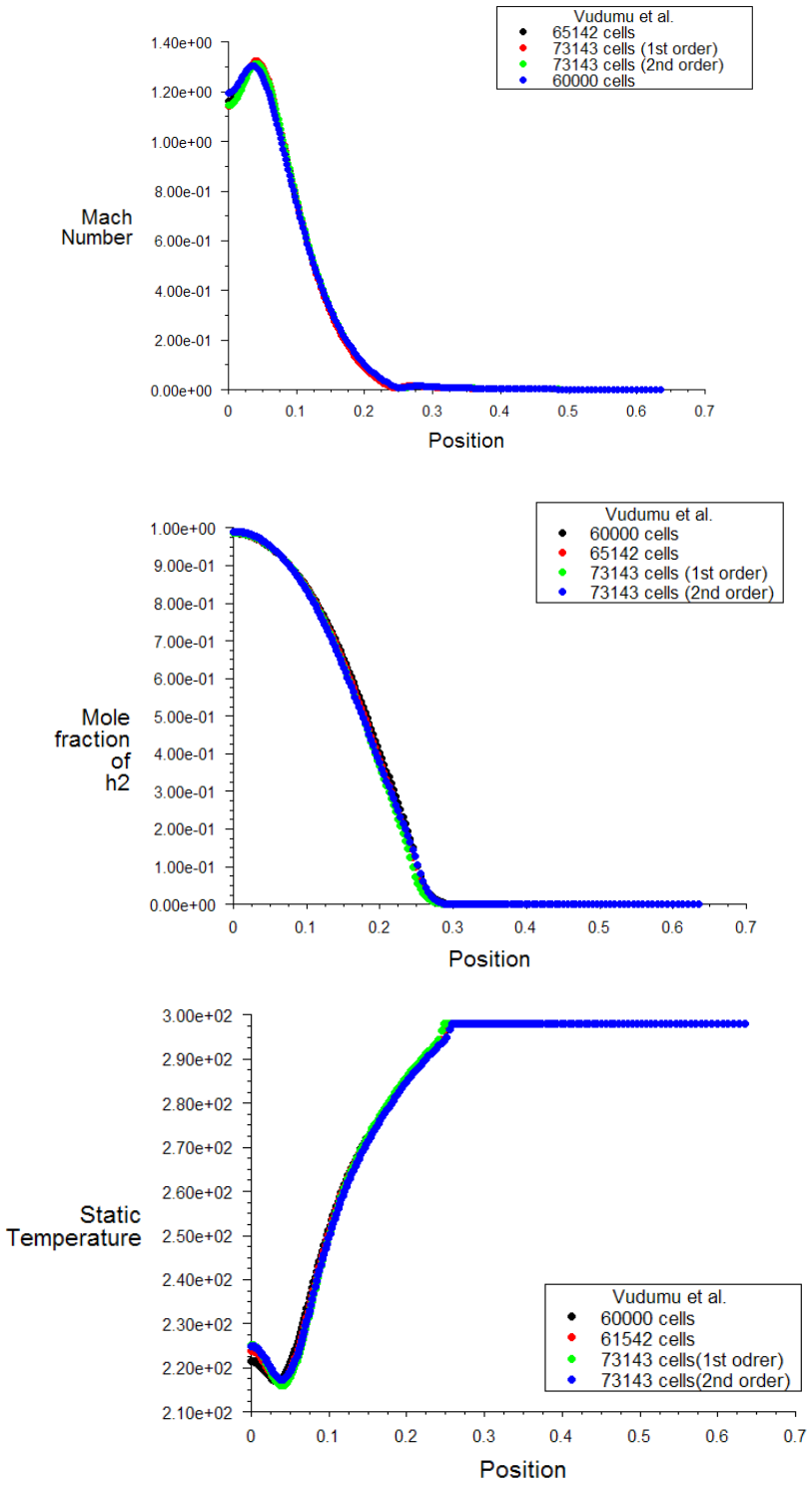

Figure A-2. Plots of grid independent study for Mach number, mole fraction and static temperature for high-pressure hydrogen leak using the underexpanded jet analysis along the radial direction

For one-dimensional engine simulations, the computations were run until the equations of continuity, momentum and energy met the following convergence criteria for mass flow rate, temperature, pressure (in all the sub-volumes) and brake power for five consecutive engine cycles:

$$df = \frac{\left|(f_{new} - f_{old})\right|}{f_{new}} \leq 0.002$$

where, df is the relative change in property for two consecutive cycles, f_{old} is the value of the property in the previous cycle, and f_{new} is the value of the property in the current cycle.

To ensure a satisfactory convergence, the above criterion was increased (made less strict) and the engine model was run again. Figure A-3 shows the variation of brake power with respect to equivalence ratio for different convergence criteria. As the convergence criterion became stricter from $df = 5$ to $df = 0.1$, the solution did not change any further. Consequently, a convergence criteria of $df = 0.002$ was adopted in this study.

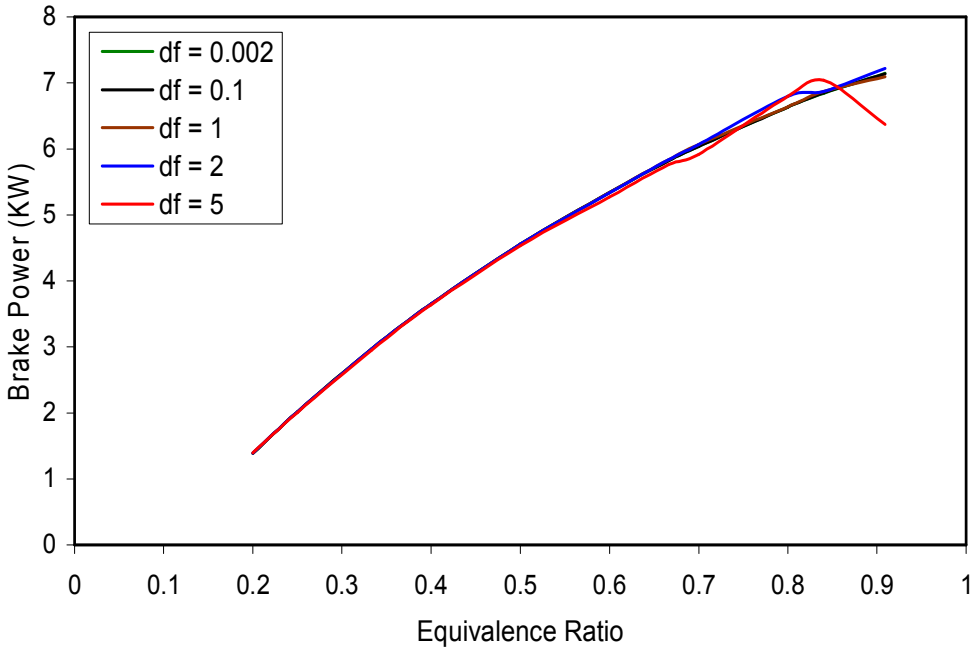

Figure A-3. Variation of brake power with equivalence ratio for various convergence criteria

APPENDIX B.

DEVELOPMENT AND INTEGRATION OF ENGINE SIMULATION PROJECTS INTO THE MECHANICAL ENGINEERING CURRICULUM AT MISSOURI S&T

PACE PROGRAM

PACE – Partners for the Advancement of Collaborative Engineering Education, is an industry and academia collaboration to develop the automotive team of the future. The PACE Partnership links GM, Autodesk, EDS, HP, Siemens and Sun Microsystems to support strategically-selected academic institutions worldwide providing hardware, software, training, automotive parts and industry projects.

PROJECT ACTIVITIES

To enhance student learning relevant to the needs of automotive industry, instructional engineering projects and necessary tutorials were developed to integrate advanced internal combustion engine simulations into the combustion related courses in the Mechanical and Aerospace Engineering Department at Missouri S&T. Specifically, GT-POWER that is used by leading vehicle manufacturers and their suppliers to design gasoline engines as well as by the present work to investigate the performance of hydrogen-powered engines (Section 5) was utilized for the first time at an academic institution with the sponsorship of PACE program. The projects included understanding and comparison of simple hand calculations using typical textbook assumptions with detailed and complicated software calculations. These projects were aimed to bridge the gap between the theoretical and simple concepts learned in the classroom and the practical and advanced skills desired by industry.

Two tutorials with step-by-step visual instructions for two semester projects were prepared for the students in the courses “Applied Thermodynamics” and “Combustion Processes”. The assigned project in Applied Thermodynamics was somewhat simpler

compared to the one in Combustion Processes because the former is an undergraduate required course and the latter is an elective undergraduate/graduate course.

Course 1: Applied Thermodynamics. The first tutorial in "Applied Thermodynamics" course introduced the basic features of the software. Already-prepared four-stroke single-cylinder engine model was given to the students to explore engine performance and emission characteristics of a gasoline and a diesel engine. For comparisons, ideal cycles typically given in thermodynamics class text books were used. Ideal Otto cycle (gasoline engine) assumes constant volume heat addition and heat rejection in the pressure-volume diagram as shown in Figure B-1. Due to inherent irreversibilities and other contributing factors, the pressure-volume diagram of an actual gasoline engine will be different from the ideal case (also shown in Figure B-1).

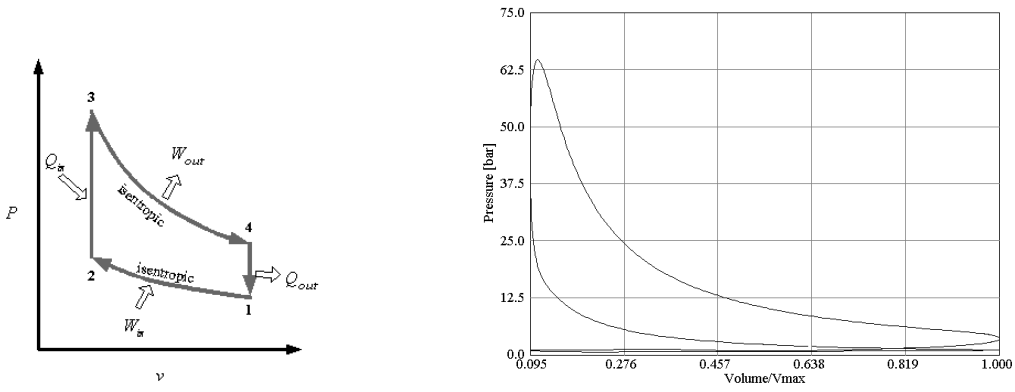

Figure B-1. Pressure-volume diagrams of an ideal Otto Cycle (left) and an actual gasoline engine (right)

The project also included varying the compression ratio of the engine and comparing efficiency values with the corresponding ideal cycle as shown in Figure B-2. The thermal efficiency of an ideal Otto cycle was hand calculated using the following equation:

$$\eta_{th,Otto} = 1 - \frac{1}{r^{k-1}} \tag{1}$$

where $r = \frac{V_{\max}}{V_{\min}}$ is the compression ratio and $k = \frac{c_p}{c_v}$ is the specific heat ratio.

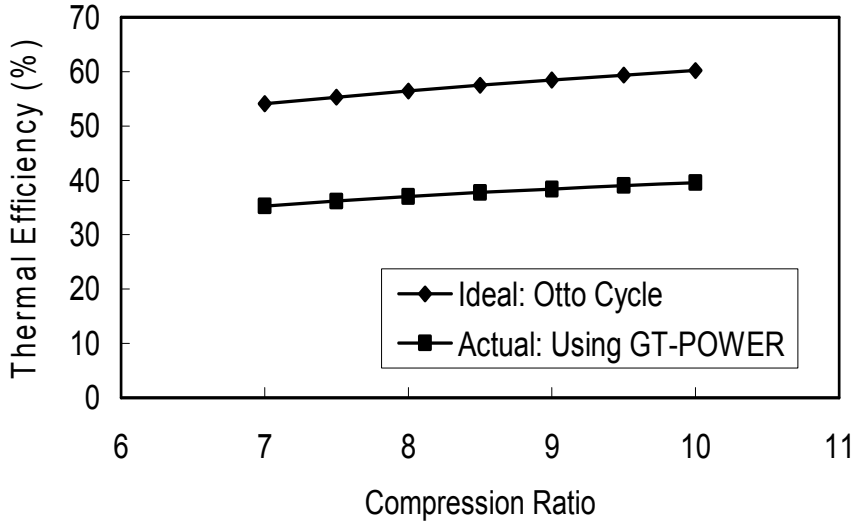

Figure B-2. Thermal efficiency vs. compression ratio using ideal Otto cycle equation and detailed simulations

A similar analysis was done for the Diesel cycle and Equation 2 was used to calculate the thermal efficiency of this ideal cycle.

$$\eta_{th,Diesel} = 1 - \frac{1}{r^{k-1}}\left[\frac{r_c^{\,k} - 1}{k(r_c - 1)}\right] \tag{2}$$

where r_c is the cutoff ratio.

Course 2: Combustion Processes. The second tutorial for the "Combustion Processes" course included building the complete detailed model for a gasoline engine and varying engine parameters such as equivalence ratio to study the performance and combustion characteristics. Figure B-3 shows the pressure vs. crank angle diagram at various equivalence ratios (1/lambda) of operation.

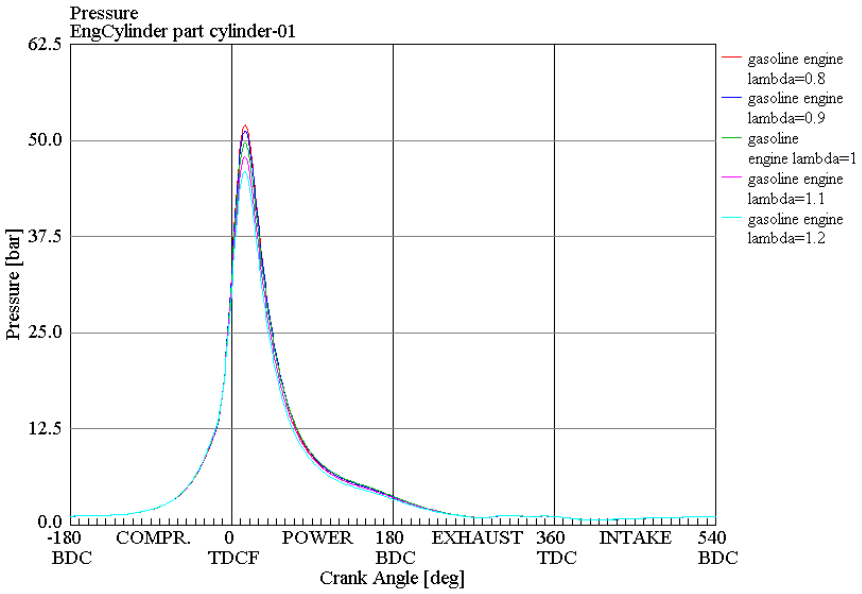

Figure B-3. Pressure vs. crank angle for a gasoline engine by varying equivalence ratio

For emissions, calculations were carried out by the students with the complete equilibrium analysis in GT-POWER and compared with the simple equilibrium hand calculations (see Table 1) by assuming only water-gas shift reaction (Equation 3), as given in the combustion textbooks. Water-gas shift reaction allows calculations of the

ideal products of combustion (with no dissociation producing minor species) to account for the incomplete products of combustion, CO and H_2.

$$CO + H_2O \Leftrightarrow CO_2 + H_2 \tag{3}$$

Table B-1. Comparison of emissions using hand calculations and GT-POWER model

Emission (mass fraction)	Hand calculations	GT-POWER model
CO_2	0.1234	0.13
CO	0.072	0.075
H_2O	0.0945	0.08
H_2	0.00147	-
O_2	0	0.01
NO	-	0.0007
HC	-	2.6 ppm
NO_x	-	625 ppm

The differences between the simple hand calculations and the complicated software computations are due to the fact that the software considers many other dissociation reactions other than water-gas shift reaction and it does not assume constant thermo-physical properties. Also, the software computes the emissions in the engine depending on the parameters chosen for modeling. Examples include geometry of the engine, compression ratio, engine speed, fuel used, air-fuel ratio, spark timing, inlet and exhaust valve opening timings, heat transfer and combustion models used to predict the engine performance.

In addition to understanding engine characteristics when powered by conventional gasoline and diesel fuels, students also explored alternative fuel-powered engines like

E85. Engine performance and emission comparisons were also done with an equivalent gasoline-powered engine.

The results of these educational activities are reported in an ASME Conference (Vudumu and Koylu, 2009).

BIBLIOGRAPHY

Anderson, J. D. (2003). Modern compressible flow with historical perspective. McGraw-Hill Companies, Inc., USA.

ANSYS FLUENT Inc., Lebanon, NH, USA. http://www.fluent.com. Mar 2010.

Barley, C.D., Gawlik, K., Ohi, J. and Hewett, R. (2007). Analysis of buoyancy-driven ventilation of hydrogen from buildings. *HYSAFE International Conference on Hydrogen Safety*, Spain, 11-13 Sep.

Barley, C.D., and Gawlik, K. (2009). Buoyancy-driven ventilation of hydrogen from buildings: Laboratory test and model validation. *International Journal of Hydrogen Energy*, 34: 5592–5603.

Birch, A.D., Brown, D.R., Dodson, M.G. and Swaffield, F. (1984). The structure and concentration decay of high pressure jets of natural gas. *Combustion Science and Technology*, 36: 249-261.

Birch, A.D., Hughes, D.J. and Swaffield, F. (1987). Velocity decay of high pressure jets. *Combustion Science and Technology*, 52: 161-171.

Bysveen, M. (2007). Engine characteristics of emissions and performance using mixtures of natural gas and hydrogen. *Energy*, 32: 482-489.

Chapra, C. and Canale, R. (2005). Numerical methods for engineers. McGraw Hill, New York, USA.

Ciccarelli, G., Jackson, D. and Verreault, J. (2006). Flammability limits of NH3-H2-N2-air mixtures at elevated initial temperatures. *Combustion and Flame*, 144: 53-63.

Cisse, P. and Karim, G.A. (2007). The rapid formation and dispersion of flammable zones within cylindrical vertical enclosures following the release of a fixed mass of hydrogen and other gaseous fuels into air. *International Journal of Hydrogen Energy*, 32: 630-636.

Coward, H.F. and Jones, G.W. (1952). Limits of flammability of gases and vapors, *US Bureau of Mines Bulletin*, 503, Pittsburg, Pennsylvania, USA.

Dahoe, A.E. and Molkov, V.V. (2007). On the development of an international curriculum on hydrogen safety engineering and its implementation into educational programmes. *International Journal of Hydrogen Energy*, 32: 1113-1120.

Crowl, D.A. and Jo, Y.D. (2007). The hazards and risks of hydrogen. *Journal of Loss Prevention in Process Industries*, 20: 158-164.

Das, L.M. (2002). Near-term introduction of hydrogen engines for automotive and agricultural application. *International Journal of Hydrogen Energy*, 27: 479-487.

Dunn, S. (2002). Hydrogen futures: toward a sustainable energy systems. *International Journal of Hydrogen Energy*, 27: 235-264.

Emmerich, S.J., Gorfain, J.E., Huag, M. and Reed, C.H. (2003). Air and Pollutant transport from attached garages to residential living spaces. *NIST publications*, NISTIR 7072.

Ewan, B.C.R. and Moodie, K. (1986). Structure and velocity measurements in underexpanded jets. *Combustion Science and Technology*, 45: 275-288.

Gamma Technologies Inc., USA. (2006). GT-POWER V6.2 User's Manual. http://www.gtisoft.com.

Groethe, M., Merilo, E., Colton, J., Chiba, S., Sato, Y. and Iwabuchi, H. (2007). Large-scale hydrogen deflagrations and detonations. *International Journal of Hydrogen Energy*, 32: 2125-2133.

Gupta, S., Brinster, J., Studer, E. and Tkatschenko, I. (2009). Hydrogen-related risks within a private garage: concentration measurements in a realistic full scale experimental facility. *International Journal of Hydrogen Energy*, 34: 5902-5911.

Heffel, J.W. (2003). NOx emission reduction in a hydrogen fueled internal combustion engine at 3000 rpm using exhaust gas recirculation. *International Journal of Hydrogen Energy*, 28: 1285-1292.

Heywood, J.B. (1988). Internal combustion engine fundamentals. McGraw Hill, New York, USA.

Houf, W. and Schefer, R. (2007). Predicting radiative heat fluxes and flammability envelopes from unintended releases of hydrogen. *International Journal of Hydrogen Energy*, 32: 136-151.

Houf, W. and Schefer, R. (2008). Analytical and experimental investigation of small-scale unintended releases of hydrogen. *International Journal of Hydrogen Energy*, 33: 1435-1444.

Houf, W.G., Evans, G.H. and Schefer, R.W. (2009). Analysis of jet flames and unignited jets from unintended releases of hydrogen. *International Journal of Hydrogen Energy*, 34: 5961-5969.

Hu, E., Huang, Z., Liu, B., Zheng, J., Gu, X. and Huang, B. (2009). Experimental investigation on performance and emissions of a spark-ignition engine fuelled with natural gas-hydrogen blends combined with EGR. *International Journal of Hydrogen Energy*, 34: 528-539.

Hustad, J.E., Sonju, O.K. (1988). Experimental studies of lower flammability of gases and mixture of gases at elevated temperatures. *Combustion and Flame*,71: 283-294.

Jorach, R., Enderle, C. and Decker, R. (1997). Development of a low-NO_x truck hydrogen engine with high specific power output. *International Journal of Hydrogen Energy*, 22: 423-427.

Jordan, T., Garcia, J., Hansen, O., Huser, A., Ledin, S., Middha, P., Molkov, V., Travis, J., Venetsanos, A.G., Verbecke, F. and Xiao, J. (2007). Results of the HySafe CFD validation benchmark SBEPV5. *HYSAFE International Conference on Hydrogen Safety*, Spain, 11-13 Sep.

Knop, V., Benkenida, A., Jay, S. and Colin, O. (2008). Modelling of combustion and nitrogen oxide formation in hydrogen-fuelled internal combustion engines within a 3D CFD code. *International Journal of Hydrogen Energy*, 33: 5083-5097.

Kumar, R.K. (1985). Flammability limits of hydrogen-oxygen-diluent mixtures. *Journal of Fire Sciences*, 3: 245-262.

Lacome, J.M., Dagba, Y., Perrette, L., Jamois, D. and Proust, C. (2007). Large-scale Hydrogen Release in an Isothermal Confined Area. *HYSAFE International Conference on Hydrogen Safety*, Spain, 11-13 Sep.

Landau, L.D. and Lifshitz, W. (1987). Fluid mechanics: volume 6 of course of theoretical physics. Pergamon Press, Ltd., England.

Launder, B.E. and Spalding, D.B. (1972). Lectures in Mathematical Models of Turbulence. Academic Press, England.

Li, H. and Karim, G.A. (2004). Knock in spark ignition hydrogen engines. *International Journal of Hydrogen Energy*, 29: 859-865.

Liu, D.D.S. and MacFarlane, R. (1983). Laminar burning velocities of hydrogen-air and hydrogen-air-stream flames. *Combustion and Flame*, 49: 59-71.

Matsuura, K., Kanayama, H., Tsukikawa, H. and Inoue, M. (2008). Numerical simulation of leaking hydrogen dispersion behavior in a partially open space. *International Journal of Hydrogen Energy*, 33: 240-247.

McDaniel, J., Glass, C., Staack, D. and Miller, C. (2002). Experimental and computational comparison of an underexpanded jet flowfield. *AIAA Paper* 2002-0305.

Medvedev, S.P., Gelfand, B.E., Polenov, A.N. and Khomik, S.V. (2002). Flammability limits of hydrogen-air mixtures in the presence of ultrafine droplets of water (fog). *Combustion, Explosion and Shock Waves*, 38: 381-386.

Negurescu, N., Panna, C., Popa, M.G. and Soare, D. (2006). Aspects regarding the combustion of hydrogen in spark ignition engine. *SAE Paper* 2006-01-0651.

Olvera, H.A and Choudhuri, A.R. (2006). Numerical simulation of hydrogen dispersion in the vicinity of a cubical building in stable stratified atmospheres. *International Journal of Hydrogen Energy*, 31: 2356-2369.

Papanikolaou, E.A. and Venetsanos, A.G. (2005). CFD modeling for helium releases in a private garage without forced ventilation. *HYSAFE International Conference on Hydrogen Safety*, Italy, 8-10 Sep.

Polasek, M., Macek, J., Takats, M. and Vitek, O. (2002). Application of advanced simulation methods and their combination with experiments to modeling of hydrogen fueled engine emission potentials. *SAE Paper* 2002-01-0373.

Prasad, K., Nelson, B., Cleary, T., Hamins, A., Marsh, N., Pitts, W. and Yang, J. (2008). Numerical simulation of hydrogen leakage and mixing in large confined spaces. *19th National Hydrogen Association Conference*, Sacramento, USA, 30 Mar-3 Apr.

Prasad, K., Pitts, W. M. and Yang, J.C. (2009). A numerical study of hydrogen or helium release and mixing in partially confined spaces. *20th National Hydrogen Association Conference*, South Carolina, USA, 30 Mar-3 Apr.

Rodgers, S.F., Vudumu, S.K., Grasman, S.E., Murray, S.L. and Koylu, U.O. (2010). Hydrogen safety in power generation applications. Accepted for publication in Professional Safety, Journal of the American Society of Safety Engineers.

Schefer, R.W., Houf, W.G., San Marchi, C., Chernicoff, W.P. and Englom, L. (2006). Characterization of leaks from compressed hydrogen dispensing systems and related components. *International Journal of Hydrogen Energy*, 31: 1247-1260.

Schefer, R.W., Houf, W.G., Williams, T.C., Bourne, B. and Colton, J. (2007). Characterization of high-pressure, underexpanded hydrogen-jet flames. *International Journal of Hydrogen Energy*, 32: 2081-2093.

Schefer, R.W., Mark. G., Houf, W.G., Marchi and Evans. G. (2009). Experimental evaluation of barrier walls for risk reduction of unintended hydrogen releases. *International Journal of Hydrogen Energy*, 34: 1590-1606.

Schmidt, D., Krause, U. and Schmidtchen, U. (1999). Numerical simulation of hydrogen gas releases between buildings. *International Journal of Hydrogen Energy*, 24: 479-488.

Shigeki, K. (2008). Consequence analysis and safety verification of hydrogen fueling stations using CFD simulations. *International Journal of Hydrogen Energy*, 33: 1425-1434.

Shudo, T. and Suzuki, H. (2002). New heat transfer equation applicable to hydrogen-fuelled engines. *Proceedings of ASME* ICEF2002-515.

Subramanian, V., Mallikarjuna, J.M. and Ramesh, A. (2005). Performance, emission and combustion characteristics of a hydrogen fueled SI engine-an experimental study. *SAE Paper* 2005-26-349.

Subramanian, V., Mallikarjuna, J.M., Ramesh, A. (2007). Intake charge dilution effects on control of nitric oxide emission in a hydrogen fueled SI engine. *International Journal of Hydrogen Energy*, 32: 2043-2056.

Swain, M.R. and Swain, M.N. (1996). Passive ventilation systems for the safe use of hydrogen. *International Journal of Hydrogen Energy*, 21: 823-835.

Swain, M.R. and Shriber, J. (1998). Comparison of hydrogen, natural gas, liquefied petroleum gas, and gasoline leakage in a residential garage. *Energy and Fuels*, 12: 83-89.

Swain, M.R., Filoso, P., Grilliot, E.S. and Swain, M.N. (2003). Hydrogen leakage into simple geometric enclosures. *International Journal of Hydrogen Energy*, 28: 229-248.

Swain, M.R., Filso, P.A. and Swain, M.N. (2005). Ignition of lean hydrogen-air mixtures. *International Journal of Hydrogen Energy*, 30: 1447-1455.

Swain, M.R., Filoso, P.A. and Swain, M.N. (2007). An experimental investigation into the ignition of leaking hydrogen. *International Journal of Hydrogen Energy*, 32: 287-295.

Takahashi, A., Urano, Y., Tokuhashi, K. and Kondo, S. (2003). Effect of vessel size and shape on experimental flammability limits of gases. *Journal of Hazardous Materials*, 105: 27-37.

Tanaka, T., Azuma, T., Evans, J.A., Cronin, P.M., Johnson, D.M. and Cleaver, R.P. (2007). Experimental study on hydrogen explosions in a full-scale hydrogen filling station model. *International Journal of Hydrogen Energy*, 32: 2162-2170.

Tchouvelev A.V., Cheng, Z., Agranat V.M. and Zhubrin S.V. (2007). Effectiveness of small barriers as means to reduce clearance distances. *International Journal of Hydrogen Energy*, 32: 1409-1415.

Venetsanos, A.G., Huld, T., Adams, P. and Bartzis, J.G. (2003). Source, dispersion and combustion modeling of an accidental release of hydrogen in an urban environment. *Journal of Hazardous Materials*, 105: 1-25.

Venetsanos, A., Papanikolaou, E., Delichatsios, M., Garcia, J., Hansen, O.R., Heitsch, M. et al. (2009). An inter-comparison exercise on the capabilities of CFD models to predict the short and long term distribution and mixing of hydrogen in a garage. *International Journal of Hydrogen Energy*, 34: 5912-5923.

Verhelst, S. and Sierens, R. (2001). Hydrogen engine-specific properties. *International Journal of Hydrogen Energy*, 26: 987-990.

Verhelst, S., Sierens, R. and Verstraeten, S. (2006). A critical review of experimental research on hydrogen fueled SI engines. *SAE Paper* 2006-01-0430.

Verhelst, S., Landtsheere, J.D., Smet, F.D., Billiouw, C., Trenson, A. and Sierens, R. (2008). Effects of supercharging, EGR and variable valve timing on power and emissions of hydrogen internal combustion engines. *SAE Paper* 2008-01-1033.

Verhelst, S., Maesschalck, P., Rombaut, N. and Sierens, R. (2009). Efficiency comparison between hydrogen and gasoline, on a bi-fuel hydrogen/gasoline engine. *International Journal of Hydrogen Energy*, 34: 2504-2510.

Versteeg, H.K. and Malalasekera, W. (2007). An introduction to computational fluid dynamics-the finite volume method. Pearson Education, Ltd., UK.

Villegas, Y.C., Moser, M.D. and Coleman, H.W. (2005). Flammability limits of hydrogen-oxygen-helium mixtures in confined spaces. *AIAA/ASME/SAE/ASEE Joint Propulsion Conference & Exhibit*, Tucson, Arizona, 10-13 July.

Vudumu, S.K. and Koylu, U.O. (2008). Hydrogen dispersion and flammability limits in simple geometric enclosures for developing safety codes and standards. *19th National Hydrogen Association Conference*, Sacramento, 30 Mar-3 Apr.

Vudumu, S.K. and Koylu, U.O. (2009). Detailed simulations of the transient hydrogen mixing, leakage and flammability in air in simple geometries. *International Journal of Hydrogen Energy*, 34: 2824–2833.

Vudumu, S.K. and Koylu, U.O. (2009). Development and integration of engine simulation projects into the mechanical engineering curriculum at Missouri S&T. *Proceedings of ASME* IMECE2009-10540.

White, C.M., Steeper, R.R. and Lutz, A.E. (2006). The hydrogen-fueled internal combustion engine: a technical review. *International Journal of Hydrogen Energy*, 31: 1292-1305.

Wierzba, I. and Wang, Q. (2006). The flammability limits of H2-CO-CH4 mixtures in air at elevated temperatures. *International Journal of Hydrogen Energy*, 31: 485-489.

Wilkening, H. and Baraldi, D. (2007). CFD modeling of accidental hydrogen release from pipelines. *International Journal of Hydrogen Energy*, 32: 2206-2215.

Winters, W.S. and Evans, G.H. (2006). Final report for the ASC gas-powder two-phase flow modeling project AD2006-09. *Sandia National Laboratories* Report No. SAND2006–7579.

Woodmansee, M.A. and Lucht, R.P. (1999). Experimental measurements of pressure, temperature, and density in an underexpanded sonic jet flowfield. *AIAA Paper* 1999-3600.

Zabetakis, M.G. (1965). Flammability characteristics of combustible gases and vapors. *US Bureau of Mines Bulletin*, 627, Washington, USA.

Zhang, J., Hereid, J., Hagen, M., Bakirtzis, D., Delichatsios, M.A. and Venetsanos, A.G. (2007). Numerical studies of dispersion and flammable volume of hydrogen in enclosures. *HYSAFE International Conference on Hydrogen Safety*, Spain, 11-13 Sep.

LIST OF PUBLICATIONS AND CONFERENCES

JOURNALS

Vudumu, S.K. and Koylu, U.O. (2009). Detailed simulations of the transient hydrogen mixing, leakage and flammability in air in simple geometries. *International Journal of Hydrogen Energy*, 34: 2824–2833.

Vudumu, S.K. and Koylu, U.O. (2010). Computational modeling, validation, and utilization for predicting the performance, combustion and emission characteristics of hydrogen IC engines. Submitted to *Energy*.

Vudumu, S.K., Koylu, U.O, Hosder, S. and Sheffield, J.W. (2010). High-pressure unsteady hydrogen leak from a storage cylinder in a mobile hydrogen unit. In preparation for submission to *International Journal of Hydrogen Energy*.

Rodgers, S.F., Vudumu, S.K., Grasman, S.E., Murray, S.L. and Koylu, U.O. (2010). Hydrogen safety in power generation applications. Accepted for publication in *Professional Safety, Journal of the American Society of Safety Engineers*.

CONFERENCES

Vudumu, S.K., Koylu, U.O, Hosder, S. and Sheffield, J.W. (2010). High-pressure unsteady hydrogen leak from a storage cylinder in a mobile hydrogen unit. *Proceedings of AIAA 40th Fluid Dynamics Conference* AIAA-2010-5107, Chicago, IL, 28 June-1 July.

Vudumu, S.K. and Koylu, U.O. (2009). A Computational study on performance, combustion and emission characteristics of a hydrogen-fueled internal combustion engine. *Proceedings of ASME* IMECE2009-11183, Lake Buena Vista, FL, 13-19 Nov.

Vudumu, S.K. and Koylu, U.O. (2009). Development and integration of engine simulation projects into the mechanical engineering curriculum at Missouri S&T. *Proceedings of ASME* IMECE2009-10540, Lake Buena Vista, FL, 13-19 Nov.

Koylu, U.O., Vudumu, S.K. and Sheffield, J.W. (2009). Hydrogen safety in accidental release scenarios. *Missouri Energy Summit*, Columbia, MO, 22-23 Apr.

Vudumu, S.K. and Koylu, U.O. (2008). CFD modeling of hydrogen dispersion and flammability limits in air in simple enclosures. *32nd International Symposium on Combustion*, Montreal, Canada, 3-8 Aug.

Vudumu, S.K., Koylu, U.O. and Drallmeier, J.A. (2008). GT-POWER for the simulations of IC engines in combustion courses at Missouri S&T. *2008 PACE Global Annual Forum*, Detroit, MI, 28 July-2 Aug.

Vudumu, S.K. and Koylu, U.O. (2008). Hydrogen dispersion and flammability limits in simple geometric enclosures for developing safety codes and standards. *19th National Hydrogen Association Conference*, Sacramento, 30 Mar-3 Apr.

VITA

Shravan Kumar Vudumu was born on August 26, 1983 in Andhra Pradesh, India. He completed his secondary education in Hyderabad, India in 2000. He joined Indian Institute of Technology - Madras in Chennai, India and obtained his Bachelor of Technology degree in Mechanical Engineering and Master of Technology degree in Energy Technology in May 2006. Mr. Vudumu then enrolled in the Ph.D. program in the Mechanical and Aerospace Engineering Department at Missouri University of Science and Technology (Formerly University of Missouri-Rolla) in August 2006. He was a National University Transportation Center Fellow, Graduate Research Assistant, and Graduate Teaching Assistant at Missouri S&T. He received his Ph.D. degree in August 2010.